

TABLE OF CONTENTS

<u>Section</u>	<u>Page No.</u>
LIST OF ILLUSTRATIONS	iv 1/A6
LIST OF TABLES	v 1/A7
SUMMARY	1 1/A8
INTRODUCTION	1 1/A8
LIST OF SYMBOLS	3 1/A10
ANALYSIS	7 1/A14
General Considerations	7 1/A14
Mathematical Representation of Solar Wind-Magneto/Ionosphere Interaction	8 1/B1
Magnetic Planet - Determination of the Magnetosphere Boundary	11 1/B4
Nonmagnetic Planet - Determination of the Ionosphere Boundary	16 1/B9
Calculation of the Gasdynamic Flow Properties	19 1/B12
Calculation of the Magnetic Field	26 1/C5
RESULTS AND DISCUSSION	29 1/C8
CONCLUDING REMARKS	32 1/C11
APPENDIX A - COMPUTER PROGRAM USER'S MANUAL	34 1/C13
APPENDIX B - LISTING OF COMPUTER PROGRAM	73 1/G1
REFERENCES	107 2/G1
TABLE 1	110 2/E4
FIGURES 1 THROUGH 15	113 2/E10

ITEM-830-H-14 NAS 1.26:2924

JAN 3 1978

COMPLETED
ORIGINAL

**NASA CONTRACTOR
REPORT**



NASA CR-2924

NASA CR-2924

**COMPUTATIONAL TECHNIQUES
FOR SOLAR WIND FLOWS
PAST TERRESTRIAL PLANETS -
THEORY AND COMPUTER PROGRAMS**

*Stephen S. Stabara, Denny S. Chaussee,
Barbara C. Trudinger, and John R. Spreiter*

Prepared by
NIELSEN ENGINEERING & RESEARCH, INC.
Mountain View, Calif. 94043
for

**MICROFILMED FROM
BEST AVAILABLE COPY**

NATIONAL AERONAUTICS AND SPACE ADMINISTRATION • WASHINGTON, D. C. • NOVEMBER 1977

136

1 Report No NASA CR- 2924		2 Government Accession No		3 Recipient's Catalog No	
4 Title and Subtitle Computational Techniques for Solar Wind Flows Past Terrestrial Planets - Theory and Computer Programs				5 Report Date November 1977	
				6 Performing Organization Code	
7 Author(s) Stephen S. Stahara, Denny S. Chaussee, Barbara C. Trudinger, and John R. Spreiter				8 Performing Organization Report No. NEAR TR 140	
				10 Work Unit No.	
9 Performing Organization Name and Address Nielsen Engineering & Research, Inc. 510 Clyde Avenue Mountain View, California 94043				11 Contract or Grant No. NASW-2945	
				13 Type of Report and Period Covered Contractor Report June 1976-July 1977	
12 Sponsoring Agency Name and Address National Aeronautics and Space Administration Washington, D.C. 20546				14 Sponsoring Agency Code	
15 Supplementary Notes					
16 Abstract Theoretical analysis and the development of user-oriented computer programs were carried out for the purpose of developing computational techniques for predicting the interaction of the solar wind with terrestrial planets. The procedures are based on a single-fluid, steady, dissipationless, magnetohydrodynamic model and are appropriate for the calculation of axisymmetric, supersonic, super-Alfvénic solar wind flow past both magnetic and nonmagnetic planets. The actual calculations are implemented by an assemblage of computer codes organized into one program. These include finite-difference codes which determine the gas-dynamic solution, together with a variety of special-purpose output codes for determining and automatically plotting both flow field and magnetic field results. <p>Theoretical results obtained using these procedures are reported for a variety of solar wind conditions and different obstacle shapes. Comparisons are made with previous results, and new results are presented for a number of solar wind flows. The computational programs developed under this work have been documented and are presented in a general user's manual included as part of this report.</p>					
17 Key Words (Suggested by Author(s)) Solar Wind Flows Finite-Difference Computations Steady Flow Magnetosphere Ionosphere			18 Distribution Statement UNCLASSIFIED-UNLIMITED Cat. 92		
19 Security Classif. (of this report) UNCLASSIFIED		20 Security Classif. (of this page) UNCLASSIFIED		22 Price* \$6.00	
				21 No. of Pages 133	

BLANK PAGE

TABLE OF CONTENTS

<u>Section</u>	<u>Page No.</u>
LIST OF ILLUSTRATIONS	iv
LIST OF TABLES	v
SUMMARY	1
INTRODUCTION	1
LIST OF SYMBOLS	3
ANALYSIS	7
General Considerations	7
Mathematical Representation of Solar Wind-Magneto/Ionosphere Interaction	8
Magnetic Planet - Determination of the Magnetosphere Boundary	11
Nonmagnetic Planet - Determination of the Ionosphere Boundary	16
Calculation of the Gasdynamic Flow Properties	19
Calculation of the Magnetic Field	26
RESULTS AND DISCUSSION	29
CONCLUDING REMARKS	32
APPENDIX A - COMPUTER PROGRAM USER'S MANUAL	34
APPENDIX B - LISTING OF COMPUTER PROGRAM	73
REFERENCES	107
TABLE 1	110
FIGURES 1 THROUGH 15	113

LIST OF ILLUSTRATIONS

Figure

- 1 Comparison of the equatorial and principal meridian traces of the magnetosphere boundary as provided by the simplified theory of equation 16.
- 2 Illustration of ionopause shapes for various values of the ionosphere scale height to shock standoff distance ratio H/R_0 .
- 3 Comparison of former and present computational procedures for determining the gasdynamic flow properties of solar wind-magneto/ionopause interactions.
- 4 Illustration of the components of the three-dimensional magnetic field.
- 5 Comparison of flow properties predicted by the present implicit method with other techniques and experiment for supersonic flow past a sphere; $M_\infty = 4.926$, $\gamma = 1.4$.
- 6 Comparison of implicit and inverse methods for shock shape and sonic line location, and density distribution along bow shock and magnetosphere boundary for $M_\infty = 8$, $\gamma = 5/3$ flow past the rotated equatorial trace of the magnetopause.
- 7 Bow wave and sonic line locations for various supersonic flows past the rotated equatorial trace of the magnetopause with $\gamma = 5/3$.
- 8 Bow shock location for solar wind flow with $M_\infty = 8$, $\gamma = 5/3$ past various ionopause shapes.
- 9 Bow shock and embedded shock locations for solar wind flow with $M_\infty = 5$, $\gamma = 5/3$ past the rotated principal meridian of the magnetosphere.
- 10 Magnetopause pressure coefficients for the principal meridian magnetopause shapes shown in figure 9.
- 11 Variation of shock stand-off distance with oncoming Mach number and ratio of specific heats for various magneto/ionopause traces as determined by the present implicit procedure.
- 12 Shock shapes for various supersonic flows past the rotated equatorial trace of the magnetopause; combined near (blunt body) and far (marching) solutions.
- 13 Shock shapes for $M_\infty = 8$, $\gamma = 5/3$ flow past an ionopause shape with $H/R_0 = 0.1$; combined near (blunt body) and far (marching) field solutions.

LIST OF ILLUSTRATIONS (CONTINUED)

Figure

- 14 Streamline, density, and velocity maps for $M_\infty = 8.0$, $\gamma = 5/3$ flow past the rotated equatorial trace of the magnetopause; combined blunt body and marching flow field.
- 15 Contours and field line locations of the in-plane magnetic field components $(B/B_\infty)_1$ and $(B/B_\infty)_2$ for $M_\infty = 8$ and $\gamma = 5/3$ flow past the rotated equatorial trace of the magnetopause.
- A.1 Card input for sample case.
- A.2 Abbreviated output for sample case.
- A.3 Plot output for sample case.

LIST OF TABLES

Table

- 1 Ordinates of various magneto/ionopause shapes.

COMPUTATIONAL TECHNIQUES FOR SOLAR
WIND FLOWS PAST TERRESTRIAL PLANETS
- THEORY AND COMPUTER PROGRAMS

by Stephen S. Stahara, Denny S. Chaussee,
Barbara C. Trudinger, and
John R. Spreiter*
Nielsen Engineering & Research, Inc.

SUMMARY

Theoretical analysis and the development of user-oriented computer programs were carried out for the purpose of developing computational techniques for predicting the interaction of the solar wind with terrestrial planets. The procedures are based on a single-fluid, steady, dissipationless, magnetohydrodynamic model and are appropriate for the calculation of axisymmetric, supersonic, super-Alfvénic solar wind flow past both magnetic and nonmagnetic planets. The actual calculations are implemented by an assemblage of computer codes organized into one program. These include finite-difference codes which determine the gasdynamic solution, together with a variety of special-purpose output codes for determining and automatically plotting both flow field and magnetic field results.

Theoretical results obtained using these procedures are reported for a variety of solar wind conditions and different obstacle shapes. Comparisons are made with previous results, and new results are presented for a number of solar wind flows. The computational programs developed under this work have been documented and are presented in a general user's manual included as part of this report.

INTRODUCTION

The gasdynamic and magnetohydrodynamic calculations of solar wind flow around magnetic and nonmagnetic planets that Spreiter et al. (refs. 1-8) carried out some years ago have been and continue to be widely used in the interpretation of data measured in space around the Earth and other planets. The objective at the time those calculations were made, was to

*Professor, Department of Applied Mechanics, Stanford University.
Consultant, Nielsen Engineering & Research, Inc.

provide some theoretical results based on a fluid rather than particle description of the flow that might be compared with measurements in space to determine the applicability of such a description. During the intervening years, the usefulness and accuracy of those results have become so well established that they are currently being used, for instance, as one of the ways in which the magnetic field of a planet such as Mercury or Mars is estimated from measurements of fly-by or orbiting spacecraft.

In such applications, the previous calculations leave much to be desired. They have been carried out for only a limited set of conditions such as obstacle shape, oncoming Mach number, angle between free-stream flow and magnetic vectors, etc., and are presented in archival publications only in the form of plots from which results for other conditions must be determined by scaling and interpolation. The usefulness of the present theoretical model, therefore, would be considerably enhanced if similar but more detailed results for the specific conditions measured by a spacecraft would be provided by the application of a documented, user-oriented, economical computer code.

That objective has been successfully accomplished in the work reported here. Based upon the identical theoretical model employed previously (refs. 1-8), and discussed in more detail below, a new more versatile means of solution far superior in efficiency and generality to the former method is now available. Current advances in computational methods have been incorporated in these programs and, in fact, an entirely new blunt body code based on a recently published algorithm was developed to determine the flow field in the region surrounding the nose of the obstacle. The new methods confirm previous results and are readily applicable to additional cases involving different geometries and flow conditions. The entire procedure is fully automated and provides detailed flow field and magnetic field properties in a convenient output format. An automatic plotting capability for generating report-quality plots is also included.

LIST OF SYMBOLS

a	speed of sound, $(\gamma p/\rho)^{1/2}$
a_e	planetary radius of earth, $6.37 \cdot 10^8$ cm
A	Alfvén speed, $(B^2/4\pi\rho)^{1/2}$
\bar{A}	Jacobian matrix associated with IMP code, equal to $\partial \hat{E}/\partial \hat{U}$
\vec{B}	magnetic field vector
B_{eq}	strength of Earth's magnetic field at geomagnetic equator, equal to 0.312 gauss
\bar{B}	Jacobian matrix associated with IMP code, equal to $\partial \hat{F}/\partial \hat{U}$
C_p	specific heat at constant pressure
C_v	specific heat at constant volume
D	geometric distance to magnetosphere nose, equal to $a_e (f^2 B_{eq}^2 / 2\pi K_p V_e)^{1/6}$
e	internal energy, eq. (5)
E	column matrix defined by eq. (29)
\hat{E}	column matrix associated with IMP code, equal to $(\xi_T U + \xi_X E + \xi_R F)/J$
f	constant associated with tangential component of Earth's magnetic dipole field at magnetopause location
F	column matrix defined by eq. (29)
\hat{F}	column matrix associated with IMP code, equal to $(\eta_T U + \eta_X E + \eta_R F)/J$
\tilde{F}	column matrix defined by eq. (34)
g	acceleration due to gravity
G	column matrix defined by eq. (29)
\tilde{G}	column matrix defined by eq. (34)
h	enthalpy, eq. (6)
H	local scale height of atmosphere, $\bar{R}T/\mu g$
H_t	total enthalpy, eq. (35)
\tilde{H}	column matrix defined by eq. (34)
J	Jacobian matrix, eq. (30)

LIST OF SYMBOLS (Continued)

K	constant defined by eq. (14)
$\Delta \vec{l}$	vector length of elemental magnetic flux tube
M	local Mach number, $ \vec{V} /a$
M_A	local Alfvén Mach number, $ \vec{V} /A$
p	pressure
q	magnitude of velocity vector, eq. (36)
Q	dummy parameter
r	spherical radial distance
R	cylindrical radial distance
\bar{R}	gas constant, 8.315×10^7 ergs/gm°K
R_i	spherical radius of ionopause, eq. (25)
R_m	spherical radius of magnetopause, eqs. (16-18)
R_O	spherical distance from center of planet to ionopause nose
S	entropy
ΔS	incremental distance along streamline
T	time
(u,v,w)	velocity components associated with the (X,R, ω) coordinate directions, respectively
U	column matrix defined by eq. (29)
\hat{U}	column matrix associated with IMP code, equal to U/J
\tilde{U}	column matrix defined by eq. (34)
\vec{V}	velocity vector
x	axial distance from center of planet measured positive upstream
X	axial distance from center of planet measured positive downstream
θ	spherical polar angle, measured with respect to planet center, from subsolar point with respect to undisturbed solar wind direction; varies from 0 in upstream direction to π in downstream direction; eq. (25)
γ	ratio of specific heats

LIST OF SYMBOLS (Continued)

δ_s	local angle of bow shock wave
$(\delta_\xi, \delta_\eta)$	second-order difference operators in (ξ, η) direction
η	transformation variable; eqs. (27), (37)
θ	polar angle measured with respect to north geomagnetic pole, eq. (15)
Λ	quantity defined by eq. (26)
μ	nondimensionalized mean molecular mass, equal to 1/2 for ionized atomic hydrogen
ξ	transformation variable, eqs. (27), (37)
ρ	density
τ	transformed time, eq. (27)
ϕ	geomagnetic longitude, eq. (16)
ψ	angle between outward normal to magneto/ionosphere boundary and oncoming undisturbed solar wind, eq. (12)
ω	azimuthal angle in axis-normal plane, eq. (33)

Subscripts

n	normal direction
P	arbitrary point on streamline
R	reference quantity
t	tangential direction
o	reference quantity at subsolar point
1	conditions upstream of a discontinuity
2	conditions downstream of a discontinuity
∞	upstream undisturbed quantity
(\parallel, \perp, n)	parallel, perpendicular, and normal magnetic field components as defined in eq. (42)

BLANK PAGE

ANALYSIS

General Considerations

An overall description of solar wind flow past terrestrial planets, including an account of the principal features of the interplanetary solar wind and a description of the physical basis of the continuum fluid model are provided in references 3 and 6. Although details of those accounts won't be repeated here, several specific points relevant to the present work will be reviewed.

The fundamental assumption underlying the theoretical analysis of large-scale features of the interaction of the solar wind with terrestrial planets is that the average bulk properties of the flow can be described adequately by the continuum equations of magnetohydrodynamics for a single-component, perfect, dissipationless (perfect electrically conducting, inviscid, nonheat-conducting) gas. Theoretical justification of this point has not yet been established, and proof remains essentially qualitative at present. The primary justification for use of the continuum fluid model is the outstanding agreement of the qualitative results predicted on this basis with those actually measured in space. It appears that the continuum model is capable of accounting both for many of the details as well as the broad features of the observations.

The primary emphasis on development of the continuum model has been on steady flow past the Earth (refs. 3, 4), a planet with a strong magnetic field. Initial applications to nonmagnetic planets have also been made (ref. 5). These particular applications are the ones toward which this study is directed.

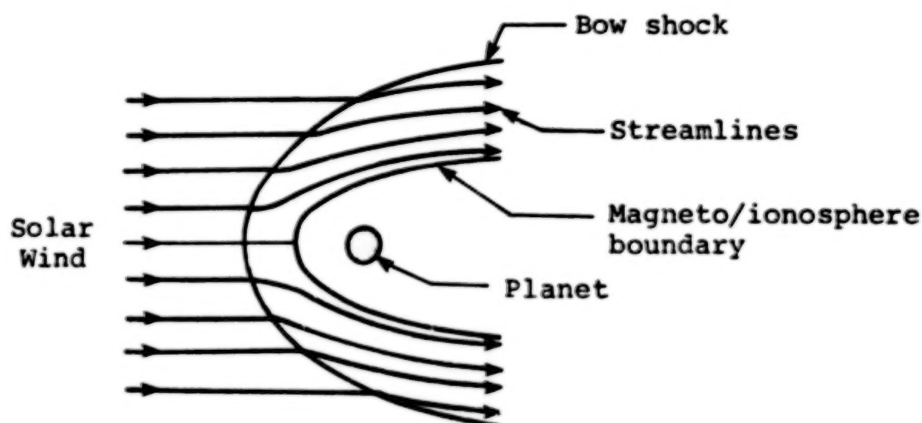
The following subsection provides the mathematical basis of the interaction of the solar wind with planetary magneto/ionospheres. The governing differential equations as well as relations for discontinuities present in the flow are discussed. The next two subsections provide the determination of the magnetosphere and ionosphere boundary shapes. The following two subsections discuss the calculation of the gasdynamic and magnetic field properties.

Mathematical Representation of Solar Wind-Magneto/Ionosphere Interaction

The differential equations governing the motion of the solar wind are the magnetohydrodynamic equations for steady flow of a dissipationless perfect gas and can be written as follows

$$\left. \begin{aligned} \vec{\nabla} \cdot \rho \vec{V} &= 0 \\ \rho (\vec{V} \cdot \vec{\nabla}) \vec{V} + \vec{\nabla} p &= -(1/4\pi) \vec{B} \times \text{Curl } \vec{B} \\ \text{Curl} (\vec{B} \times \vec{V}) &= 0 \\ \text{div } \vec{B} &= 0 \\ (\vec{V} \cdot \vec{\nabla}) S &= 0 \\ S - S_0 &= C_v \ln \frac{p/p_0}{(\rho/\rho_0)^\gamma} \end{aligned} \right\} \quad (1)$$

and apply in the region exterior to the magneto/ionosphere boundary, as shown in the sketch below.



In these equations, ρ , p , S , and \vec{V} refer to the density, pressure, entropy, and velocity of the gas, \vec{B} denotes the magnetic field, and $\gamma = C_p/C_v$ is the ratio of specific heats, equal to 5/3 for a monatomic gas. The temperature T is related to the pressure and density by the equation of state for a perfect gas

$$p = \rho \bar{R} T / \mu \quad (2)$$

in which $\bar{R} = (C_p - C_v)\mu = 8.315 \times 10^7$ ergs/gm $^\circ$ K is the universal gas constant, and μ is the mean molecular mass nondimensionalized so that $\mu = 16$ for atomic oxygen. For fully ionized hydrogen, μ is thus 1/2. The magnetic field B is expressed in terms of gaussian units.

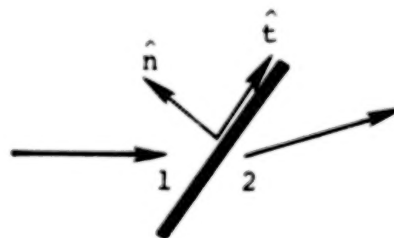
We note that it is fully equivalent and convenient for some purposes to replace the entropy equation $(V \cdot \nabla)S = 0$ in equation (1) by the following energy equation:

$$\text{div}[\rho V (\frac{1}{2} V^2 + h) + VB^2/4\pi - (B \cdot V)B/4\pi] = 0 \quad (3)$$

Because of the omission of dissipative terms in equation (1), surfaces of discontinuity, such as the bow shock and the magneto/ionosphere boundary indicated in the sketch above, may develop in the flow. Across these surfaces, continuous solutions of the dissipationless differential equations cease to exist. The flow is no longer governed solely by the differential equations (1), but must be supplemented by additional considerations. Mass, momentum, magnetic flux, and energy must be conserved across these surfaces, and these conditions lead to the following relations which relate quantities on the two sides of any such discontinuity:

$$\left. \begin{aligned} [\rho V_n] &= 0 \\ [\rho V_n V + (p + B^2/8\pi)\hat{n} - B_n B_t/4\pi] &= 0 \\ [B_{nt} - B_t V_n] &= 0 \\ [B_n] &= 0 \\ [\rho V_n (h + V^2/2) + V_n B^2/4\pi - (B \cdot V)B_n/4\pi] &= 0 \end{aligned} \right\} \quad (4)$$

Here, (\hat{n}, \hat{t}) denote unit vectors normal and tangential to the discontinuity surface, as sketched below,



and the subscripts (n, t) refer to vector components in the normal and tangential directions. The square brackets denote the difference between the enclosed quantities on the two sides of the discontinuity as in $[Q] = Q_2 - Q_1$ where subscripts (1, 2) denote conditions on the upstream and downstream sides of the discontinuity. The symbol h in the energy equation represents the enthalpy, which is related to the internal energy

$$e = c_v T \quad (5)$$

according to

$$h = C_p T = C_v T + p/\rho \quad (6)$$

Of the five classes of discontinuities possible (refs. 2-6), two of these, the fast shock wave and the tangential discontinuity, are of concern in the present applications. The first relates conditions on the two sides of the bow shock wave, and any other shock waves present. The latter has properties compatible both with those required to describe a boundary surface (magnetopause) that separates the geomagnetic field and the external flow in the case of a magnetic planet, and also to relate conditions on the two sides of an ionopause in an application to a non-magnetic planet with atmosphere. More detailed consideration of the tangential discontinuity condition leads to a determination of the magneto/ionopause shapes, as described in the following sections.

Two important parameters which characterize the solar wind flow at any point as described by equations (1) are the Mach number $M = V/a$ and the Alfvén Mach number $M_A = V/A$. The former is the ratio of the flow velocity to the speed of sound $a = (\gamma p/\rho)^{1/2}$, while the latter is the ratio of the flow velocity to the speed $A = (B^2/4\pi\rho)^{1/2}$ of a rotational or Alfvén wave propagating along the direction of the magnetic field.

For typical solar wind conditions (refs. 2-6), both the oncoming Mach number and the Alfvén Mach number are high ($M_\infty \sim M_{Ax} \sim 0(10)$). In this case, an important simplification of the magnetohydrodynamic equations occurs. The magnetic terms in equations (1), (3), and (4) decouple from the gasdynamic portion of those equations, with the result that the fluid motion can be determined by solving the equations of gasdynamics, while the magnetic field \underline{B} can be determined subsequently by solving the

remaining equations using the values for \underline{V} already determined. The magnetic field, determined in this fashion, is usually interpreted as being "frozen in" or moving with the fluid (ref. 3).

This results in the following differential and conservation equations; for the flow field

$$\left. \begin{aligned} \underline{\nabla} \cdot \rho \underline{V} &= 0 \\ \rho (\underline{V} \cdot \underline{\nabla}) \underline{V} + \underline{\nabla} p &= 0 \\ \text{div} \left(\rho \underline{V} \left(\frac{1}{2} V^2 + h \right) \right) &= 0 \\ [\rho V_n] &= 0 \\ [\rho V_n V + p] &= 0 \\ [\rho V_n \left(\frac{1}{2} V^2 + h \right)] &= 0 \end{aligned} \right\} \quad (7)$$

and for the magnetic field

$$\left. \begin{aligned} \text{Curl}(\underline{B} \times \underline{V}) &= 0 \\ \text{div } \underline{B} &= 0 \\ [\underline{B}_n \underline{V}_t - \underline{B}_t \underline{V}_n] &= 0 \\ [\underline{B}_n] &= 0 \end{aligned} \right\} \quad (8)$$

Equations (7) and (8) provide the governing equations which form the basis of the mathematical representation of the solar wind-magneto/ionosphere interaction problem considered here.

Magnetic Planet - Determination of the Magnetosphere Boundary

Determination of the magnetosphere boundary formed by the interaction of the solar wind and a planetary magnetic field, simultaneously accounting for the distortion of the geomagnetic field contained therein, results in a free-boundary problem of sufficient complexity that even approximate solutions were not obtained until recently. The various approximations introduced for applications to the Earth are summarized here. More detailed descriptions are provided in references 3, 6, and 9.

The basis for important simplifying approximations to the governing tangential discontinuity conditions

$$\begin{aligned} V_n = B_n = [p + B^2/8\pi] &= 0 \\ [V_t] \neq 0; [B_t] \neq 0; [\rho] \neq 0 \end{aligned} \quad (9)$$

which apply at the Earth's magnetosphere boundary are that the gas pressure p is much less than the magnetic pressure $B^2/8\pi$ in the confined region interior to the magnetopause, and that p is much greater than $B^2/8\pi$ in the exterior flow region around the forward part of the magnetopause. Consequently, the boundary condition to be satisfied by the exterior flow at the magnetopause can be satisfactorily approximated by the limiting case of the tangential discontinuity conditions in equation (9) in which there is a vacuum ($p = \rho = 0$) on one side, and no magnetic field on the other. Thus, the condition $[p + B^2/8\pi] = 0$ becomes

$$(B^2/8\pi)_{\text{mag}} = (p)_{\text{flow}} \quad (10)$$

while the equations governing the magnetic field interior to the magnetopause are

$$\text{div } \underline{B} = 0, \text{Curl } \underline{B} = 0 \quad (11)$$

Furthermore, it has been shown (refs. 3, 6) that the gas pressure of the flow on the forward portion of the magnetosphere boundary - $(p)_{\text{flow}}$ in equation (10) - can be approximated adequately by the Newtonian formula

$$p = p_{\text{st}} \cos^2 \psi \quad (12)$$

Here, ψ is the angle between the outward normal to the magnetosphere boundary and the flow direction of the oncoming undisturbed solar wind, and p_{st} is the stagnation or ram pressure exerted on the nose of the magnetosphere and is given by

$$p_{\text{st}} = K \rho_{\infty} V_{\infty}^2 \quad (13)$$

In this relation, K is a constant usually taken as one, but whose actual value is

$$K = \frac{1}{\gamma} \left[\frac{(\gamma + 1)(\gamma + 1)}{\gamma - (\gamma - 1)/2M_{\infty}^2} \right]^{\frac{1}{\gamma - 1}} \quad (14)$$

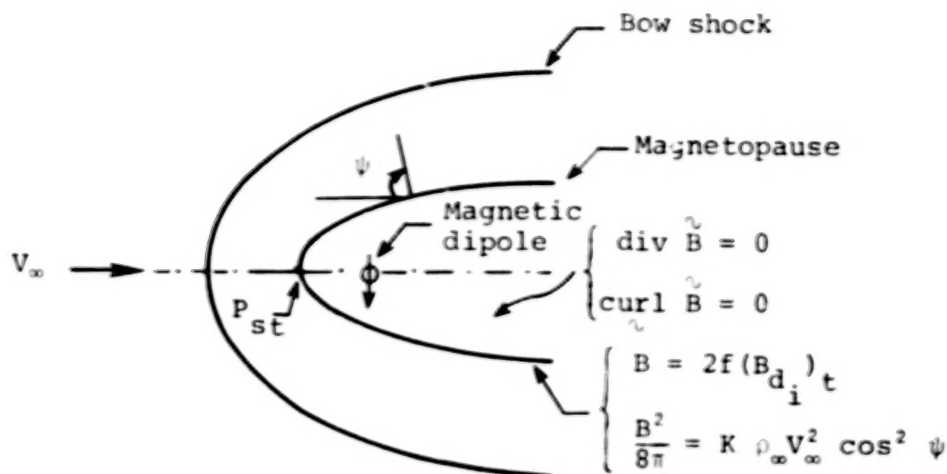
For the high Mach number flows typical of solar wind conditions, K approaches 0.844 for $\gamma = 2$ and 0.881 for $\gamma = 5/3$. The important implication associated with the introduction of the Newtonian approximation is that the calculation of the shape of the magnetosphere boundary decouples from the calculation of the external flow.

Implementation of the above analysis requires a representation of the Earth's magnetic field. This is provided with sufficient accuracy for the present application by a magnetic dipole located at the center of the Earth and given by

$$\vec{B} = -B_{eq} (a_e/r)^3 (\sin \theta \hat{e}_\theta + 2 \cos \theta \hat{e}_r) \quad (15)$$

where $B_{eq} = 0.312$ gauss is the strength of the field at the geomagnetic equator, $a_e = 6.37 \times 10^8$ cm is the radius of the Earth, r is the geocentric distance, and θ is the polar angle measured with respect to the north geomagnetic pole which is at 78.6° north latitude and 70.1° west longitude. The problem for determining the magnetopause and the distortion of the confined geomagnetic field is then reduced to finding a solution of equations (11) which has the dipole singularity equation (15) at the origin, and which satisfies the tangential discontinuity conditions $B_n = 0$ and $B^2/8\pi = K \rho_\infty V_\infty^2 \cos^2 \psi$ at the unknown location of the magnetopause. This problem is identical to the classical steady-state Chapman-Ferraro problem (ref. 10) specified over four decades ago, and based on particle rather than continuum concepts. Even at this stage, however, the problem still remains sufficiently complex that only a few numerical solutions have been carried out (refs. 11-13) at the present time. An early approximation which has proven quite successful in providing accurate magnetopause shapes (refs. 9, 12, 14) is to replace the $B_n = 0$ condition with the condition that the magnetic-field intensity at the magnetosphere boundary is equal to $2f$ times the tangential component of the Earth's dipole field, where f is a constant usually taken as unity (refs. 15-17).

The final mathematical statement for the free-boundary problem for the shape of the magnetosphere boundary, then, is summarized in the sketch below:



This formulation leads to the following partial differential equation for the geocentric distance r to the magnetopause for the case in which the dipole axis is perpendicular to the solar-wind flow (ref. 18)

$$\left[\frac{1 + 3 \cos^2 \theta}{R_m^3} \left(\frac{1}{R_m \sin \theta} \frac{\partial R_m}{\partial \phi} \right)^2 + \frac{1}{R_m^3} \left(\sin \theta + \frac{2 \cos \theta}{R} \frac{\partial R_m}{\partial \phi} \right)^2 \right] = \left[\sin \phi \sin \theta - \frac{\sin \phi \cos \theta}{R_m} \frac{\partial R_m}{\partial \theta} - \frac{\cos \phi}{R_m \sin \theta} \frac{\partial R_m}{\partial \phi} \right]^2 \quad (16)$$

where $R_m = r/D$, $D = a_e (f^2 B_{eq}^2 / 2\pi K \rho_\infty V_\infty^2)^{1/6}$ is the geocentric distance to the magnetosphere nose, ϕ is the geomagnetic longitude measured with respect to a line through the origin that is normal to both the dipole axis and the free-stream direction, and is equal to $\pi/2$ when directed in the upstream direction, and $3\pi/2$ when directed downstream.

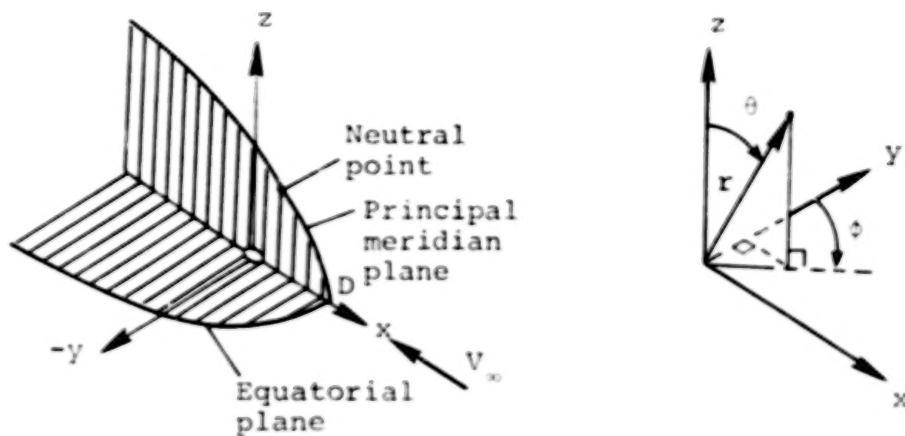
A considerable simplification occurs if attention is confined to either the geomagnetic equatorial plane or the principal meridian plane defined by the dipole axis and the direction of the incident solar wind. These equations are; in the equatorial plane ($\theta = \pi/2$, $\partial R_m / \partial \theta = 0$)

$$\frac{dR_m}{d\phi} = R_m \left(\frac{R_m^6 \sin \phi \cos \phi + \sqrt{R_m^6 - 1}}{R_m^6 \cos^2 \phi - 1} \right) \quad \pi/2 \leq \phi \leq \frac{3\pi}{2} \quad (17)$$

and in the principal meridian plane ($\phi = \pm \pi/2$, $\frac{\partial R}{\partial \phi} = 0$)

$$\frac{dR_m}{d\theta} = (R_m \tan \theta) \frac{R_m^3 \mp 1}{R_m^3 \pm 2} \quad -\pi/2 \leq \theta \leq \frac{\pi}{2} \quad (18)$$

A sketch of the traces of the magnetosphere boundary in the equatorial and principal meridian planes is provided below together with the spherical (r, θ, ϕ) coordinate system. We note in particular that the



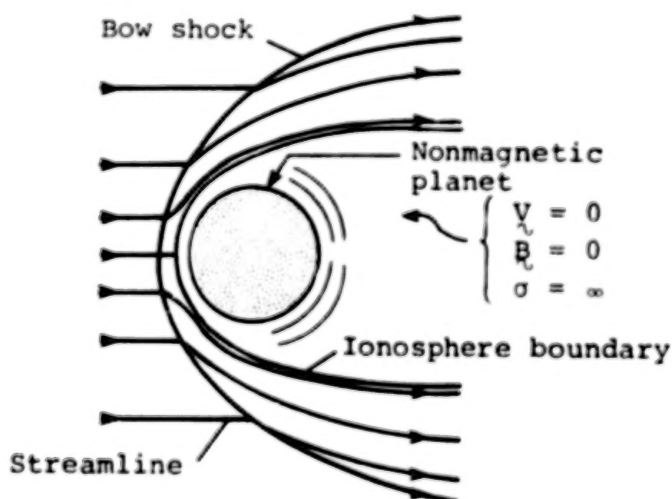
shape of the equatorial trace is a smooth curve, while that of the principal meridian contains a pronounced dent at the location of the neutral point where the magnetic field vanishes in the ideal theory. In all of the reported work to date (refs. 1-4, 6, 8) concerning flow fields past the magnetosphere, the magnetopause has been approximated by an axisymmetric shape obtained by rotating the equatorial trace of the boundary about the longitudinal axis. That this provides a very good approximation to the actual three-dimensional shape is shown in figure 1 which displays in more detail the comparison of the equatorial and principal meridian traces of the magnetopause as calculated by equations (17) and (18), respectively. Also shown on the principal meridian trace is a dashed line which forms a tangent surface across the cusped neutral point region, and which represents the free-streamline surface which will

most likely appear in nature (ref. 19). We note that all three of these shapes are quite close to one another so that the rotated equatorial trace provides a satisfactory approximation to the three-dimensional shape. Furthermore, it has been shown (ref. 3, 13) that higher-order approximations to the Chapman-Ferraro problem for the magnetosphere shape are in reasonable agreement with the approximate shape given by the solution to equation (16).

Consequently, the boundary shape of the magnetosphere for which the majority of results are presented here is the rotated equatorial trace given by equation (17). That shape has been incorporated in the associated computer codes developed herein as the default shape for magnetosphere calculations. Tabulated ordinates (Y_m/D - vs. $-x/D$) for the equatorial trace are provided in Table 1 where Y_m is the cylindrical radial coordinate of the profile.

Nonmagnetic Planet - Determination of the Ionosphere Boundary

The determination of the ionosphere boundary initiates from the assumptions that the ionosphere, or at least the outer part of it that participates in the interaction with the solar wind, is idealized as a spherically symmetric and hydrostatically supported plasma having infinite electrical conductivity, effectively bound to the planet and incapable of mixing with the solar wind, as indicated in the sketch below:



This interior plasma is separated from the flowing solar plasma by a tangential discontinuity across which the same relations, given previously by equations (9) for the analogous problem for a magnetic planet, must hold. The assumption of hydrostatic support implies a quiescent ionosphere in which the bulk motions of the gas with respect to the planet are sufficiently small ($V = 0$) that equilibrium exists between the pressure gradient and gravity, viz.

$$\frac{dp}{dr} = -\rho g \quad (19)$$

where p and ρ are the gas pressure and density, r is the radial distance measured from the center of the planet, and g is the acceleration due to gravity. The variation of g is inversely proportional to r^2 , so that $g = g_s (r_s/r)^2$ where the subscript s denotes values at the surface of the planet. Since the density ρ is related to the pressure according to the perfect gas law equation (2), equation (19) can be integrated to yield

$$p = p_R \exp \left(- \int_{R_R}^r \frac{dr}{H} \right) \quad (20)$$

where p_R is the pressure at some reference radius R_R and H is the local scale height of the atmosphere given by $H = RT/g$. If H is regarded as constant; that is, if variations of g and T with r are neglected, equation (20) can be integrated directly to yield

$$p = p_R \exp \left(- \frac{r - R_R}{H} \right) \quad (21)$$

In view of uncertainties associated with measurements of the atmospheric properties of Venus and Mars, the variation of p with r as given by equation (21) was adopted in previous solar wind/ionosphere applications (ref. 5) and has also been used herein.

In the present application, it is also evident that the gas pressure p is much larger than the magnetic pressure $B^2/8\pi$ on both sides of the ionopause. Therefore, the discontinuity pressure balance relation $[p + B^2/8\pi] = 0$ of equation (9) reduces to a simple equality between the ionospheric pressure given by equation (21) and the static pressure of the flowing solar plasma adjacent to the ionopause. Introducing as in the magnetosphere application the Newtonian approximation equation (12) for

the static pressure of the flowing plasma on the exterior boundary of the ionosphere, we arrive at the following equation for the pressure balance at the ionopause R_i :

$$p_{st} \cos^2 \psi = K \rho_{\infty} V_{\infty}^2 \cos^2 \psi = p_R \exp \left(- \frac{R_i - R_O}{H} \right) \quad (22)$$

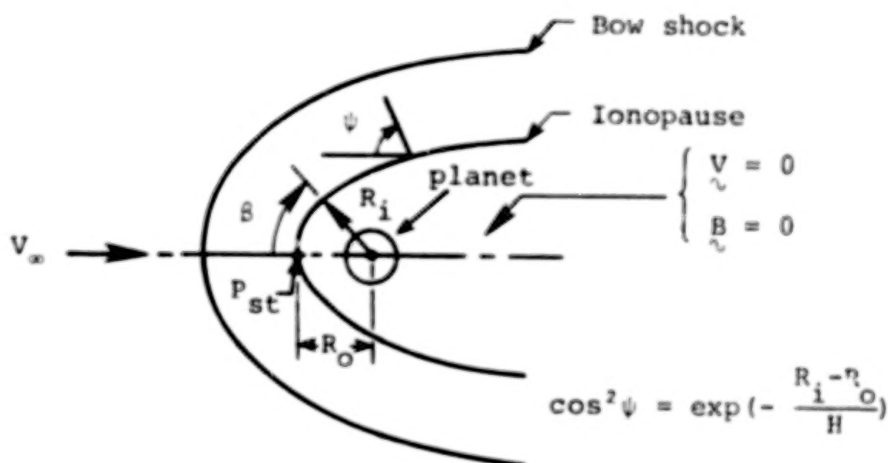
It is convenient to choose as the reference radius and location the stagnation point on the ionopause; that is, $R_R = R_O$ where R_O is the distance from the center of the planet to the nose of the ionopause. This implies that

$$p_R = p_O = K \rho_{\infty} V_{\infty}^2 \quad (23)$$

and that at all points along the ionosphere boundary

$$\cos^2 \psi = \exp \left(- \frac{R_i - R_O}{H} \right) \quad (24)$$

The final mathematical statement of the free-boundary problem for determining the shape of the ionosphere boundary then is summarized in the sketch below:



By relating the local angle ψ to the slope of the ionopause, the following ordinary differential equation results for the ordinates of the ionosphere boundary

$$\frac{dR_i}{d\theta} = R_i \left[\frac{\sin 2\theta - 2\sqrt{\Lambda - \Lambda^2}}{2(\Lambda - \sin^2 \theta)} \right] \quad 0 \leq \theta \leq \pi \quad (25)$$

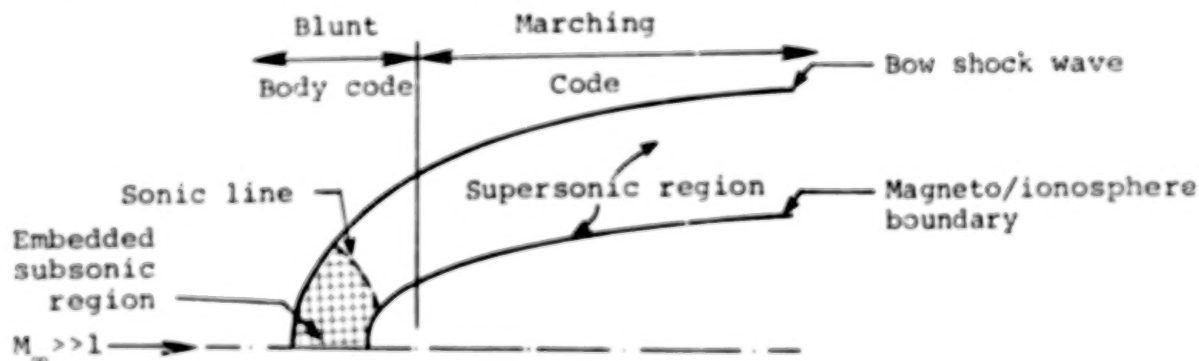
where

$$\Lambda = \exp[-(R_i - R_o)/H] \quad (26)$$

and θ is the angle measured from the subsolar point as indicated above. Results for various ionopause shapes obtained by integrating equation (25) for different values H/R_o in the range $0.001 \leq H/R_o \leq 1.0$ are provided in figure 2. We note that the range of interest for planetary applications to Venus and Mars appears to be $0.01 \leq H/R_o \leq 0.30$ (ref. 5). Tabulated ordinates (Y_i/R_o - vs. $-X/R_o$) are provided in Table 1 for $H/R_o = 0.01, 0.1, 0.2$, and 0.5 , where $Y_i = R_i \sin \theta$ is the cylindrical radial coordinate of the ionopause profile.

Calculation of the Gasdynamic Flow Properties

Computation of the gasdynamic flow properties consists of determining solutions to the differential equations and discontinuity conservation equations given by equations (7). Because both the downstream tail region (far field) as well as the region in the vicinity of the obstacle nose (near field) are generally of interest in solar wind-magneto/ionopause interactions, the computational methods selected must be capable of determining this entire flow field. In view of the need to carry the flow calculation to an arbitrary downstream distance, the most computationally efficient procedure to employ is to subdivide the flow field into two regions, as indicated in the sketch below:



Illustrated here are the essential features of the high supersonic Mach number flow typical of solar wind flows past terrestrial planets. Of special note is the embedded subsonic pocket, located at the nose of the magneto/ionopause. The presence of this pocket necessitates use of a computational technique capable of treating a mixed subsonic/supersonic flow. Downstream of this region, the flow becomes supersonic and remains so for the convex shapes typical of magneto/ionopause boundaries. In that far field region, a more economical procedure than that used near the nose can be employed.

We note that this subdivision of flow field and use of different solution procedures in each region is common practice for calculating hypersonic blunt-body flows, and was employed in the former solar wind method (ref. 3) as well as in a more recent application to space shuttle re-entry flows (ref. 20). Indicated in figure 3 is a comparison of the former and present computational procedures which illustrates the breakdown of the various solution domains. The previous method treated the nose region by the inverse iteration method, and the remainder of the flow field by the method of characteristics. In light of recent advances, both of those techniques, particularly the inverse method, are now considered dated and inferior to more current methods. In the present study, those two methods have been superseded by: (1) a new axisymmetric implicit unsteady Euler equation solver (IMP) specifically developed under this contract (ref. 21) and which determines the steady state solution in the nose region by a time-marching procedure, and (2) a shock-capturing marching solution (SCT) which spatially advances the solution downstream as far as required by solving the steady Euler equations. As indicated in figure 3, the implicit unsteady Euler equation (IMP) code is used to determine the flow in the region between the stagnation streamline on the symmetry axis and a body-axis normal plane ($x = \text{constant}$) conveniently chosen at the $\beta = 90^\circ$ ($x = 0$) location. For the magneto/ionopause shapes considered here, purely supersonic flow exists on this plane and the conditions there provide the starting data for the SCT code. The SCT code then marches the solution downstream in axis normal planes to the final specified location.

Obstacle nose solution - implicit unsteady Euler equation (IMP) code.-

The partial differential equations employed in the implicit (IMP) code are the unsteady axisymmetric versions of the gasdynamic Euler equations given

by equations (7). To implement the calculation, those equations are written in conservation-law form under the generalized independent variable transformation

$$\left. \begin{aligned} \tau &= T \\ \xi &= \xi(T, X, R) \\ \eta &= \eta(T, X, R) \end{aligned} \right\} \quad (27)$$

as follows:

$$\begin{aligned} (U/J)_{\tau} + [(\xi_T U + \xi_X E + \xi_R F)/J]_{\xi} \\ + [(\eta_T U + \eta_X E + \eta_R F)/J]_{\eta} + G = 0 \end{aligned} \quad (28)$$

where

$$\begin{aligned} U &= \begin{pmatrix} \rho \\ \rho u \\ \rho v \\ e \end{pmatrix} & E &= \begin{pmatrix} \rho u \\ p + \rho u \\ \rho uv \\ (e + p)u \end{pmatrix} \\ F &= \begin{pmatrix} \rho v \\ \rho uv \\ p + \rho v^2 \\ (e + p)v \end{pmatrix} & G &= \frac{1}{RJ} \begin{pmatrix} \rho v \\ \rho uv \\ \rho v^2 \\ (e + p)v \end{pmatrix} \end{aligned} \quad (29)$$

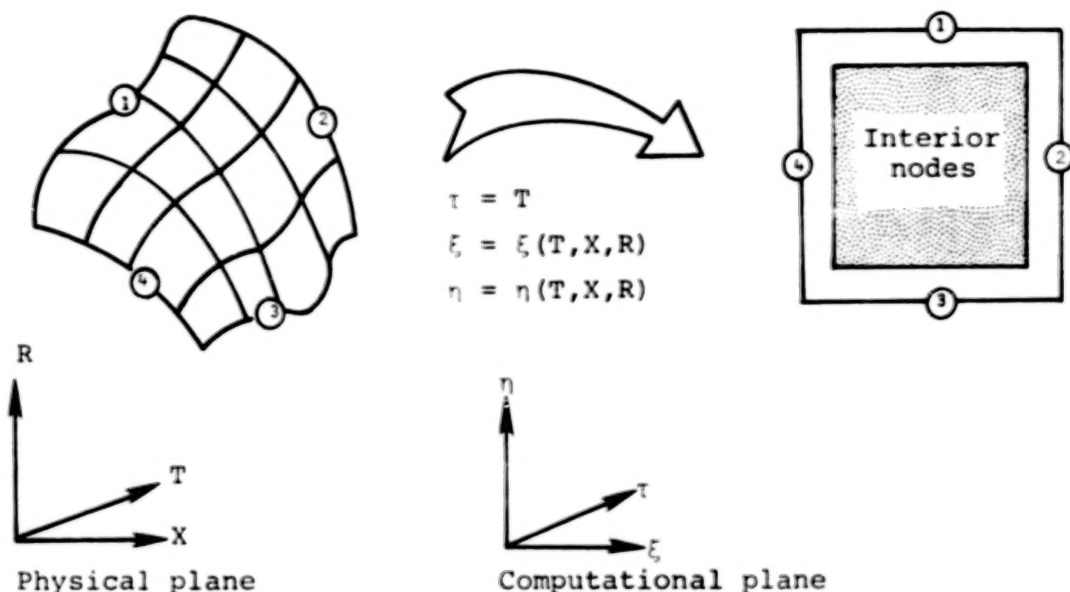
and the Jacobian

$$J = \xi_X \eta_R - \xi_R \eta_X \quad (30)$$

In equations (27) to (30), T denotes time, X is the axial downstream direction, and R is the cylindrical radial distance; p represents the pressure; ρ the density; u and v the velocity components in the X and R directions, respectively; and e the total energy per unit volume. The following equation relates the pressure, density, and velocity components to the energy for an ideal gas

$$e = p/(\gamma - 1) + \rho(u^2 + v^2)/2 \quad (31)$$

Using the independent variable transformation equation (27), the physical plane with boundaries 1-4 in X, Y, T space is mapped into the rectangular computational plane ξ, η , and τ space as shown in the sketch below. Generally, at each time step the transformation metrics are not known beforehand and must be determined numerically. Integration step size is established by using the eigenvalues of the Jacobian matrices \bar{A} and \bar{B} , where $\bar{A} = \partial \hat{E} / \partial \hat{U}$, $\bar{B} = \partial \hat{F} / \partial \hat{U}$ and $\hat{U} = U/J$, $\hat{E} = (\xi_T U + \xi_X E + \xi_R F)/J$, and $\hat{F} = (\eta_T U + \eta_X E + \eta_R F)/J$.



The boundaries, as indicated in the sketch, at which appropriate conditions are imposed on the present problem consist of: (1) the bow shock surface at which the Rankine-Hugoniot relations are satisfied, (2) the downstream outflow boundary where the flow is assumed to be entirely supersonic, (3) the obstacle surface at which a no flow condition in the normal direction is imposed, and (4) the stagnation streamline where symmetry conditions are implemented. Initial flow field conditions are determined by guessing a bow shock shape for the particular blunt obstacle at hand and by prescribing a Newtonian pressure distribution on the body. Since the maximum entropy streamline wets the body, that fact plus the known surface flow direction serve to determine the remainder of the flow properties on the obstacle surface. A linear variation for the flow properties between the bow shock and the obstacle is then prescribed.

This provides the initial flow field which is then integrated in a time-asymptotic fashion until the steady-state solution is obtained.

The basic numerical algorithm used in the IMP code was developed by Beam and Warming (ref. 22) and is second-order accurate, noniterative, and spatially factored. In particular, the "delta form" with Euler time differencing is employed. When applied to equation (28) the algorithm assumes the form

$$(I + \Delta\tau\delta_{\xi}\bar{A}^n)(I + \Delta\tau\delta_{\eta}\bar{B}^n)(\hat{U}^{n+1} - \hat{U}^n) = -\Delta\tau(\delta_{\xi}E^n + \delta_{\eta}F^n + G) \quad (32)$$

where \bar{A} and \bar{B} are the Jacobian matrices, I is the identity matrix, δ_{ξ} and δ_{η} are second-order, central difference operators, $U^{n+1} = U(n\Delta\tau)$ and $\Delta\tau$ is the integration step size.

Equation (32) is solved at the interior points only. It requires two 4×4 block tridiagonal inversions at each time step of the integration. The solution procedure is as follows:

1. Define $\Delta\hat{U} = U^{n+1} - \hat{U}^n$.
2. Form the right-hand side of equation (32) and store results in the \hat{U}^{n+1} array.
3. Define $\bar{U} = (I + \Delta\tau\delta_{\eta}\bar{B}^n)\Delta\hat{U}$ and solve the matrix equation $(I + \Delta\tau\delta_{\xi}\bar{A}^n)\bar{U} = \hat{U}^{n+1}$ for \bar{U} storing the result in the \hat{U}^{n+1} array.
4. Solve the matrix equation $(I + \Delta\tau\delta_{\eta}\bar{B}^n)\Delta\hat{U} = \hat{U}^{n+1}$ for $\Delta\hat{U}$.
5. Obtain the values of \hat{U}^{n+1} from the relation $\hat{U}^{n+1} = \Delta\hat{U} + \hat{U}^n$.
6. Obtain the final solution after applying the smoothing; $\hat{U}^{n+1} = \hat{U}^{n+1} - (\epsilon/8)S/J$.

A fourth-order smoothing term S is usually required to eliminate nonlinear instabilities which may arise since the use of central differences in the spatial directions results in a neutrally stable algorithm.

Downstream solution - shock capturing steady Euler equations (SCT) code. - Since the shock-capturing technique employed has been established previously (refs. 23, 24, 25) only a brief description will be provided here. The steady, full three-dimensional Euler equations are written in cylindrical coordinates in the form:

$$\frac{\partial \tilde{U}}{\partial X} + \frac{\partial \tilde{F}}{\partial R} + \frac{\partial \tilde{G}}{\partial \omega} + \tilde{H} = 0 \quad (33)$$

where

$$\left. \begin{aligned} \tilde{U} &= \begin{pmatrix} \rho u \\ p + \rho u^2 \\ \rho uv \\ \rho uw \end{pmatrix} & \tilde{G} &= \frac{1}{R} \begin{pmatrix} \rho w \\ \rho uw \\ \rho vw \\ p + \rho w^2 \end{pmatrix} \\ \tilde{F} &= \begin{pmatrix} \rho v \\ \rho uv \\ p + \rho v^2 \\ \rho vw \end{pmatrix} & \tilde{H} &= \frac{1}{R} \begin{pmatrix} \rho v \\ \rho uv \\ \rho(v^2 - w^2) \\ 2\rho vw \end{pmatrix} \end{aligned} \right\} \quad (34)$$

Here p and ρ represent dimensional pressure and density and (u, v, w) denote velocity components in the cylindrical coordinate directions (X, R, ω) , respectively, where X is the axial downstream direction, R is the cylindrical radius in an axis-normal plane, and ω is the azimuthal angle measured in the axis-normal plane. This set of equations is closed by the use of energy conservation as provided by the equation for total enthalpy

$$H_t = h(p, \rho) + \frac{q^2}{2} = \text{constant} \quad (35)$$

where

$$q = \sqrt{u^2 + v^2 + w^2} \quad (36)$$

is the magnitude of the velocity vector and $h(p, \rho)$ is the caloric equation of state.

The equations are then transformed to a computational plane by using the independent variable transformation

$$X = X$$

$$\xi(X, R, \omega) = \frac{(R - R_b)}{(R_s - R_b)} \quad (37)$$

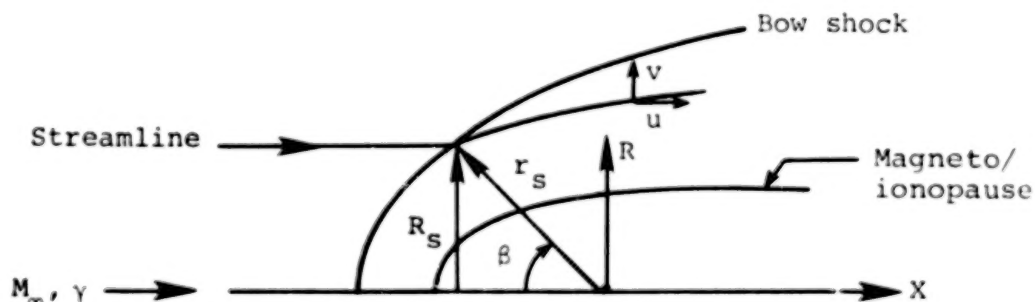
$$\xi(\omega) = f(\omega)$$

where the subscripts (b,s) denote body and shock surfaces, respectively. This change of variable is employed in equation (33) and the result then rearranged into the following conservation law form (refs. 23,24,25).

$$\frac{\partial U}{\partial X} + \frac{\partial F}{\partial \xi} + \frac{\partial G}{\partial \eta} + H = 0 \quad (38)$$

The finite-difference formulation of MacCormack (ref. 26) is used to integrate equation (38) with respect to the hyperbolic coordinate X to yield values of the conservative variable U . This procedure is calculable as long as the flow velocity in the axial (X) direction is greater than the local speed of sound. We note that for the axisymmetric obstacle shapes considered here, $\partial/\partial\omega = 0$; however, the version of the SCT code employed has the capability for treating full three-dimensional geometries.

Streamline and contour calculations.- A number of special purpose subroutines were written to calculate streamlines and contour maps of various flow field properties, and also to provide automated plots of these quantities. The streamlines are determined by integrating trajectories through the known velocity field as this procedure was found to be more accurate than a mass flow calculation. The calculation of a particular streamline is initiated at the point where the streamline crosses the bow shock, as shown below:



At that point, exact values of the streamline slope dR_s/dX are known in terms of the local shock angle δ_s and free-stream quantities according to the relation

$$\frac{dR_s}{dX} = \frac{2 \cdot \cot \delta_s \cdot (M_\infty^2 \sin^2 \delta_s - 1)}{2 + M_\infty^2 (\gamma + 1 - 2 \sin^2 \delta_s)} \quad (39)$$

which is implicit in the blunt-body (IMP) and marching (SCT) code solutions. At other points in the flow field, the local streamline slope is given by the ratio of radial to downstream velocity, i.e.

$$\frac{dR_s}{dX} = \frac{v}{u} \quad (40)$$

and the streamline determination is made by stepwise integration in X of equation (40) according to a modified third-order Euler predictor/corrector method. Two-dimensional linear interpolation from the flow field grid points is employed to obtain the velocity components (u,v) required at the stepwise points along the streamline trajectory. Separate streamline calculations are made for the near field (IMP results) and far field (SCT results) because of the different coordinate systems employed in those two regions.

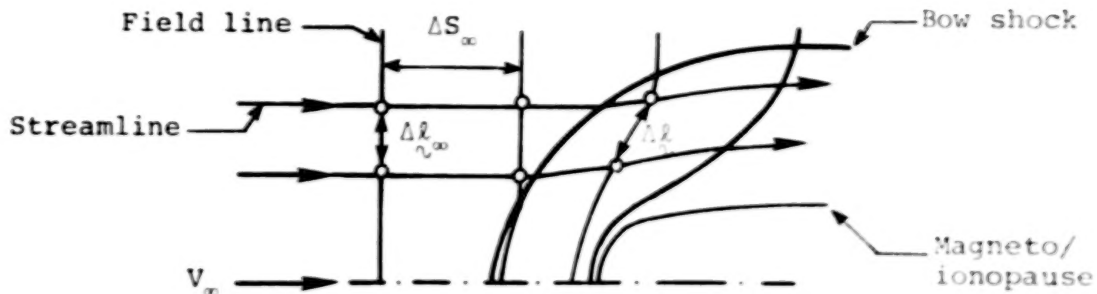
Contours of various flow field quantities are determined for the entire flow field (near field plus far field) by using a modified version of the contour package developed by R. Sorensen at NASA/Ames Research Center. Pertinent details of that package are provided in the user's manual section of this report.

Calculation of the Magnetic Field

With the flow properties known from the gasdynamic calculations, determination of the magnetic field \vec{B} proceeds by integrating equations (8). Those equations are commonly interpreted as indicating the field lines move with the fluid. This leads to a straightforward, although tedious, calculation in which the vector distance from each point on an arbitrarily selected fluid line to its corresponding point on an adjacent field line in the downstream direction is determined by numerically integrating $\int \vec{v} dt$ over a fixed time interval δt . While that calculation determines the location of the field lines, the intensity of the magnetic field at any point may then be calculated from the relation

$$\frac{|\vec{B}|}{|\vec{B}_\infty|} = \frac{c |\Delta \vec{\ell}|}{c_\infty |\Delta \vec{\ell}_\infty|} \quad (41)$$

where $\Delta \vec{\ell}$ is the vector length of a small element of a flux tube. The sketch below clarifies these quantities for the case when the oncoming \vec{B} field is perpendicular to the flow:



where the open symbol \odot denotes locations of points on the streamlines corresponding to a fixed time interval $\Delta t = \Delta S_\infty / V_\infty$.

Because of the axisymmetry of the gasdynamic quantities and the linearity of the equations for \vec{B} , Alksne and Webster (ref. 27) have shown that the magnetic field at any point in the flow field can be calculated by vectorially summing the contributions of the three component fields indicated in figure 4. At any point P, the magnetic field \vec{B}_P is given by

$$\vec{B}_P = \left(\frac{B_P}{B_\infty} \right)_\parallel \vec{B}_\infty_\parallel + \left(\frac{B_P}{B_\infty} \right)_\perp \vec{B}_\infty_\perp + e_n \left(\frac{B_P}{B_\infty} \right)_n \vec{B}_\infty_n \quad (42)$$

where the subscripts (\parallel , \perp , n) refer respectively to the contributions associated with the components of \vec{B}_∞ parallel to \vec{V}_∞ ; perpendicular to \vec{V}_∞ in the plane that contains the point P, the center of the planet, and the vector \vec{V}_∞ ; and normal to the latter plane.

For the contribution associated with the parallel component \vec{B}_∞_\parallel , it has been shown (refs. 28,29) that $(B_P)_\parallel$ is proportional to ΔV throughout the entire flow field. Consequently, this component can be calculated directly from the gasdynamic solution by the expression

$$\left(\frac{B_P}{B_\infty} \right)_\parallel = \frac{c_p V_p}{c_\infty V_\infty} \quad (43)$$

Similarly, the normal component $(B_P/B_\infty)_n$ can be shown to be equal to

$$\left(\frac{B_P}{B_\infty} \right)_n = \frac{R_P \rho_P}{R_{P_\infty} \rho_\infty} \quad (44)$$

where R_P is the radial cylindrical coordinate of the streamline, as indicated in figure 4.

The determination of the contribution $(B_P/B_\infty)_t$ cannot be made directly from the gasdynamic properties as can the other two components. For this component, recourse must be made to the general computation associated with equation (41). Details of the calculation procedure for $(B_P/B_\infty)_t$ are provided in the user's manual section of this report.

RESULTS AND DISCUSSION

In order both to verify the correctness of the procedures developed under this study as well as to demonstrate their flexibility and power for calculating solar wind flows for a variety of conditions, a large number of test cases have been run. A representative sample of the results obtained from those calculations is reported here. Because the implicit blunt-body procedure (IMP code) is new, that code was tested and compared to previously established theoretical methods to substantiate its validity prior to solar wind applications. We have prepared figure 5 to exhibit such a comparison. Here, flow field results predicted by the present implicit method are compared with those of other theoretical techniques and also experimental data for supersonic flow past a sphere with $M_\infty = 4.926$ and $\gamma = 1.4$. The variation of density and Mach number along the stagnation streamline are provided in the two plots on the left, while the variation of surface pressure and shock standoff distance with spherical angle are given in the two plots on the right. In all of these comparisons, the present theoretical results are in excellent agreement with both established theoretical methods and experiment.

Figure 6 exhibits a comparison of results predicted by the implicit method for a solar wind calculation. The upper plot of the figure displays the locations of the bow wave and sonic line for flow past the equatorial trace of the magnetopause for $M_\infty = 8$ and $\gamma = 5/3$. The density distribution along the magnetosphere boundary and along the shock wave for this flow are given in the lower plot. Included in both of these figures is the solution calculated by Spreiter et al. (ref. 3) using the inverse method of Inouye and Lomax (ref. 30). Excellent agreement is obtained between the present implicit technique and the inverse method. Figure 7 provides analogous results for the equatorial trace of the magnetopause for a variety of Mach numbers typical of solar wind flows, and illustrates the Mach number capability of the present IMP code.

With regard to solar wind flows past nonmagnetic planets, figure 8 displays results for the bow shock location for $M_\infty = 8$ and $\gamma = 5/3$ flow past various ionopause shapes with $H/R_0 = 0.01, 0.1, 0.2, 0.25, 0.50, 0.75$ and 1.0 . Not included in that figure for clarity of presentation are the results of Spreiter et al. (ref. 5) obtained by using the inverse method. Those results and the predictions of the present implicit method given in figure 8 are essentially indistinguishable.

As an illustration of the geometric flexibility of the present implicit method and also as a critical test of its ability to capture embedded shock waves besides the bow shock, a feature which the inverse method cannot duplicate, figures 9 and 10 have been prepared. This calculation corresponds to the $M_\infty = 5$ and $\gamma = 5/3$ flow around the axisymmetric shape generated by rotating the principal meridian of the magnetopause about its axis and compares with an experimental test by Spreiter et al. (ref. 3). This particular profile shape contains a pronounced dent with a concave corner in the vicinity of the neutral point. Spreiter et al. (ref. 3) have argued that the presence of a concave corner in the magnetopause is unrealistic and would not occur in nature, but should be replaced by a free surface created by drawing a tangent line across the corner. In figure 9, we present results for both the concave and the free surfaces, denoted by solid and dashed lines, respectively. For the concave surface, a pocket of embedded subsonic flow is seen to form behind the embedded shock wave which was caused by the indented profile. If the surface is modified to the free surface shape, the embedded wave disappears completely as expected. The corresponding pressure coefficients on the magnetosphere boundary are presented in figure 10. For the concave surface, the shock wave is located on the body at approximately $\theta = 80^\circ$, while for the free surface, the pressure coefficient displays a constant value as anticipated. Finally, we note that the calculation of a supersonic flow with an embedded shock and subsequent subsonic pocket provides a severe test for any blunt body procedure. The ability of the present code to provide convergent results for such a flow demonstrates the capability for further extension and application to more generalized profiles than was heretofore possible.

As a final indication of the range of solar wind flows over which the implicit code has been tested, we have prepared figure 11 which displays the variation of shock stand-off distance with oncoming Mach number and ratio of specific heats for three different magneto/ionopause shapes. These include the rotated equatorial trace of the magnetopause, and the ionopause shapes for $H/R_0 = 0.01$ and 0.5 . Those shapes and the corresponding ranges of M_∞ and γ essentially span the entire range of interest of geometry and solar wind conditions for which the computer programs developed herein would be normally applied.

In order to demonstrate the ability of the marching code to continue the blunt-body IMP solution downstream to some arbitrarily-specified

downstream location, and also to verify its stability and convergence for application to these classes of flows, we have calculated marching solutions for a variety of cases typical of solar wind interactions. Figure 12 exhibits the location of the bow wave for flows with $\gamma = 5/3$ and $M_\infty = 3, 8, \text{ and } 25$ past the rotated equatorial trace of the magnetopause as the flow proceeds downstream from the nose region to $x/D = -11$. For this calculation, starting conditions for the marching code (SCT) have been provided by the blunt-body (IMP) code on the line $x/D = 0.0$, which is the usual location at which the two solutions are joined by the computer program. The marching code then determines the remainder of the flow field back to the specified downstream location. Since for the particular shapes considered herein the downstream flows are quite smooth, the marching calculation is very efficient (less than 30 sec., CDC 7600, OPT=2 compiler). Similar results are presented in figure 13 for $M_\infty = 8$ and $\gamma = 5/3$ flow past an ionopause shape with $H/R_0 = 0.1$. Those results have been carried downstream to $x/R_0 = -20$ since this distance is more typical of the region of interest for nonmagnetic planets. This is so because of the different scalings (D, R_0) used for the magnetic and nonmagnetic applications. For Venus and Mars, the location of the ionopause nose is at a distance only slightly greater than the planetary radius, as compared with the location of the magnetopause nose for the Earth which is of the order of 10 planetary radii.

In order to illustrate the capability of the present procedures to determine streamlines, contour maps of various flow properties, and magnetic field lines and contours, as well as to demonstrate the automated plotting capability for displaying these results, figures 14 and 15 have been prepared. Figure 14 illustrates the computer generated streamline locations and contour maps of density ρ/ρ_∞ and velocity ratio V/V_∞ for the complete near and far field flow about the equatorial trace of the magnetosphere for $M = 8$ and $\gamma = 5/3$. Based on this gasdynamic solution, figure 15 exhibits the corresponding results for the magnetic field components $(B/B_\infty)_\perp$ and $(B/B_\infty)_\parallel$ in the plane of symmetry. Both magnetic field line locations and contours are provided. In addition to demonstrating the overall smoothness of the computed results, these two figures illustrate the ability of the present techniques to provide the completely automated production of report quality plots of both gasdynamic and magnetic field properties for solar wind flows past axisymmetric magneto/ionopause shapes

CONCLUDING REMARKS

Theoretical analysis and associated development of computer programs were carried out for the purpose of developing computational techniques for predicting the interaction of solar wind flows with both magnetic and nonmagnetic terrestrial planets. Based on the identical theoretical model employed in previous work, i.e. the steady, dissipationless, magnetohydrodynamic model for axisymmetric, supersonic, super-Alfvénic solar wind flow a new and more powerful solution procedure has been developed. The procedure is built upon an assemblage of computer codes, including:

- Blunt-body code - to determine gasdynamic solution near obstacle nose
- Marching code - to determine gasdynamic solution downstream of obstacle nose
- Streamline code - to determine flow field streamlines
- Contour code - to determine contour maps of flow and magnetic field properties
- Magnetic field code - to determine frozen-in magnetic field
- Plotting code - to plot selected flow and magnetic field results

Comparisons are reported which demonstrate the accuracy of the present techniques by comparison with previously-established theoretical methods as well as limited experimental data. Furthermore, new results are presented for a variety of solar wind flows which illustrate the flexibility and generality of the component methods. The computational procedures are fully automated and provide detailed flow field and magnetic field properties in convenient output format, including an automatic plot capability. The programs are documented and are presented in a general user's manual included as part of this report.

With regard to improvements of the present techniques to provide a more accurate mathematical representation of solar wind flow, a number of items for further study are recommended. The first of these involves extension of the present capability from axisymmetric to three-dimensional nonaxisymmetric obstacle shapes representative of planetary magnetopauses. The second involves the merging of the present procedures for determining the magnetic field exterior to the magnetosphere boundary with a method, such as the Olsen-Pfitzer model, for calculating the confined magnetic field so as to provide a complete magnetic field representation. Lastly, the capability for determining numerical solutions of the complete magnetohydrodynamic equations, rather than the frozen magnetic field approximation,

should be actively pursued. Although this extension represents a major advance in magnetospheric physics and computational fluid dynamics, in view of the success of the currently employed methods, its successful achievement appears highly promising. The component methods on which the present procedure is based are directly capable of extension in these as well as other directions. Moreover, the efficiency of the present calculations indicates that the improved representation achieved by these improvements will not result in prohibitive computational costs.

APPENDIX A

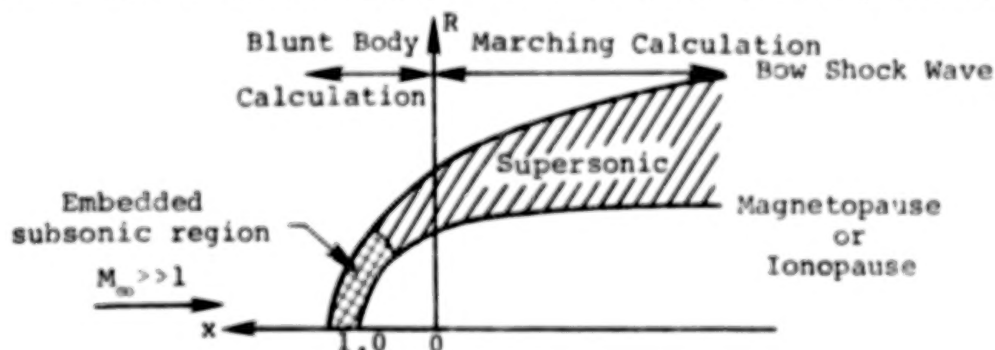
A.1 Introduction

The purpose of this appendix is to describe the operation of the assemblage of computer codes which were developed in conjunction with the theoretical work presented in this report and organized into one program, and to provide sufficient detail to permit understanding and use of the program. The program computes the flow field of the solar wind about a terrestrial planet, using a procedure for the calculation of supersonic/hypersonic flow about an axisymmetric blunt body. The corresponding frozen-in magnetic field is then calculated from the previously determined velocity and density fields. Streamlines and contour lines of various flow field properties and magnetic field components are also determined.

A description of the general operating procedure of the program is given, with descriptions of input and output. The program is written in FORTRAN IV and has been developed on a CDC 7600 computer. University Computing Company (UCC) Standard Plotting Software and Functional Software packages are used to produce automated plots. Files used, besides TAPE5 for INPUT and TAPE6 for OUTPUT, are TAPE1 for the plot file (system default), TAPE4 for input file for rerun option, and TAPE9 for storing data for rerun. Typical run times for cases using the default parameters are 40 to 50 seconds, using the OPT=2 compiler. For a case using the rerun option, which employs a previously calculated flow field, the run time is approximately 5 seconds.

A.2 Program Description

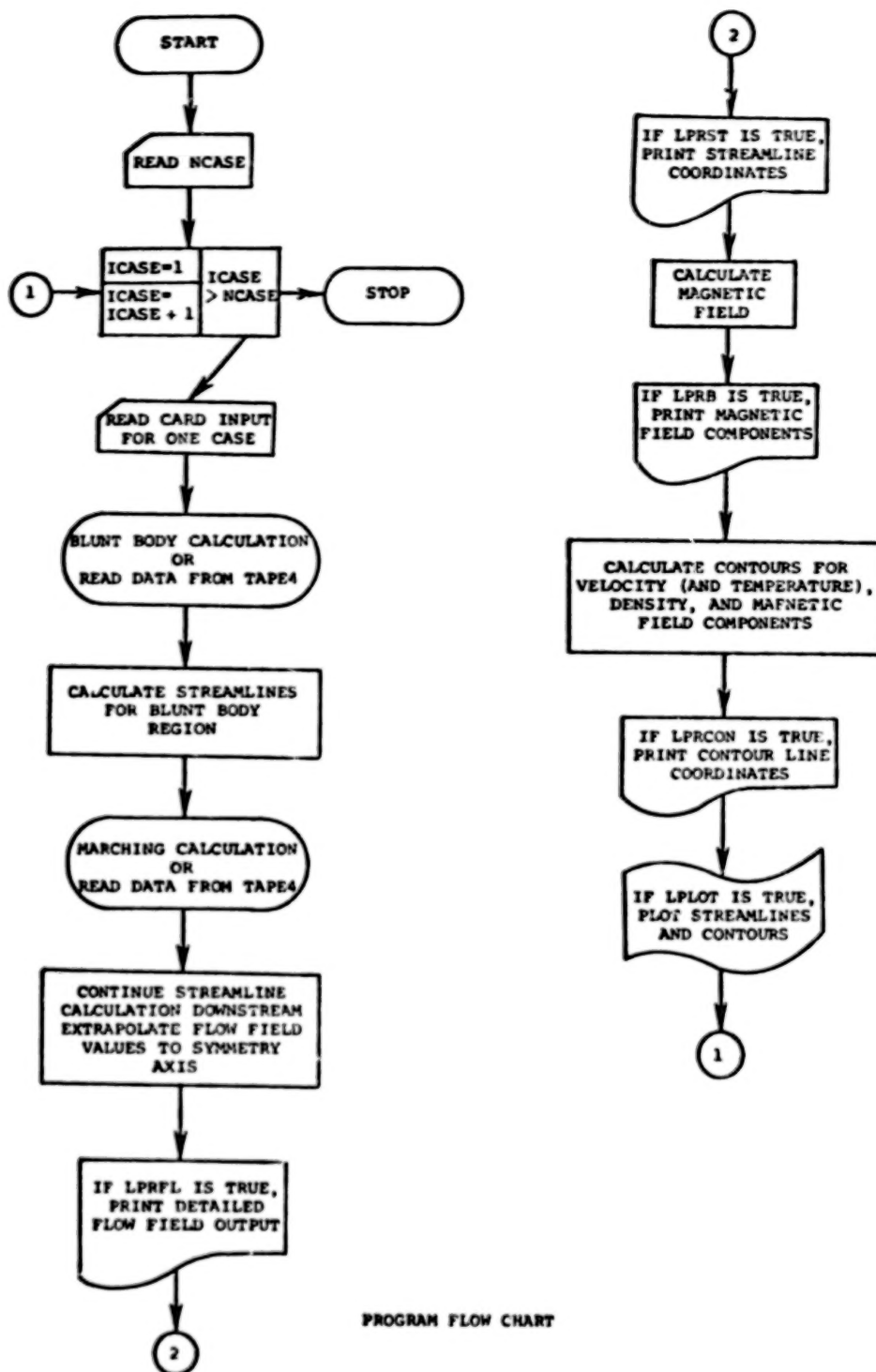
For computational purposes, the flow is subdivided into two regions, as indicated in the sketch below, with the center of the planet as origin.



The region near the nose of the magnetopause/ionopause includes all of the imbedded subsonic flow and part of the supersonic flow. An axisymmetric

implicit unsteady Euler equation solver is used to calculate this part of the flow field. Using the solution plane at $x = 0.0$ to provide starting conditions, the flow field in the purely supersonic downstream region is determined by integrating the steady Euler equations using a spatial marching procedure. Streamlines, the magnetic field, and contours are calculated using the entire flow field, distinguishing between the two regions as required by the different forms of the computational grids. A rerun capability is provided, where flow field data is read from a file written on a previous run, rather than repeating the blunt body and marching calculations. The computations proceed as shown in the sketch below, which provides an overall flow chart of the complete program. The program provides for several cases to be run consecutively.

APPENDIX A

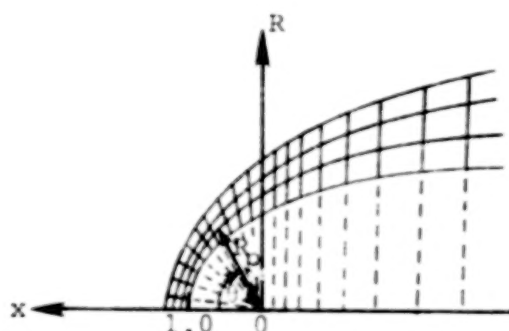


PROGRAM FLOW CHART

A.2.1 Calculation Procedure

After reading in the number of cases in the run, each case is calculated independently. Subroutine INPUT reads in all card input required for one case, viz. a title, flow conditions, obstacle geometry, calculation and print control parameters, and desired contour values. The user may supply the obstacle geometry in the form of a shape table for an axisymmetric body, or use one of the default shapes which are calculated internally by the program. These default shapes are the magnetopause equatorial trace and a constant scale-height ionopause for which H/R_0 is specified by the user. The input is printed as the first item of output.

A computational mesh in polar (R_p, θ) coordinates is established for the blunt body calculation; then, for the marching calculation, this is extended into a cylindrical (x, R) system, as indicated below:



All lengths, x , R , R_p , are scaled so that the nose of the obstacle is at $x = 1.0$. For the default shapes, rays at equal angular increments of $\Delta\theta$ are used, starting at $-\Delta\theta/2$, up to $90^\circ + \Delta\theta$, where $\Delta\theta = 90^\circ / (\text{NBLUNT} - 1.5)$ and NBLUNT is an input parameter describing the number of angular mesh points to be used in the blunt-body calculation. Program default value is NBLUNT = 24, so that for the default mesh, $\Delta\theta = 4^\circ$. The obstacle shape is determined by integrating the appropriate differential equation by a trapezoidal predictor-corrector method. For a user-supplied shape, the θ grid is determined by rays from the origin through the first NBLUNT points, and the reflection of the first ray in the x -axis. Values for R_p are determined by dividing the line segments between the body and bow shock wave into NR-1 equal intervals. Thus, including the obstacle and bow shock wave, the grid forms NR arcs around the obstacle. A starting solution for the blunt-body calculation is obtained by guessing a bow shock shape and by prescribing a Newtonian pressure distribution on the body.

APPENDIX A

Noting that the maximum entropy streamline wets the body, other flow properties on the body surface can then be calculated. An initial flow field is then established by linear interpolation between the obstacle and the guessed bow shock, where the Rankine-Hugoniot relations hold. The integration proceeds in time for ITER steps. The initial bow shock shape used for the magnetopause equatorial trace and for an ionopause with $H/R_0 \geq 0.1$ is a correlation shape depending on $(M_\infty, \gamma, H/R_0)$ and given by the parabola $R_p = \delta_1 \sqrt{\delta_0 - x} / \sqrt{\delta_0}$ where

$$\delta_0 = 1.0 + 1.1 \left[((\gamma-1)M_\infty^2 + 2) / (\gamma+1)M_\infty^2 \right] \times (0.9 + 0.5 H/R_0)$$

$$\delta_1 = \Delta_0 \{ (1.273 + 0.009 M_\infty^2) (0.904 + 0.655 H/R_0) \\ \times (3.95 - 5.3 H/R_0 + 3.85 (H/R_0)^2) \} + (R_{\text{body}})_x = 0.0$$

$$\Delta_0 = \left[(\gamma-1)M_\infty^2 + 2 \right] / \left[(\gamma+1)M_\infty^2 \right] \times 0.78$$

For a user-supplied obstacle shape and for an ionopause with $H/R_0 < 0.1$, the initial shock shape used is the curve $R_p = \sqrt{(1 + \Delta_0 (1 + 0.68\theta^2 + 0.16\theta^4))}$. Information on convergence, the final sonic line locations, and the body and final bow shock shape are printed from this calculation.

The results at $\theta = 90^\circ$, i.e. at $x = 0.0$, are used as starting conditions for the marching calculation, after proper normalization. For default geometries, the integration of the appropriate differential equation is continued downstream at equal θ increments to form a body shape table. The stepsize along the x-axis is recalculated at every ICNST(49) with ICNST(49) being set to 10. At each x-location, R_{body} is determined by linear interpolation. The computational mesh is extended by adding the line perpendicular to the x-axis at each step, divided in the same manner as for the blunt nose. The calculation marches downstream with a maximum stepsize of 1.0 until the terminal location specified by the user has been passed. However, the number of steps is limited to 75, after which the calculation will end regardless of the x-location. The coordinates of the obstacle and bow shock are printed at each step.

The grid coordinates and flow field values are written to a file, TAPE9, which may be saved to use as input for a later run. This rerun option, which replaces constructing the computational mesh and performing

the blunt body and marching calculations with reading the rerun input file, TAPE4, is described in section A.2.2.

The streamlines are calculated in two sections, following each of the flow field calculations. Using the results of the blunt body calculation, i.e. the (x, R) grid coordinates, (R_p, θ) grid coordinates, density ρ/ρ_∞ , and velocity components v_X/v_∞ and v_R/v_∞ , the velocity magnitude $|v|/v_\infty$ and flow angle are calculated. Density ρ/ρ_∞ and velocity $|v|/v_\infty$ are smoothed along the rays of constant- θ , using a third degree least squares fit with respect to R_p . Streamlines are then calculated downstream to $x = 0.0$, using the trajectory method, integrating through the velocity field by means of a third-order modified Euler integration procedure, using the grid locations on the bow shock as starting positions. The flow angle $\phi = \tan^{-1}(v_R/v_X)$ at each point is determined using bivariate linear interpolation in θ , then R_p . Points for which $\theta < 0^\circ$ or $\theta > 90^\circ$ are discarded in the interpolation.

The marching calculation provides (x, R) grid coordinates, and values of density ρ/ρ_t , and velocity components v_X/v_t and v_R/v_t , where t denotes free-stream stagnation conditions. For compatibility with the blunt body solution, the flow field values are converted to ρ/ρ_∞ , v_X/v_∞ , v_R/v_∞ before calculating the resultant velocity magnitude $|v|/v_\infty$ and flow angle ϕ . The streamline calculation is continued downstream, employing the same method as in the nose region. Starting positions on the shock wave for the streamline calculation in the marching zone are set at equal R -increments, with a maximum of 50 streamlines calculated. The flow angle is determined using bivariate linear interpolation first in x , then in R .

Along the symmetry axis, values of x , ρ/ρ_∞ , and $|v|/v_\infty$ are determined by extrapolation, using a third-order Lagrangian polynomial in θ on each arc of the computational grid. Exact values for the stagnation streamline are used where possible, viz.

at the bow shock

$$\rho/\rho_\infty = (\gamma+1)M_\infty^2 / \left[(\gamma-1)M_\infty^2 + 2 \right]$$

$$|v|/v_\infty = 1/(\rho/\rho_\infty)$$

APPENDIX A

at the body surface

$$\rho/\rho_\infty = (\rho/\rho_\infty)_{\text{shock}} \left\{ \left[\frac{(\gamma+1)M_\infty^2}{4\gamma M_\infty^2 - 2(\gamma-1)} \right]^{1/(\gamma-1)} \right\}$$

$$|\underline{v}|/v_\infty = 0.0$$

$$x = 1.0$$

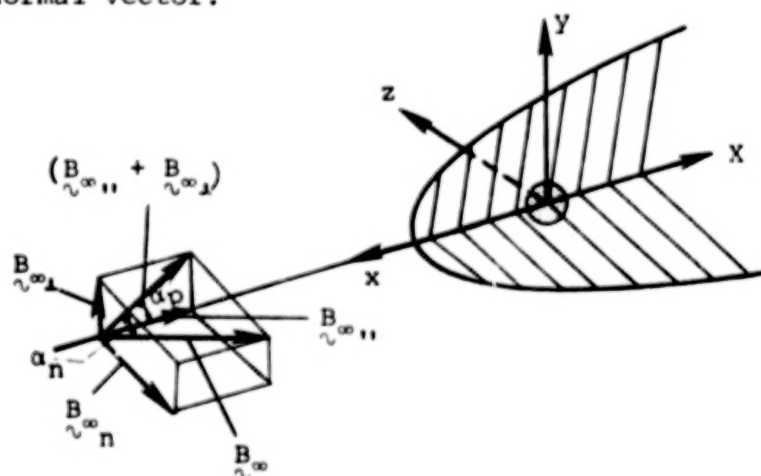
Detailed flow field output may now be printed by subroutine FLØUT, with LPRFL as print control variable. In addition to grid coordinates, density, velocities and flow angle, values of temperature T/T_∞ and pressure P/P_∞ are output, where

$$T/T_\infty = 1 + \left[(\gamma-1)/2 \right] M_\infty^2 \left(1 - (|\underline{v}|/v_\infty)^2 \right)$$

$$P/P_\infty = (\rho/\rho_\infty) (T/T_\infty)$$

Streamline coordinates may also be printed by subroutine STØUT, with LPRST as print control variable.

The magnetic field is determined by separately calculating the components whose field lines are parallel, perpendicular, and normal to the flow, in the undisturbed solar wind. These components are then added vectorially, the resultant being expressed in orthogonal (x,y,z) components. The angles in the free stream α_p and α_n between the magnetic field and the flow, as shown in the sketch below, are input variables. The components are calculated using the following formulae, in which \underline{e} signifies a vector of magnitude e, in the direction of the component field line, and \hat{n} the unit normal vector.



$$\left(\frac{B}{B_{\infty}}\right)_{\parallel} = \left(\frac{V}{V_{\infty}}\right)\left(\frac{\rho}{\rho_{\infty}}\right) ; \left(\frac{B}{B_{\infty}}\right)_{\perp} = \left(\frac{\Delta \ell}{\Delta \ell_{\infty}}\right)\left(\frac{\rho}{\rho_{\infty}}\right) ; \left(\frac{B}{B_{\infty}}\right)_n = \left(\frac{R}{R_{\infty}}\right)\left(\frac{\rho}{\rho_{\infty}}\right)$$

$$\left(\frac{B}{B_{\infty}}\right) = \left(\frac{B}{B_{\infty}}\right)_{\parallel} \left(\frac{B_{\infty \parallel}}{B_{\infty}}\right) + \left(\frac{B}{B_{\infty}}\right)_{\perp} \left(\frac{B_{\infty \perp}}{B_{\infty}}\right) + n \left(\frac{B}{B_{\infty}}\right)_n \left(\frac{B_{\infty n}}{B_{\infty}}\right)$$

The magnetic field line vector component B_{\parallel} , which results from the interplanetary component $B_{\infty \parallel}$ that is parallel to the undisturbed solar flow has local magnitude given by $(|V|/V_{\infty})(\rho/\rho_{\infty})$, and the same local direction ϕ as the fluid flow. Determination of the normal magnetic field component B_n requires calculation of R/R_{∞} , where R_{∞} is the free stream cylindrical R-ordinate of the streamline through the point under consideration. This is calculated by linearly interpolating in the local radial cylindrical coordinate R between the streamlines, with $R/R_{\infty} = 1.0$ along the x-axis. The magnetic field vector component B_{\perp} resulting from the interplanetary component $B_{\infty \perp}$ which is perpendicular to the undisturbed solar wind flow requires the distance vector $\Delta \ell / \Delta \ell_{\infty}$, whose magnitude is $\Delta \ell / \Delta \ell_{\infty}$ and direction is ψ , where $\Delta \ell / \Delta \ell_{\infty}$ is the stretching factor of the perpendicular field at the point, and ψ is the direction of the field line through the point. The perpendicular field lines are determined by integrating $\int v dt$ along each streamline, using trapezoidal integration to locate points along the streamline at regular increments in time, Δt , starting at a perpendicular field line ahead of the bow shock. Values for $\Delta \ell / \Delta \ell_{\infty}$ and ψ are calculated at the points where the perpendicular field lines and streamlines intersect, interpolating only along the field lines. A generalized quadrilateral interpolation scheme is then employed to determine $\Delta \ell / \Delta \ell_{\infty}$ and ψ at the computational grid points, using the quadrilateral containing the point formed by the intersection of pairs of adjacent streamlines and perpendicular field lines. At the bow shock, an exact formula is used, viz.

$$(\Delta \ell / \Delta \ell_{\infty})^2 = 1 + \cot^2 \theta (1 + D^2) - 2D \times \csc \theta \times \cot \theta \times \cos(\theta - \delta)$$

$$\psi = \theta + \sin^{-1}\{D \times \cot \theta \times \sin(\theta - \delta) / (\Delta \ell / \Delta \ell_{\infty})\}$$

APPENDIX A

where

$$D^2 = 1 - 4(M_\infty^2 \sin^2 \theta - 1)(\gamma M_\infty^2 \sin^2 \theta + 1) / [(\gamma + 1)^2 M_\infty^4 \sin^2 \theta]$$

$$\cot \delta = \tan \theta \times \left\{ (\gamma + 1) M_\infty^2 / [2(M_\infty^2 \sin^2 \theta - 1)] - 1 \right\}$$

$$\theta = \tan^{-1} \left\{ \frac{dR_{\text{shock}}}{dx} \right\}$$

The values of $\Delta l / \Delta l_\infty$ at the grid points are smoothed using fifth-order least squares fit with respect to arc length along the arcs of the grid. The resultant magnetic field is expressed in orthogonal (x,y,z) components, where

$$B_x / B_\infty = \cos \alpha_n \times \left(\cos \phi \times \cos \alpha_p \times (B/B_\infty)_n + \cos \psi \times \sin \alpha_p \times (B/B_\infty)_\perp \right)$$

$$B_y / B_\infty = \cos \alpha_n \times \left(\sin \phi \times \cos \alpha_p \times (B/B_\infty)_n + \sin \psi \times \sin \alpha_p \times (B/B_\infty)_\perp \right)$$

$$B_z / B_\infty = \sin \alpha_n \times (B/B_\infty)_n$$

Magnetic field components may now be printed by subroutine BOUT, with LPRB as print control parameter. The magnetic field is not calculated when LPRB = .FALSE. and KBCON=0.

Contours are calculated for velocity $|v|/v_\infty$, density ρ/ρ_∞ , and magnetic field components $(B/B_\infty)_n$ and $(B/B_\infty)_\perp$. The method used is a modified version of a procedure developed by R. Sorenson of NASA/Ames Research Center. The boundary is searched for intervals which bracket a contour point. Having found one point, the remainder of the contour is determined by 'walking' around the contour, searching at each step for the interval through which the contour line next passes, until a boundary point is reached. Then closed contours are found in a similar manner. Linear interpolation is used throughout the process. Note that since T/T_∞ is a function of $|v|/v_\infty$ only, velocity contours may also be considered as temperature contours. The coordinates of the contour lines can be printed by subroutine CONOUT, with LPRCON as print control parameter. The section of the program which creates the plots is accessed only when the control parameter LPLOT = .TRUE.

A.2.2 Rerun Option

The rerun option is used when $LRERUN = .TRUE.$ The blunt body and marching calculations are replaced with reading the grid coordinates and flow field values from the rerun file, TAPE4, which contains data written to TAPE9, then saved, on a previous run. Different values for any parameter not used in the flow field calculations may be specified, viz. contour values, plot length, magnetic field angles, and output options. Values of AMACH, GAMMA, and H/R_0 are required input, to ensure that the input rerun file does contain the case desired for rerun. If the geometry is user-supplied, the body shape table will be read from TAPE4, and should not be input from cards.

After reading the card input, AMACH, GAMMA, and H/R_0 are tested against values from TAPE4. The grid coordinates and flow field values from the blunt body calculation are read in, then smoothed, and streamlines calculated for this region, as previously described. The results of the marching calculation are then read, and the streamline calculation continued downstream. The calculations then proceed as described in section A.2.1.

A run must not contain more than one case which uses the rerun option.

A.2.3 Program Limitations and Precautions

The program makes some assumptions about the geometry of the obstacle shape around which flow is to be calculated, and about the flow field. The obstacle shape is assumed to be monotonically increasing in R , going downstream. The nose of the obstacle is at $x = 1.0$. The origin of the (x, R) coordinate system is the center of the planet. Obstacle shapes with sharp corners should be avoided. The flow at $x = 0.0$, which is used as the starting plane for the marching calculation, must be such that the axial (x -direction) Mach number is purely supersonic. This is a basic requirement of the marching code and is associated with the manner in which the code advances the solution. That condition is violated for ionopause shapes with $H/R_0 > 0.5$, so that with the present joining procedure employed (i.e. at $x = 0.0$) those shapes cannot be treated. In the magnetic field calculation, the first streamline is assumed to be inside the arc described by the grid points immediately off the body, downstream of $x = 0.0$. To reduce computational costs, a grid using $NR = 10$ may be used, in which case a lower value of CN may be required. This would

APPENDIX A

reduce the running line by approximately 40 percent. A free stream Mach number less than 3.0 is not advised.

A.2.4 Convergence Criteria for Blunt Body Calculation

The output provides two measures of the convergence of the blunt body calculation. The RMS of shock speed and maximum shock speed are printed at each iteration. These quantities should both tend to zero. A value for q_{RMS} , RMS of shock speed, of

$$q_{RMS} < \sqrt{\gamma} \times M_{\infty} \times 10^{-3}$$

where γ is the specific heat ratio, and M_{∞} is the free stream Mach number, usually indicates a converged solution. The RMS of error in enthalpy, HT, should be less than 1 percent, with the maximum enthalpy error also of that order.

The Courant number, CN, determines the time step size used by the calculation. A value not greater than the default of 3.0 should be used. For low Mach numbers or a coarser mesh than the default, a lower value may be preferable. If the default value does not generate a converged solution, or if the error message from subroutine SHOCK is printed, try lowering CN in increments of 0.5 to find a better value of CN. User-supplied bodies may also require a lower Courant number.

A.3 Description of Input

This section describes the card input for the program. An alphabetized dictionary of input variables is provided, defining the variables, listing default values and limitations. A discussion of the preparation of the card input is then presented, followed by a description of the input card format.

A.3.1 Dictionary of Input Variables

AMACH	free-stream Mach number; $3.0 \leq AMACH \leq 25.0$ is recommended
ANGN	the angle, in degrees, measuring the deviation of the free-stream magnetic field from the plane in which $B_{\infty 1}$ and $B_{\infty 2}$ lie; equal to $\tan^{-1}(B_{\infty 2}/\sqrt{ B_{\infty 1} ^2 + B_{\infty 2} ^2})$
ANGP	the angle, in degrees, measuring the deviation of the in-plane magnetic component ($B_{\infty 1}$ + $B_{\infty 2}$) from the direction of flow; equal to $\tan^{-1}(B_{\infty 2}/B_{\infty 1})$

BCØN(I)	KBCØN-dimensional array specifying values to be used for magnetic field strength contours
CN	Courant number used for blunt body calculation; program default value is 3.0
GAMMA	free-stream ratio of specific heats
HRØ	obstacle geometry indicator: $HRØ > 0$ - ionopause with $H/R_0 = HRØ$ $HRØ = 0$ - magnetopause equatorial trace $HRØ < 0$ - geometry is user-supplied
ITER	integer, number of iterations for blunt body calculation; program default value is 300
KBCØN	integer, number of values specified for magnetic field contours; $0 \leq KBCØN \leq 20$
KRCØN	integer, number of values specified for density contours; $0 \leq KRCØN \leq 20$
KVCØN	integer, number of values specified for velocity contours; $0 \leq KVCØN \leq 20$
LPLØT	logical variable indicating whether to create plots or plot file FALSE - no TRUE - yes
LPRB	logical variable indicating whether to print magnetic field output FALSE - no TRUE - yes
LPRCØN	logical variable indicating whether to print coordinates of contour lines FALSE - no TRUE - yes
LPRFL	logical variable indicating whether to print detailed flow field output FALSE - no TRUE - yes
LPRST	logical variable indicating whether to print coordinates of streamlines FALSE - no TRUE - yes

APPENDIX A

LRERUN	logical variable indicating whether this case uses rerun option FALSE - perform blunt body and marching calculations TRUE - read results of a previous calculation from TAPE4
NBLUNT	integer, number of angular mesh points for blunt body calculation; for user-supplied geometry, $XX(NBLUNT-1)=0.0$; program default value, and maximum, is 24
NBØD	integer, number of points in body shape table when geometry is user-supplied; $1 \leq NBØD \leq 100$
NCASE	integer, number of cases to be run consecutively; $NCASE \geq 1$
NR	integer, number of radial mesh points; program default value, and maximum, is 19
RCØN(I)	KRCØN - dimensional array specifying values to be used for density contours
RR(I)	NBØD - dimensional array representing the R-locations, in cylindrical (x,R) coordinates, of the user-supplied body shape
TITLE	descriptive heading of the case, to be printed on the first page of output; may contain up to 80 characters, including blanks
VCØN(I)	KVCØN - dimensional array specifying values to be used for velocity contours
XCALC	terminal downstream x-location for marching calculation of flow field; $XCALC < 0.0$; program default value is -1.0
XPLØT	terminal downstream x-location for calculation of streamlines, magnetic field, and contours; $XCALC \leq XPLØT < 0.0$; program default value is -1.0
XX(I)	NBØD - dimensional array representing the x-locations, in cylindrical (x,R) coordinates, of the user-supplied body shape

A.3.2 Preparation of Input Data

The card input for a run consists of one card containing the number of cases to be run consecutively, Item 0, followed by a set of input for each case, Item 1 through Item 7, and Item 8 if required. Where a default value is to be used, the input field should be left blank. For each case, all required variables which do not assume their default values should be specified. The input format for all cards is described in section A.3.3.

Item 0 - This item consists of one card, containing the number of cases in this run, NCASE.

Item 1 - This card provides identification of the case, TITLE, which is printed on the first page of the output for this case.

Item 2 - This card contains information on the flow conditions and body geometry, and parameters required for the blunt body and marching calculations. AMACH, GAMMA, and HRØ must be specified for each case. For the rerun option, the values are tested against the values from the rerun file. The parameters XCALC, NR, NBLUNT, CN, ITER are used only when the flow field is to be calculated. These variables each assume a default value if the input field is blank.

Item 3 - This item consists of one card containing the rerun indicator, LRERUN, and the output control variables LPRFL, LPRST, LPRCØN, LPRB, and LPLØT.

Item 4 - This card contains the variables XPLØT, ANGP, and ANGN. The value for XPLØT is changed by the program to be the x-location of the marching calculation immediately upstream of the input value for XPLØT. The angles describing the deviation of the magnetic field from the flow, ANGP and ANGN, are not required when LPRB=.FALSE. and KBCØN=0, since the magnetic field is not calculated under these conditions. ANGP is the angle between the vectors $(B_{\infty\Delta} + B_{\infty\eta})$ and v_{∞} , while ANGN is the angle between B_{∞} and $(B_{\infty\Delta} + B_{\infty\eta})$, where $B_{\infty\eta}$, $B_{\infty\Delta}$, $B_{\infty n}$ are the components of the free-stream magnetic field, B_{∞} , which are parallel, perpendicular, and normal to v_{∞} , and are as indicated in figure 4 of the text. The two angles ANGP and ANGN fully determine the half plane for which the magnetic field is to be calculated. The magnetic field for the other half of the plane may be calculated by rerunning with the sign of ANGP reversed. When $(B_{\infty\Delta} + B_{\infty\eta}) = 0$, $ANGN = \pm 90^\circ$, $ANGP = 0^\circ$; and, when $B_{\infty n} = 0$, $ANGN = 0^\circ$.

Item 5 - This item contains the values for the velocity contours. The first card contains KVCØN, the number of values specified for VCØN. If KVCØN=0, only this card is required, and no velocity contours are calculated. If KVCØN > 0, the contour values are then read. Up to three cards may be required to accommodate the values, eight per card, maximum of 20. The contour values should be monotonically increasing, with at least one value within the range of the magnitude of the velocity in the region for which contours are to be calculated.

Item 6 - This item contains the values for the density contours. The description is similar to that for item 5, with KRCØN being the number of values specified, and RCØN the array of values.

Item 7 - This item contains the values for the magnetic field contours. The description is similar to that for item 5, with KBCØN

APPENDIX A

being the number of values specified, and BCØN the array of values. Note that the same contour values are used for the parallel and perpendicular components.

Item 8 - This optional item is required when $HRØ < 0.0$ and $LRERUN = .FALSE.$, and contains the body shape table for the user-supplied geometry. The first card contains NBØD, the number of points in the shape table. The next NBØD cards contain the cylindrical (x,R) coordinates of these points, (XX(I), RR(I)), one point per card. The points supplied by the user determine the θ -spacing of the mesh used for the blunt body calculation. The first point should be near, but not on, the x-axis. A suggested location is such that the θ -spacing between the first point and the x-axis is half the θ -spacing between the first two points. The blunt body calculation adds a point which is the reflection about the x-axis of the first point in the body shape table. The $(NBLUNT-1)^{th}$ point should be at $x=0.0$. The $BLUNT^{th}$ point is also used to create the grid for the blunt body calculation. The coordinates must be normalized so that the planet center is at (0.,0.) and the nose of the body at (1.,0.).

A.3.3 Format of Input Data

Four format types are used for the input data. For real numbers (F-format), a decimal point is required. Integers (I-format) should be right-adjusted in the field. For logical variables (L-format), the first non-blank character in the field, which should be 'T' or 'F', determines the value. Note that a blank input field is interpreted as 'FALSE'. The title, which is in A-format, may contain any valid character.

A description of the card format of the input data follows, with item numbers corresponding to those in section A.3.2:

BLANK PAGE

BLANK PAGE

Item No. 0: 1 card

Variable	NCASE
Card Column	10
Format Type	I

Item No. 1: 1 card

Variable	TITLE									
Card Column	1									80
Format Type	A									

Item No. 2: 1 card

Variable	AMACH	GAMMA	HRØ	XCALC	NR	NBLUNT	CN	ITER
Card Column	10	20	30	40	50	60	70	80
Format Type	F	F	F	F	I	I	F	I

Item No. 3: 1 card

Variable	LRERUN	LPRL	LPRST	LPRCØN	LPRB	LPLØT
Card Column	10	20	30	40	50	60
Format Type	L	L	L	L	L	L

Item No. 4: 1 card

Variable	XPLØT	ANGP	ANGN
Card Column	10	20	30
Format Type	F	F	F

Item No. 5:

Variable	KVCØN	(1) 1 card
Card Column	10	
Format Type	I	

(2) 0 to 3 cards as needed for up to 20 values, 8 per card

Variable	VCØN(1)	VCØN(2)			VCØN(KVCØN)			
Card Column	10	20	30	40	50	60	70	80
Format Type	F	F	F	F	F	F	F	F

Input Data Card Format

Item No. 6:

Variable	KRCØN	(1) 1 card
Card Column	10	
Format Type	I	

(2) 0 to 3 cards as needed for up to 20 values, 8 per card

Variable	RCØN(1)	RCØN(2)			RCØN(KRCØN)			
Card Column	10	20	30	40	50	60	70	80
Format Type	F	F	F	F	F	F	F	F

Item No. 7:

Variable	KRCØN	(1) 1 card
Card Column	10	
Format Type	I	

(2) 0 to 3 cards as needed for up to 20 values, 8 per card

Variable	BCØN(1)	BCØN(2)			BCØN(KBCØN)			
Card Column	10	20	30	40	50	60	70	80
Format Type	F	F	F	F	F	F	F	F

Item No. 8: (required only when HRØ < 0.0 and LRERUN=.FALSE.)

Variable	NBØD	(1) 1 card
Card Column	10	
Format Type	I	

(2) I = 1 to NBØD; NBØD cards

Variable	XX(I)	RR(I)
Card Column	10	20
Format Type	F	F

A.4 Description of Output

This section describes the output of the computer program. The contents of each output item are specified and discussed. The printed output consists of six items, four of which are optional, with input control parameters. Plotted output is also optional.

The first output item consists of the input data. The title for the case is printed first, followed by all input variables, with identification of each variable. Default values are printed as if they were input. Parameters CN, NR, NBLUNT, ITER for the blunt body calculation and XCALC, the terminal location for the marching calculation, are printed only when the flow field is to be calculated. When the geometry is user-supplied, the input body shape table is printed. For a default geometry, the body shape is indicated by the description "default magnetopause coordinates - equatorial trace" or "default ionopause coordinates - $H/R_0 =$ ".

The second output item is not printed when LRRUN=.TRUE. From the blunt body calculation, the shock speed at each iteration, the final enthalpy error, final sonic line location, and body and final bow shock shape are printed. For convergence criteria of this calculation, the downstream location and body and shock ordinates are output. There is no control variable allowing the user to suppress this item of output when the flow field is calculated.

Detailed flow field output is the third item, and is printed only when LPRFL=.TRUE. Coordinates are labeled as X/D , R/D , RP/D , or X/R_0 , R/R_0 , RP/R_0 , to emphasize that distances are normalized by the distance from the center of the planet to the nose of the body, D for the magnetopause, R_0 for an ionopause. Along the symmetry axis, the values printed are velocity magnitude V/V_{∞} , density ρ/ρ_{∞} , temperature T/T_{∞} , and pressure P/P_{∞} . Over the rest of the flow field values are also given for velocity components V_x/V_{∞} , V_r/V_{∞} , and flow angle ϕ . Note that the flow angle is the deviation of the flow about the obstacle, and so $0^\circ \leq \phi < 90^\circ$.

The next output item is the (x, R) coordinates of the streamlines. For the blunt body region, the (R_p, θ) coordinates of the starting position on the bow shock wave are also given. This item is printed only when LPRST=.TRUE.

APPENDIX A

The magnetic field components are then printed, if LPRB=.TRUE. .The location of each point is defined in (R_p, θ) coordinates for the blunt body region, and (x, R) coordinates for the downstream marching region. The components along field lines parallel, perpendicular, and normal to the flow in the free stream are printed as B/BINF(PARALLEL), B/BINF(PERP), B/BINF(NORMAL). The orthogonal (x, y, z) components of the resultant are printed as BX/BINF(RESULTANT), BY/BINF(RESULTANT), BZ/BINF(RESULTANT). The magnetic field in the symmetry (x, y) plane, defined by the vector sum $\{(B/B_\infty)_x + (B/B_\infty)_y\}$, is also printed, and is given by the magnitude B/BINF(IN-PLANE) and direction B-ANGLE(IN-PLANE) of the vector. The B-ANGLE ψ is the angle between the magnetic field and the flow, and generally has the same sign as ANGP.

The last item printed is the (x, R) coordinates of the contours, for which LPRCON is the logical control variable. Noting that temperature and velocity contours coincide, the corresponding value of T/TINF is printed along with V/VINF for the velocity contours. There are three nonfatal error messages which may occur - see section A.5.

The program also has the capability of producing plotted output, using UCC plot routines AXIS, CHAR, DASH, DOTLN, ENPLT, GREEK, MATH, NUMPLT, PLOT, PTLN, POLAR, SCALF, VECTOR. Plots are not produced when LPLPT=.FALSE. The plots provide pictorial representation of the streamlines and contours, with a maximum of six frames produced. The first frame is a plot of the streamlines. Then contour plots of velocity, temperature, and density are drawn. The last two frames are contour plots of the parallel and perpendicular magnetic field components, with field lines added to indicate direction. Frames are omitted when no contour levels are provided.

A.5 Program Error Messages

This section lists the messages printed by the program, and indicates what action should be taken by the user.

- (1) ***** EXECUTION TERMINATED *****
 RERUN DATA ON TAPE4 DOES NOT AGREE
 WITH CASE SPECIFIED ON CARD INPUT:
 MACH NO. GAMMA M/RO

FROM CARDS
 FROM TAPE4

The first three parameters of item 2 of the input for a case using the rerun option should agree with those used when creating the file. The tolerance used in comparing the values is 10^{-5} . For a user-supplied geometry, it is sufficient for both values of H/R_0 to be negative.

- (2) ***** EXECUTION TERMINATED *****
 ARRAY OF CONTOUR VALUES IMPROPERLY SPECIFIED

When specified, the contour values should be monotonically increasing, with at least one value in the range of the velocity, density, or magnetic field strength for the region under consideration. This error does not inhibit generation of the rerun file.

- (3) CONTOUR SEARCH ABORTED - TABLE OVERFLOW IN NAD

The program allows for 29 contour lines to be found, storing the starting address of each contour in array NAD. This message indicates that at least one more contour line could be found. If the user requires all the contours of the levels specified, the case should be rerun in two parts. Otherwise, reduce the number of contour levels specified.

- (4) CONTOUR SEARCH ABORTED - TABLE OVERFLOW IN (X,Y)

The contour lines may be described by up to 1000 points, stored in arrays X and Y. This message indicates that more points would be required for the contour lines requested. The last contour line found will be incomplete. As with (3), either reduce the number of contour levels or run as two cases.

- (5) NEGATIVE PRESSURE DETECTED BY SHOCK AT J=
 PN= PØ= PTAU=

This message is printed when a negative pressure has been calculated at the shock on this iteration, at radial location J. The quantities printed are: PN, the pressure calculated on this step; PØ, the pressure from the previous step; and PTAU, the partial derivative of pressure with

APPENDIX A

respect to time. This condition indicates that the shock wave motion is too extreme. Lowering the value of CN, and thus reducing the time step, may remove the problem.

The following messages (6)-(10) usually result from using an obstacle geometry which is in some way too severe for the program to handle in its present form. The obstacle slope may be sufficiently high at $x = 0.0$ that the axial Mach number becomes subsonic in the starting solution for the marching calculation, or there may be a sharp corner in the profile. Check input, particularly free stream Mach number and body geometry.

(6) NEGATIVE PRESSURE ON BODY DETECTED BY BNDRY, PB= AT J=

This message indicates that a negative pressure on the body, PB, has been calculated at radial location J.

(7) NEGATIVE PRESSURE OR DENSITY ON BODY DETECTED BY BNDRYM AT X=
PB= RHOB= VXB= VRB=

The program makes internal corrections when this condition occurs, resulting pressure PB, density RHOB, and velocity components VXB and VRB.

(8) NEGATIVE SIGMA-BAR-1 IN EIGENM INDICATES SUBSONIC FLOW AT I=

(9) NEGATIVE SIGMA-BAR-2 IN EIGENM INDICATES SUBSONIC FLOW AT I=

These messages are printed when subsonic flow is detected by the marching calculation. The computed stepsize for this region will be quite small.

(10) -----BODY TURN STOPPED AT M2=100-----

This message indicates that the body has a sharp corner, which has been limited to 100° when being transformed.

A.6 Sample Case

A sample case is presented in this section. Figures A.1, A.2, and A.3 illustrate the input data, portions of the printed output, and the plotted output, respectively.

The sample case is run alone and is set up so as to produce all possible output. Flow is to be calculated about the rotated equatorial

trace of the magnetopause to a downstream location of $x = -10.0$, with $M_\infty = 8$, $\gamma = 5/3$. Streamlines, magnetic field components, and contours are desired to a downstream location of $x = -5.0$. The magnetic field forms angles of $\alpha_p = -45^\circ$, $\alpha_n = 45^\circ$ with the solar wind flow. Contour values are specified for all quantities.

The input data is tabulated in figure A.1, with item numbers corresponding to those in sections A.3.2 and A.3.3. The first card, item 0, indicates that there is one case to be run. The remaining 13 cards provide the data required for this case. Item 1 contains the identifying title. On the next card, item 2, values are specified for AMACH, GAM, HRØ, and XCALC. The other data fields are left blank to indicate that the default values will be used. The values of the logical variables of item 3 specify that the flow field is to be calculated, and that full printed and plotted output is to be produced. Item 4 defines the plot length to be -5.0 , and the magnetic field angles as $ANGP = -45.0$ and $ANGN = 45.0$. Items 5, 6, 7 specify the contour levels to be used - 12 for velocity and temperature, 10 for density, and 12 for magnetic field strength. Item 8 is omitted, since the obstacle geometry is one of the default shapes for which the coordinates are calculated internally by the program.

Figure A.2 presents portions of the printed output from the sample case using the data deck of figure A.1. The full printed output for this case is approximately 5,000 lines. The first item of printed output, figure A.2(a), is the input variables. Then in figure A.2(b), the output from the blunt body calculation is shown, omitting shock speed values for iterations 6 to 295. Note that the convergence criteria described in section A.2.4 are satisfied. Figure A.2(c) provides the output from the marching calculation. Figures A.2(d), (e), (f) show the detailed flow field output in four areas: near the symmetry axis; near $x = 0.0$, when the two calculation schemes are joined; around $x = -5.0$, the value of $XPLØT$; and the last two locations calculated. An example of the streamline output is shown in figures A.2(g), (h). Figures A.2(h), (i), (j) provide the magnetic field components at the same locations chosen to illustrate the flow field output. Examples of the printed output of the contour lines are shown in figures A.2(k), (l), (m), choosing two contour lines for each quantity. Note that for $(|B|/B_\infty)_1$, the different contour lines for the same contour level are considered to be two separate and distinct lines.

Figure A.3 shows the six plots which are produced by the program for this case.

Column No.	10	20	30	40	50	60	70	80
Item No.								
0	1							
1	SAMPLE CASE		DEFAULT MAGNETO PAUSE EQUATORIAL TRACE					
2	8.0	1.66666667	0.0	-10.0				
3	FALSE	TRUE	TRUE	TRUE	TRUE	TRUE		
4	-5.0	-45.0	45.0					
5	12							
	0.1	0.2	0.3	0.4	0.5	0.6	0.7	0.75
	0.8	0.85	0.88	0.9				
6	10							
	0.8	1.2	1.6	2.0	2.5	3.0	3.5	3.8
	4.0	4.2						
7	12							
	0.5	0.75	1.0	1.25	1.5	2.0	2.5	3.0
	3.5	4.0	5.0	6.0				

Figure A-1. - Card input for sample case.

FIGURE A.2

ABBREVIATED OUTPUT FOR SAMPLE CASE

SAMPLE CASE DEFAULT MAGNETOPAUSE EQUATORIAL TRACE

INPUT VARIABLES

FREESTREAM MACH NO. = 0.22
 SPECIFIC HEAT RATIO = 1.007
 OBSTACLE GEOMETRY: DEFAULT MAGNETOPAUSE COORDINATES = EQUATORIAL TRACE
 PARAMETERS FOR BLUNT BODY CALCULATION
 NO. OF RADIAL MESH POINTS = 19
 NO. OF ANGULAR MESH POINTS = 24
 COLLIMANT HUMIDITY = 3.00
 NO. OF ITERATIONS = 30
 TERMINAL DOWNSTREAM LOCATION FOR MARCHING CALCULATION = 10.0
 TERMINAL DOWNSTREAM LOCATION FOR PLOTTING = -5.0
 IN-PLANE DEVIATION OF MAGNETIC FIELD FROM FLOW = -45.00 DEGREES
 DEVIATION OF MAGNETIC FIELD FROM PLANE OF FLOW = 45.00 DEGREES
 LDEPTH = F
 LPHL = T
 LPHST = T
 LPHCDH = T
 LPHB = T
 LPLST = T

VALUES SPECIFIED FOR CONTOUR CALCULATION

12 CONTOUR LEVELS FOR VELOCITY

0.200	0.210	0.220	0.230	0.240	0.250
0.260	0.270	0.280	0.290	0.300	0.310

12 CONTOUR LEVELS FOR DENSITY

0.000	0.001	0.002	0.003	0.004	0.005
0.006	0.007	0.008	0.009	0.010	0.011

12 CONTOUR LEVELS FOR MAGNETIC FIELD STRENGTH

0.000	0.750	1.000	1.250	1.500	2.000
2.500	3.000	3.500	4.000	4.500	5.000

Figure A.2(a)

APPENDIX A

BLUNT BODY CALCULATION

ITERATION 1	RMS OF SHOCK SPEED= 1.2458E-02	MAXIMUM SHOCK SPEED= 3.6539E-02 AT J=29
ITERATION 2	RMS OF SHOCK SPEED= 1.2445E-02	MAXIMUM SHOCK SPEED= 3.1748E-02 AT J=29
ITERATION 3	RMS OF SHOCK SPEED= 2.1994E-02	MAXIMUM SHOCK SPEED= 3.2079E-02 AT J=29
ITERATION 4	RMS OF SHOCK SPEED= 3.4882E-02	MAXIMUM SHOCK SPEED= 3.8379E-02 AT J=16
ITERATION 5	RMS OF SHOCK SPEED= 4.9444E-02	MAXIMUM SHOCK SPEED= 7.2299E-02 AT J=16
ITERATION 200	RMS OF SHOCK SPEED= 3.7948E-03	MAXIMUM SHOCK SPEED= 9.6732E-03 AT J=17
ITERATION 247	RMS OF SHOCK SPEED= 3.7524E-03	MAXIMUM SHOCK SPEED= 9.1115E-03 AT J=15
ITERATION 247	RMS OF SHOCK SPEED= 3.7140E-03	MAXIMUM SHOCK SPEED= 9.1274E-03 AT J=17
ITERATION 249	RMS OF SHOCK SPEED= 3.6731E-03	MAXIMUM SHOCK SPEED= 8.9772E-03 AT J=17
ITERATION 249	RMS OF SHOCK SPEED= 3.6332E-03	MAXIMUM SHOCK SPEED= 8.6374E-03 AT J=16

FINAL SHOCK LINE LOCATION

XSL= .8992	XSL= .9040
XSL= .8171	XSL= .8979
XSL= .8247	XSL= .8972
XSL= .8040	XSL= .8922
XSL= .8741	XSL= .8876
XSL= .8456	XSL= .8885
XSL= .7187	XSL= 1.0347
XSL= .7425	XSL= 1.0141
XSL= .7865	XSL= 1.0172
XSL= .7914	XSL= 1.0114
XSL= .8172	XSL= 1.0045
XSL= .8437	XSL= 1.0102
XSL= .8646	XSL= 1.0114
XSL= .8907	XSL= .9951
XSL= .9146	XSL= .9871
XSL= .9316	XSL= .9776
XSL= .9791	XSL= .9661
XSL= 1.0177	XSL= .9514
XSL= 1.0376	XSL= .9377

*** X SPACD IN 4T = .1802E+01 RMS OF X SPACD IN 4T = .0475E+01 ***

BODY AND FINAL SHOCK SHAPE

J	X(BOODY)	Y(BOODY)	X(SHOCK)	Y(SHOCK)
2	-.0000	.0000	-1.2716	.0000
3	-.0057	.0046	-1.2862	.1331
4	-.0279	.0741	-1.2581	.2718
5	-.0794	.2434	-1.2436	.4136
6	-.0811	.3242	-1.2282	.5494
7	-.0443	.3871	-1.2162	.6882
8	-.0187	.4441	-1.1874	.8277
9	-.0015	.5047	-1.1537	.9681
10	-.0017	.5681	-1.1211	1.1094
11	-.0216	.6359	-1.0814	1.2449
12	-.0774	.7166	-1.0343	1.3849
13	-.1746	.7729	-.9898	1.5250
14	-.3094	.8183	-.9420	1.6653
15	-.4687	.8549	-.8977	1.8061
16	-.6438	.8844	-.8580	1.9477
17	-.8357	.9172	-.8216	2.0901
18	-.1072	.9489	-.7884	2.2344
19	-.4014	.9797	-.7583	2.3806
20	-.6341	1.0098	-.7304	2.5282
21	-.8226	1.0388	-.7049	2.6782
22	-.9772	1.0664	-.6816	2.8307
23	-.1013	1.0937	-.6603	2.9858
24	-.0000	1.1200	-.6417	3.1445

BEST AVAILABLE COPY
MICROFILMED FROM

Figure A.2(b) - continued

MARCKING CALCULATION

STEP NO.	DOWNSIDE LOCATION	N BY ORIGINATE	LOCK ORIGINATE
1	-0.362	1.3622	2.1483
2	-0.604	1.3751	2.1719
3	-0.798	1.3879	2.1951
4	-0.950	1.3995	2.2181
5	-1.056	1.4108	2.2408
6	-1.122	1.4219	2.2631
7	-1.214	1.4328	2.2855
8	-1.248	1.4430	2.3074
9	-1.270	1.4531	2.3292
10	-1.320	1.4639	2.3511
11	-1.378	1.4755	2.3731
12	-1.432	1.4878	2.3954
13	-1.482	1.5009	2.4179
14	-1.530	1.5132	2.4403
15	-1.578	1.5258	2.4628
16	-1.644	1.5388	2.4853
17	-1.698	1.5518	2.5078
18	-1.730	1.5643	2.5303
19	-1.815	1.5768	2.5528
20	-1.868	1.5898	2.5753
21	-1.908	1.6019	2.5978
22	-1.978	1.6149	2.6203
23	-2.048	1.6279	2.6428
24	-2.128	1.6409	2.6653
25	-2.198	1.6539	2.6878
26	-2.258	1.6669	2.7103
27	-2.328	1.6799	2.7328
28	-2.418	1.6929	2.7553
29	-2.478	1.7059	2.7778
30	-2.558	1.7189	2.8003
31	-2.608	1.7319	2.8228
32	-2.648	1.7449	2.8453
33	-2.698	1.7579	2.8678
34	-2.748	1.7709	2.8903
35	-2.808	1.7839	2.9128
36	-2.858	1.7969	2.9353
37	-2.918	1.8099	2.9578
38	-2.968	1.8229	2.9803
39	-3.018	1.8359	3.0028
40	-3.068	1.8489	3.0253
41	-3.118	1.8619	3.0478
42	-3.168	1.8749	3.0703
43	-3.218	1.8879	3.0928
44	-3.268	1.8999	3.1153
45	-3.318	1.9129	3.1378
46	-3.368	1.9259	3.1603
47	-3.418	1.9389	3.1828
48	-3.468	1.9519	3.2053
49	-3.518	1.9649	3.2278
50	-3.568	1.9779	3.2503
51	-3.618	1.9909	3.2728
52	-3.668	1.9999	3.2953
53	-3.718	2.0129	3.3178
54	-3.768	2.0259	3.3403
55	-3.818	2.0389	3.3628
56	-3.868	2.0519	3.3853
57	-3.918	2.0649	3.4078
58	-3.968	2.0779	3.4303
59	-4.018	2.0909	3.4528
60	-4.068	2.1039	3.4753

Figure A.2(c) - continued

DETAILED FLOW FIELD OUTPUT

FLOW FIELD VALUES EXTRAPOLATED TO SYMMETRY AXIS, THETA = 1.00 DEGREES

I	X/D	V/VINF	RQD/RQDINF	T/TINF	P/PINF
1	1.0000	0.0000	4.2201	22.3333	94.4497
2	1.0150	0.0144	4.2200	22.3276	94.2214
3	1.0300	0.0287	4.2196	22.3133	94.0045
4	1.0450	0.0431	4.2189	22.2999	93.8164
5	1.0600	0.0577	4.2188	22.2872	93.6476
6	1.0750	0.0725	4.2183	22.2749	93.4980
7	1.0900	0.0874	4.2174	22.2629	93.3577
8	1.1050	0.1023	4.2162	22.2512	93.2269
9	1.1200	0.1172	4.2145	22.2399	93.1041
10	1.1350	0.1321	4.2125	22.2289	92.9892
11	1.1500	0.1470	4.2101	22.2189	92.8819
12	1.1650	0.1619	4.2073	22.2099	92.7822
13	1.1800	0.1768	4.2042	22.2019	92.6898
14	1.1950	0.1917	4.2008	22.1949	92.6045
15	1.2100	0.2066	4.1971	22.1889	92.5262
16	1.2250	0.2214	4.1931	22.1839	92.4548
17	1.2400	0.2363	4.1888	22.1789	92.3898
18	1.2550	0.2511	4.1842	22.1739	92.3308
19	1.2700	0.2659	4.1793	22.1689	92.2772

FLOW FIELD VALUES FROM BLUNT BODY CALCULATION

ANGULAR LOCATION NO. 3, AT THETA = 2.00 DEGREES

I	X/D	R/D	X/D	V/VINF	VX/VINF	FLOW ANGLE	V/VINF	RQD/RQDINF	T/TINF	P/PINF
1	1.0000	0.0000	1.0000	0.0000	0.0000	88.4170	0.0103	4.2204	22.3311	94.3002
2	1.0150	0.0144	1.0146	0.0179	0.0159	48.3361	0.0245	4.2230	22.3206	94.2396
3	1.0300	0.0287	1.0295	0.0358	0.0315	32.0864	0.0386	4.2175	22.3016	94.0967
4	1.0450	0.0431	1.0446	0.0539	0.0486	21.7493	0.0526	4.2099	22.2742	93.7714
5	1.0600	0.0577	1.0597	0.0719	0.0658	16.1277	0.0667	4.2001	22.2394	93.4034
6	1.0750	0.0725	1.0747	0.0899	0.0828	12.5421	0.0808	4.1882	22.1941	92.9527
7	1.0900	0.0874	1.0898	0.1079	0.0994	10.0370	0.0948	4.1740	22.1419	92.4194
8	1.1050	0.1023	1.1048	0.1259	0.1170	9.3428	0.1088	4.1577	22.0806	91.8036
9	1.1200	0.1172	1.1199	0.1439	0.1341	8.1878	0.1228	4.1399	22.0114	91.1036
10	1.1350	0.1321	1.1349	0.1619	0.1511	7.2955	0.1368	4.1181	21.9339	90.3238
11	1.1500	0.1470	1.1499	0.1799	0.1681	6.5784	0.1508	4.0948	21.8482	89.4668
12	1.1650	0.1619	1.1649	0.1979	0.1859	5.9916	0.1648	4.0692	21.7542	88.5283
13	1.1800	0.1768	1.1799	0.2159	0.1997	5.4997	0.1787	4.0413	21.6521	87.5019
14	1.1950	0.1917	1.1949	0.2339	0.2176	5.0828	0.1926	4.0109	21.5419	86.4017
15	1.2100	0.2066	1.2099	0.2519	0.2354	4.7228	0.2065	3.9780	21.4239	85.2237
16	1.2250	0.2214	1.2249	0.2699	0.2533	4.4117	0.2204	3.9428	21.2970	83.9699
17	1.2400	0.2363	1.2399	0.2879	0.2714	4.1354	0.2343	3.9050	21.1629	82.6387
18	1.2550	0.2511	1.2549	0.3059	0.2894	3.9001	0.2481	3.8646	21.0200	81.2346
19	1.2700	0.2659	1.2699	0.3239	0.3071	3.6835	0.2620	3.8218	20.8693	79.7581

ANGULAR LOCATION NO. 3, AT THETA = 4.00 DEGREES

I	X/D	R/D	X/D	V/VINF	VX/VINF	FLOW ANGLE	V/VINF	RQD/RQDINF	T/TINF	P/PINF
1	1.0000	0.0000	1.0000	0.0000	0.0000	85.2322	0.0409	4.2139	22.2977	93.9609
2	1.0150	0.0144	1.0147	0.0179	0.0160	71.1386	0.0523	4.2102	22.2745	93.7792
3	1.0300	0.0287	1.0297	0.0358	0.0337	58.4397	0.0642	4.2045	22.2494	93.5316
4	1.0450	0.0431	1.0448	0.0539	0.0518	48.1188	0.0760	4.1970	22.2182	93.2169
5	1.0600	0.0577	1.0598	0.0719	0.0697	39.4164	0.0878	4.1875	22.1809	92.8339
6	1.0750	0.0725	1.0748	0.0899	0.0877	33.3384	0.0997	4.1761	22.1372	92.3799
7	1.0900	0.0874	1.0899	0.1079	0.1057	28.0607	0.1117	4.1625	22.0879	91.8566
8	1.1050	0.1023	1.1049	0.1259	0.1237	23.6199	0.1239	4.1469	22.0336	91.2599
9	1.1200	0.1172	1.1199	0.1439	0.1417	20.0317	0.1362	4.1291	21.9736	90.5823
10	1.1350	0.1321	1.1349	0.1619	0.1597	17.2983	0.1487	4.1091	21.9019	89.8221
11	1.1500	0.1470	1.1499	0.1799	0.1777	15.3485	0.1613	4.0868	21.8284	88.9839
12	1.1650	0.1619	1.1649	0.1979	0.1957	13.2744	0.1741	4.0622	21.7536	88.0791
13	1.1800	0.1768	1.1799	0.2159	0.2137	11.0878	0.1871	4.0352	21.6763	87.1090
14	1.1950	0.1917	1.1949	0.2339	0.2317	9.7585	0.2004	4.0058	21.5968	86.0817
15	1.2100	0.2066	1.2099	0.2519	0.2497	8.3866	0.2139	3.9739	21.5136	84.9737
16	1.2250	0.2214	1.2249	0.2699	0.2677	7.2866	0.2276	3.9395	21.4282	83.7893
17	1.2400	0.2363	1.2399	0.2879	0.2857	6.4107	0.2416	3.9025	21.3401	82.5272
18	1.2550	0.2511	1.2549	0.3059	0.3037	5.7344	0.2559	3.8629	20.2464	80.1766
19	1.2700	0.2659	1.2699	0.3239	0.3217	5.2386	0.2705	3.8206	20.1776	79.3649

Figure A.2(d) - continued

ANNUAL LOCATION NO. 24, AT FIFTA - 97,000 - 11,000

TABLE 1. P-VALUE VALUES FROM REGRESSING CALCULATION

ADDITIONAL SERIAL LOCATION NO. 1 OF 870 • 0-2002

ADDITIONAL SERIAL LOCATIONS NO. 2 OF 970 • 04.070

Figure A.2(e) - continued

APPENDIX A

ADDITIONAL AXIAL LOCATION NO.45, AT R/D = -0.0009

I	R/D	WR/VINF	VR/VINF	FLDN ANGLE	V/VINF	RND/RNDINF	T/TINF	P/PINF
1	1.7801	0.073	0.043	0.007	0.004	0.028	0.0048	2.1132
2	1.9071	0.105	0.070	0.009	0.007	0.004	0.0051	2.1421
3	2.0349	0.129	0.092	0.009	0.010	0.008	0.0058	2.1613
4	2.1628	0.154	0.114	0.009	0.010	0.009	0.0063	2.1808
5	2.2906	0.179	0.136	0.009	0.010	0.010	0.0068	2.2003
6	2.4185	0.204	0.158	0.009	0.010	0.011	0.0073	2.2198
7	2.5463	0.229	0.180	0.009	0.010	0.012	0.0078	2.2393
8	2.6742	0.254	0.202	0.009	0.010	0.013	0.0083	2.2588
9	2.8020	0.279	0.224	0.009	0.010	0.014	0.0088	2.2783
10	2.9299	0.304	0.246	0.009	0.010	0.015	0.0093	2.2978
11	3.0577	0.329	0.268	0.009	0.010	0.016	0.0098	2.3173
12	3.1856	0.354	0.290	0.009	0.010	0.017	0.0103	2.3368
13	3.3134	0.379	0.312	0.009	0.010	0.018	0.0108	2.3563
14	3.4413	0.404	0.334	0.009	0.010	0.019	0.0113	2.3758
15	3.5691	0.429	0.356	0.009	0.010	0.020	0.0118	2.3953
16	3.6970	0.454	0.378	0.009	0.010	0.021	0.0123	2.4148
17	3.8248	0.479	0.400	0.009	0.010	0.022	0.0128	2.4343
18	3.9527	0.504	0.422	0.009	0.010	0.023	0.0133	2.4538
19	4.0805	0.529	0.444	0.009	0.010	0.024	0.0138	2.4733

ADDITIONAL AXIAL LOCATION NO.46, AT R/D = -0.0170

I	R/D	WR/VINF	VR/VINF	FLDN ANGLE	V/VINF	RND/RNDINF	T/TINF	P/PINF
1	1.7714	0.073	0.043	0.007	0.004	0.028	0.0047	2.0999
2	1.9033	0.105	0.065	0.007	0.007	0.004	0.0050	2.1288
3	2.0351	0.129	0.087	0.007	0.010	0.008	0.0057	2.1480
4	2.1669	0.154	0.109	0.007	0.010	0.009	0.0062	2.1675
5	2.2987	0.179	0.131	0.007	0.010	0.010	0.0067	2.1870
6	2.4305	0.204	0.153	0.007	0.010	0.011	0.0072	2.2065
7	2.5623	0.229	0.175	0.007	0.010	0.012	0.0077	2.2260
8	2.6941	0.254	0.197	0.007	0.010	0.013	0.0082	2.2455
9	2.8259	0.279	0.219	0.007	0.010	0.014	0.0087	2.2650
10	2.9577	0.304	0.241	0.007	0.010	0.015	0.0092	2.2845
11	3.0895	0.329	0.263	0.007	0.010	0.016	0.0097	2.3040
12	3.2213	0.354	0.285	0.007	0.010	0.017	0.0102	2.3235
13	3.3531	0.379	0.307	0.007	0.010	0.018	0.0107	2.3430
14	3.4849	0.404	0.329	0.007	0.010	0.019	0.0112	2.3625
15	3.6167	0.429	0.351	0.007	0.010	0.020	0.0117	2.3820
16	3.7485	0.454	0.373	0.007	0.010	0.021	0.0122	2.4015
17	3.8803	0.479	0.395	0.007	0.010	0.022	0.0127	2.4210
18	4.0121	0.504	0.417	0.007	0.010	0.023	0.0132	2.4405
19	4.1439	0.529	0.439	0.007	0.010	0.024	0.0137	2.4600

ADDITIONAL AXIAL LOCATION NO.49, AT R/D = -0.0220

I	R/D	WR/VINF	VR/VINF	FLDN ANGLE	V/VINF	RND/RNDINF	T/TINF	P/PINF
1	1.7628	0.073	0.043	0.007	0.004	0.028	0.0046	2.0866
2	1.8946	0.105	0.065	0.007	0.007	0.004	0.0049	2.1155
3	2.0264	0.129	0.087	0.007	0.010	0.008	0.0056	2.1347
4	2.1582	0.154	0.109	0.007	0.010	0.009	0.0061	2.1542
5	2.2900	0.179	0.131	0.007	0.010	0.010	0.0066	2.1737
6	2.4218	0.204	0.153	0.007	0.010	0.011	0.0071	2.1932
7	2.5536	0.229	0.175	0.007	0.010	0.012	0.0076	2.2127
8	2.6854	0.254	0.197	0.007	0.010	0.013	0.0081	2.2322
9	2.8172	0.279	0.219	0.007	0.010	0.014	0.0086	2.2517
10	2.9490	0.304	0.241	0.007	0.010	0.015	0.0091	2.2712
11	3.0808	0.329	0.263	0.007	0.010	0.016	0.0096	2.2907
12	3.2126	0.354	0.285	0.007	0.010	0.017	0.0101	2.3102
13	3.3444	0.379	0.307	0.007	0.010	0.018	0.0106	2.3297
14	3.4762	0.404	0.329	0.007	0.010	0.019	0.0111	2.3492
15	3.6080	0.429	0.351	0.007	0.010	0.020	0.0116	2.3687
16	3.7398	0.454	0.373	0.007	0.010	0.021	0.0121	2.3882
17	3.8716	0.479	0.395	0.007	0.010	0.022	0.0126	2.4077
18	4.0034	0.504	0.417	0.007	0.010	0.023	0.0131	2.4272
19	4.1352	0.529	0.439	0.007	0.010	0.024	0.0136	2.4467

ADDITIONAL AXIAL LOCATION NO.50, AT R/D = -0.0370

I	R/D	WR/VINF	VR/VINF	FLDN ANGLE	V/VINF	RND/RNDINF	T/TINF	P/PINF
1	1.7542	0.073	0.043	0.007	0.004	0.028	0.0045	2.0733
2	1.8860	0.105	0.065	0.007	0.007	0.004	0.0048	2.1022
3	2.0178	0.129	0.087	0.007	0.010	0.008	0.0055	2.1214
4	2.1496	0.154	0.109	0.007	0.010	0.009	0.0060	2.1409
5	2.2814	0.179	0.131	0.007	0.010	0.010	0.0065	2.1604
6	2.4132	0.204	0.153	0.007	0.010	0.011	0.0070	2.1799
7	2.5450	0.229	0.175	0.007	0.010	0.012	0.0075	2.1994
8	2.6768	0.254	0.197	0.007	0.010	0.013	0.0080	2.2189
9	2.8086	0.279	0.219	0.007	0.010	0.014	0.0085	2.2384
10	2.9404	0.304	0.241	0.007	0.010	0.015	0.0090	2.2579
11	3.0722	0.329	0.263	0.007	0.010	0.016	0.0095	2.2774
12	3.2040	0.354	0.285	0.007	0.010	0.017	0.0100	2.2969
13	3.3358	0.379	0.307	0.007	0.010	0.018	0.0105	2.3164
14	3.4676	0.404	0.329	0.007	0.010	0.019	0.0110	2.3359
15	3.5994	0.429	0.351	0.007	0.010	0.020	0.0115	2.3554
16	3.7312	0.454	0.373	0.007	0.010	0.021	0.0120	2.3749
17	3.8630	0.479	0.395	0.007	0.010	0.022	0.0125	2.3944
18	3.9948	0.504	0.417	0.007	0.010	0.023	0.0130	2.4139
19	4.1266	0.529	0.439	0.007	0.010	0.024	0.0135	2.4334

Figure A.2(2) - continued

STREAMLINE TRAJECTORY CALCULATION

43 STREAMLINES CALCULATED

STREAMLINE NO. 1, STARTING AT $X/D = 1.2733$, $Y/D = 0.000$
ICORRESPONDS TO $\theta = 2.00$ DEGREES, $RP/D = 1.27110$

X/D	Y/D
1.2733	0.0000
1.2740	0.0001
1.2750	0.0002
1.2760	0.0003
1.2770	0.0004
1.2780	0.0005
1.2790	0.0006
1.2800	0.0007
1.2810	0.0008
1.2820	0.0009
1.2830	0.0010
1.2840	0.0011
1.2850	0.0012
1.2860	0.0013
1.2870	0.0014
1.2880	0.0015
1.2890	0.0016
1.2900	0.0017
1.2910	0.0018
1.2920	0.0019
1.2930	0.0020
1.2940	0.0021
1.2950	0.0022
1.2960	0.0023
1.2970	0.0024
1.2980	0.0025
1.2990	0.0026
1.3000	0.0027
1.3010	0.0028
1.3020	0.0029
1.3030	0.0030
1.3040	0.0031
1.3050	0.0032
1.3060	0.0033
1.3070	0.0034
1.3080	0.0035
1.3090	0.0036
1.3100	0.0037
1.3110	0.0038
1.3120	0.0039
1.3130	0.0040
1.3140	0.0041
1.3150	0.0042
1.3160	0.0043
1.3170	0.0044
1.3180	0.0045
1.3190	0.0046
1.3200	0.0047
1.3210	0.0048
1.3220	0.0049
1.3230	0.0050
1.3240	0.0051
1.3250	0.0052
1.3260	0.0053
1.3270	0.0054
1.3280	0.0055
1.3290	0.0056
1.3300	0.0057
1.3310	0.0058
1.3320	0.0059
1.3330	0.0060
1.3340	0.0061
1.3350	0.0062
1.3360	0.0063
1.3370	0.0064
1.3380	0.0065
1.3390	0.0066
1.3400	0.0067
1.3410	0.0068
1.3420	0.0069
1.3430	0.0070
1.3440	0.0071
1.3450	0.0072
1.3460	0.0073
1.3470	0.0074
1.3480	0.0075
1.3490	0.0076
1.3500	0.0077
1.3510	0.0078
1.3520	0.0079
1.3530	0.0080
1.3540	0.0081
1.3550	0.0082
1.3560	0.0083
1.3570	0.0084
1.3580	0.0085
1.3590	0.0086
1.3600	0.0087
1.3610	0.0088
1.3620	0.0089
1.3630	0.0090
1.3640	0.0091
1.3650	0.0092
1.3660	0.0093
1.3670	0.0094
1.3680	0.0095
1.3690	0.0096
1.3700	0.0097
1.3710	0.0098
1.3720	0.0099
1.3730	0.0100
1.3740	0.0101
1.3750	0.0102
1.3760	0.0103
1.3770	0.0104
1.3780	0.0105
1.3790	0.0106
1.3800	0.0107
1.3810	0.0108
1.3820	0.0109
1.3830	0.0110
1.3840	0.0111
1.3850	0.0112
1.3860	0.0113
1.3870	0.0114
1.3880	0.0115
1.3890	0.0116
1.3900	0.0117
1.3910	0.0118
1.3920	0.0119
1.3930	0.0120
1.3940	0.0121
1.3950	0.0122
1.3960	0.0123
1.3970	0.0124
1.3980	0.0125
1.3990	0.0126
1.4000	0.0127
1.4010	0.0128
1.4020	0.0129
1.4030	0.0130
1.4040	0.0131
1.4050	0.0132
1.4060	0.0133
1.4070	0.0134
1.4080	0.0135
1.4090	0.0136
1.4100	0.0137
1.4110	0.0138
1.4120	0.0139
1.4130	0.0140
1.4140	0.0141
1.4150	0.0142
1.4160	0.0143
1.4170	0.0144
1.4180	0.0145
1.4190	0.0146
1.4200	0.0147
1.4210	0.0148
1.4220	0.0149
1.4230	0.0150
1.4240	0.0151
1.4250	0.0152
1.4260	0.0153
1.4270	0.0154
1.4280	0.0155
1.4290	0.0156
1.4300	0.0157
1.4310	0.0158
1.4320	0.0159
1.4330	0.0160
1.4340	0.0161
1.4350	0.0162
1.4360	0.0163
1.4370	0.0164
1.4380	0.0165
1.4390	0.0166
1.4400	0.0167
1.4410	0.0168
1.4420	0.0169
1.4430	0.0170
1.4440	0.0171
1.4450	0.0172
1.4460	0.0173
1.4470	0.0174
1.4480	0.0175
1.4490	0.0176
1.4500	0.0177
1.4510	0.0178
1.4520	0.0179
1.4530	0.0180
1.4540	0.0181
1.4550	0.0182
1.4560	0.0183
1.4570	0.0184
1.4580	0.0185
1.4590	0.0186
1.4600	0.0187
1.4610	0.0188
1.4620	0.0189
1.4630	0.0190
1.4640	0.0191
1.4650	0.0192
1.4660	0.0193
1.4670	0.0194
1.4680	0.0195
1.4690	0.0196
1.4700	0.0197
1.4710	0.0198
1.4720	0.0199
1.4730	0.0200
1.4740	0.0201
1.4750	0.0202
1.4760	0.0203
1.4770	0.0204
1.4780	0.0205
1.4790	0.0206
1.4800	0.0207
1.4810	0.0208
1.4820	0.0209
1.4830	0.0210
1.4840	0.0211
1.4850	0.0212
1.4860	0.0213
1.4870	0.0214
1.4880	0.0215
1.4890	0.0216
1.4900	0.0217
1.4910	0.0218
1.4920	0.0219
1.4930	0.0220
1.4940	0.0221
1.4950	0.0222
1.4960	0.0223
1.4970	0.0224
1.4980	0.0225
1.4990	0.0226
1.5000	0.0227

Figure A.2(g) - continued

APPENDIX A

STREAMLINE NO.42, STARTING AT X/D = -4.3769, Y/D = 4.3233

X/D	Y/D
-4.3769	4.3233
-4.3863	4.3717
-4.7098	4.4187
-4.9175	4.4442

STREAMLINE NO.43, STARTING AT X/D = -4.6915, Y/D = 4.4391

X/D	Y/D
-4.6915	4.4391
-4.9024	4.4851
-4.9175	4.4893

MAGNETIC FIELD COMPONENTS

ANGULAR LOCATION NO. 1, AT THETA = (1.50) DEGREES

I	PP/D	B/BIHF (PARALLEL)	B/BIHF (PERP)	B/BIHF (IN-PLANE)	B-ANGLE (IN-PLANE)	B/BIHF (NORMAL)	BX/BIHF (RESULTANT)	BY/BIHF (RESULTANT)	BZ/BIHF (RESULTANT)
1	1.0000	0.0000							
2	1.0010	0.0003	19.5008	19.7949	-89.7964	4.2200	0.0347	-9.7544	2.9886
3	1.0030	0.0012	19.7315	19.8321	-89.8076	4.2155	0.0446	-7.5177	2.9809
4	1.0050	0.0030	11.7017	8.2804	-89.1712	4.2089	0.0449	-5.0544	2.9781
5	1.0070	0.0054	4.8738	4.4841	-88.5443	4.1998	0.0454	-4.9389	2.9697
6	1.0090	0.0081	0.1004	0.0619	-87.9137	4.1885	0.0461	-4.2633	2.9616
7	1.0110	0.0111	7.3505	5.3567	-87.2821	4.1744	0.0466	-3.7403	2.9518
8	1.0130	0.0147	0.8444	0.5521	-86.6459	4.1582	0.0469	-3.4241	2.9403
9	1.0150	0.0188	0.2913	0.4051	-85.9990	4.1395	0.0468	-3.1476	2.9271
10	1.0170	0.0234	0.0912	0.2841	-85.3424	4.1185	0.0462	-2.9456	2.9122
11	1.0190	0.0284	0.0111	0.2019	-84.6660	4.0951	0.0450	-2.7980	2.8957
12	1.0210	0.0338	0.0119	0.1517	-83.9722	4.0693	0.0430	-2.6969	2.8775
13	1.0230	0.0396	0.0442	0.1011	-83.2596	4.0412	0.0401	-2.6471	2.8575
14	1.0250	0.0458	0.0724	0.0779	-82.5244	4.0106	0.0364	-2.6442	2.8360
15	1.0270	0.0524	0.0912	0.0744	-81.7698	3.9777	0.0311	-2.6836	2.8127
16	1.0290	0.0594	0.0914	0.0811	-80.9977	3.9424	0.0245	-2.7622	2.7877
17	1.0310	0.0668	0.0899	0.1005	-80.1478	3.9046	0.0166	-2.8856	2.7611
18	1.0330	0.0746	0.0819	0.1202	-79.2392	3.8647	0.0077	-2.9949	2.7328
19	1.0350	0.0828	0.0814	0.1398	-78.2838	3.8229	0.0000	-1.9104	2.7018

ANGULAR LOCATION NO. 2, AT THETA = 2.00 DEGREES

I	PP/D	B/BIHF (PARALLEL)	B/BIHF (PERP)	B/BIHF (IN-PLANE)	B-ANGLE (IN-PLANE)	B/BIHF (NORMAL)	BX/BIHF (RESULTANT)	BY/BIHF (RESULTANT)	BZ/BIHF (RESULTANT)
1	1.0000	0.0000							
2	1.0010	0.0003	19.5008	19.8129	-91.8200	4.2133	-0.2080	-9.7690	4.0177
3	1.0030	0.0012	19.7315	19.8521	-92.7384	4.2024	-0.0999	-7.4417	4.7039
4	1.0050	0.0030	11.7017	8.2808	-93.0175	4.1889	-0.0118	-5.0331	4.9431
5	1.0070	0.0054	4.8738	4.4847	-93.6830	4.1727	0.0030	-4.8954	4.9051
6	1.0090	0.0081	0.1004	0.0619	-94.4184	4.1536	0.0036	-4.2460	4.2492
7	1.0110	0.0111	7.3505	5.3567	-95.0814	4.1319	0.0087	-3.7571	4.0516
8	1.0130	0.0147	0.8444	0.5521	-95.6891	4.1076	0.0142	-3.3422	3.9129
9	1.0150	0.0188	0.2913	0.4051	-96.2467	4.0812	0.0218	-3.1167	3.7695
10	1.0170	0.0234	0.0912	0.2841	-96.7591	4.0524	0.0280	-2.9143	3.6178
11	1.0190	0.0284	0.0111	0.2019	-97.2324	4.0211	0.0324	-2.7246	3.5168
12	1.0210	0.0338	0.0119	0.1517	-97.6698	3.9885	0.0353	-2.5729	3.3982
13	1.0230	0.0396	0.0442	0.1011	-98.0741	3.9546	0.0366	-2.4467	3.2916
14	1.0250	0.0458	0.0724	0.0779	-98.4423	3.9195	0.0352	-2.3275	3.1941
15	1.0270	0.0524	0.0912	0.0744	-98.7698	3.8834	0.0326	-2.2225	3.0980
16	1.0290	0.0594	0.0914	0.0811	-99.0517	3.8461	0.0287	-2.1219	2.9952
17	1.0310	0.0668	0.0899	0.1005	-99.2892	3.8076	0.0232	-2.0254	2.8868
18	1.0330	0.0746	0.0819	0.1202	-99.4878	3.7680	0.0156	-1.9346	2.7971
19	1.0350	0.0828	0.0814	0.1398	-99.6425	3.7274	0.0073	-1.8480	2.7024

Figure A.2(h) - continued

ANGULAR LOCATION NO. 3, AT THETA = 0.0000 DEGREES

I	RP/D	S/RINF (PARALLEL)	S/RINF (PERP)	S/RINF (IN-PLANE)	S-ANGLE (IN-PLANE)	S/RINF (NORMAL)	SX/RINF (RESULTANT)	SY/RINF (RESULTANT)	SZ/RINF (RESULTANT)
1	1.0011	.1723							
2	1.0169	.2211	19.7354	13.8038	-94.0993	12.5951	-.0977	-9.7358	8.5525
3	1.0314	.2706	14.8020	10.2979	-93.4037	11.6319	-.4326	-7.2508	8.2391
4	1.0460	.3208	11.6097	8.9349	-92.1443	10.9325	-.2126	-5.6791	7.7466
5	1.0616	.3676	9.8224	8.7739	-91.0505	10.3597	-.0878	-4.7691	7.3294
6	1.0767	.4104	8.5379	5.8698	-89.9227	9.8352	.0056	-4.1526	6.1060
7	1.0918	.4551	7.5758	5.1945	-88.9634	7.5321	.0864	-3.6725	5.5968
8	1.1069	.5138	6.8514	4.8877	-87.9982	6.8321	.1161	-3.3127	4.8310
9	1.1221	.5624	6.3034	4.5063	-87.0325	6.3863	.1576	-3.0059	4.4592
10	1.1372	.6119	5.8859	4.0167	-86.0642	5.9080	.1990	-2.8039	4.1776
11	1.1523	.6592	5.5598	3.7568	-85.2820	5.5322	.2194	-2.6074	3.9210
12	1.1674	.7073	5.2036	3.5460	-84.4222	5.1748	.2437	-2.4455	3.6941
13	1.1825	.7551	4.9275	3.3572	-83.5894	4.9048	.2692	-2.3588	3.4862
14	1.1976	.8027	4.7526	3.2041	-82.6889	4.6555	.2899	-2.2470	3.2919
15	1.2126	.8499	4.6067	3.0578	-81.7625	4.4481	.3098	-2.1199	3.1453
16	1.2279	.8966	4.2843	2.9220	-80.7732	4.2862	.3312	-2.0195	3.0190
17	1.2430	.9429	4.1259	2.8149	-79.8069	4.0980	.3583	-1.9415	2.8977
18	1.2581	.9885	3.9738	2.7231	-78.8669	3.9595	.3850	-1.8866	2.7998
19	1.2732	1.0334	3.8123	2.6216	-77.1725	3.8206	.4116	-1.8375	2.7016

ANGULAR LOCATION NO. 23, AT THETA = 90.0000 DEGREES

I	RP/D	S/RINF (PARALLEL)	S/RINF (PERP)	S/RINF (IN-PLANE)	S-ANGLE (IN-PLANE)	S/RINF (NORMAL)	SX/RINF (RESULTANT)	SY/RINF (RESULTANT)	SZ/RINF (RESULTANT)
1	1.3692	1.1539							
2	1.3844	1.2145	3.5172	1.1726	-144.3591	11.8723	-3.1469	-1.8661	8.3950
3	1.3995	1.2577	3.7415	2.2113	-146.2984	7.1832	-1.8891	-4.2099	5.0793
4	1.4146	1.3044	4.5946	4.3029	-147.7891	5.8294	-1.2965	-.9932	3.9826
5	1.4299	1.3738	3.6240	1.7525	-138.9333	4.8498	-.9363	-.8141	3.4293
6	1.5044	1.4370	3.3987	1.4204	-133.7244	4.3286	-.8942	-.7258	3.0688
7	1.5441	1.5157	3.2193	1.1903	-127.5793	4.0145	-.8132	-.6671	2.8877
8	1.5832	1.5787	2.9417	1.0300	-120.5963	3.7970	-.7307	-.6089	2.6899
9	1.6223	1.6369	2.7663	.9111	-112.9630	3.6526	-.6513	-.5431	2.5828
10	1.6615	1.7407	2.6534	.8274	-104.3051	3.5498	-.6146	-.5564	2.5101
11	1.7006	1.8837	2.5709	.7682	-95.5531	3.4850	-.6528	-.5427	2.4693
12	1.7397	1.9472	2.5202	.7392	-85.8723	3.4386	-.6376	-.5213	2.4414
13	1.7789	2.0307	2.4878	.7373	-75.2899	3.4192	-.6238	-.5005	2.4177
14	1.8180	2.1415	2.4593	.7604	-67.5293	3.4158	-.6023	-.4897	2.4034
15	1.8571	2.2884	2.4524	.7576	-59.3933	3.4262	-.5836	-.4793	2.4227
16	1.8963	2.3889	2.4456	.8376	-51.7832	3.4525	-.5689	-.4690	2.4413
17	1.9354	2.5223	2.4446	.9086	-44.9234	3.4900	-.5499	-.4607	2.4678
18	1.9745	2.6889	2.4489	.9694	-38.9013	3.5389	-.5335	-.4515	2.5024
19	2.0137	2.8821	2.4432	1.0402	-33.8877	3.5984	-.5162	-.4413	2.5430

ANGULAR LOCATION NO. 24, AT THETA = 90.0000 DEGREES

I	RP/D	S/RINF (PARALLEL)	S/RINF (PERP)	S/RINF (IN-PLANE)	S-ANGLE (IN-PLANE)	S/RINF (NORMAL)	SX/RINF (RESULTANT)	SY/RINF (RESULTANT)	SZ/RINF (RESULTANT)
1	1.3491	1.1443							
2	1.3642	1.1943	7.7661	4.6839	-151.7632	10.8083	-2.9163	-1.5700	7.8424
3	1.3792	1.2484	5.3287	2.9243	-148.1338	6.5661	-1.7585	-1.0112	4.8430
4	1.3943	1.2567	4.1933	2.0885	-144.2240	5.1983	-1.1981	-.8534	3.8744
5	1.5214	1.3194	3.5221	1.5807	-134.7697	4.4765	-.8932	-.7229	3.1639
6	1.5645	1.3844	3.1303	1.2785	-123.7249	4.0266	-.8239	-.6523	2.8672
7	1.6076	1.4552	2.6746	1.0080	-117.0528	3.7522	-.7454	-.6019	2.6532
8	1.6506	1.5314	2.7171	.9232	-109.2854	3.5697	-.6191	-.5595	2.5234
9	1.6937	1.6133	2.5728	.8176	-100.9357	3.4484	-.5068	-.5143	2.4384
10	1.7368	1.7016	2.4613	.7494	-91.2532	3.3707	-.4598	-.5197	2.3834
11	1.7799	1.7968	2.4151	.7034	-81.8848	3.3286	-.4045	-.4975	2.3466
12	1.8230	1.8992	2.3695	.6884	-70.6933	3.2954	-.3799	-.4873	2.3302
13	1.8660	2.0195	2.3428	.6983	-61.5558	3.2924	-.3562	-.4882	2.3261
14	1.9091	2.1281	2.3295	.7355	-52.1828	3.3035	-.2427	-.4900	2.3399
15	1.9522	2.2754	2.3311	.7869	-44.2423	3.3327	-.3251	-.4915	2.3505
16	1.9953	2.3920	2.3313	.8436	-36.9440	3.3742	-.4673	-.4939	2.3859
17	2.0384	2.5383	2.3372	.9186	-30.4137	3.4282	-.4946	-.4911	2.4291
18	2.0814	2.6946	2.3469	.9984	-24.8920	3.4919	-.3793	-.4910	2.4691
19	2.1245	2.8813	2.3530	1.0732	-20.3214	3.5676	-.6617	-.4916	2.5226

Figure A.2(1) - continued

APPENDIX A

ADDITIONAL AXIAL LOCATION NO. 1, AT R/D = -0.3332

I	R/D	R/RINF (PARALLEL)	R/RINF (PERP)	R/RINF (IN-PLANE)	R-ANGLE (IN-PLANE)	R/RINF (NORMAL)	R/RINF (RESULTANT)	R/RINF (RESULTANT)	R/RINF (RESULTANT)
1	1.3823	1.174	7.5038	4.5138	-1.573782	15.2705	-2.8292	-1.4835	7.2623
2	1.4050	1.1148	7.1878	2.8980	-1.497239	8.3951	-1.7138	-1.2421	4.4938
3	1.4497	1.1004	6.1878	2.0263	-1.443821	3.5824	-1.1807	-0.8112	3.3797
4	1.4993	1.0289	4.0804	1.5925	-1.430458	4.3898	-0.9307	-0.6959	3.0899
5	1.557	1.0127	3.4377	1.2388	-1.337162	3.4452	-0.8053	-0.632	2.7897
6	1.6247	1.0004	2.8174	0.9351	-1.258438	3.5841	-0.688	-0.557	2.6051
7	1.6991	1.0177	2.4444	0.651	-1.194109	3.5105	-0.5694	-0.4547	2.4823
8	1.7717	1.0564	2.1249	0.401	-1.134089	3.3907	-0.441	-0.384	2.4018
9	1.8493	1.0894	1.8355	0.234	-1.083043	3.2754	-0.3193	-0.287	2.3514
10	1.9299	1.1264	1.5740	0.078	-1.037821	3.1778	-0.2068	-0.203	2.3176
11	2.0127	1.1674	1.3316	0.029	-0.997319	3.0948	-0.1088	-0.110	2.2951
12	2.0983	1.2127	1.1040	0.009	-0.962015	3.0210	-0.057	-0.058	2.2859
13	2.1867	1.2621	0.8980	0.001	-0.931233	2.9578	-0.013	-0.018	2.2872
14	2.2779	1.3153	0.7130	0.000	-0.904910	2.9051	0.003	-0.003	2.2906
15	2.3719	1.3724	0.5497	0.000	-0.883210	2.8627	0.016	-0.022	2.2979
16	2.4683	1.4334	0.4080	0.000	-0.865445	2.8300	0.030	-0.030	2.3080
17	2.5671	1.4984	0.2869	0.000	-0.851930	2.8064	0.045	-0.045	2.3203
18	2.6683	1.5674	0.1919	0.000	-0.842030	2.7917	0.061	-0.061	2.3345
19	2.7719	1.6404	0.1247	0.000	-0.835200	2.7857	0.078	-0.078	2.3505

ADDITIONAL AXIAL LOCATION NO. 2, AT R/D = -0.3334

I	R/D	R/RINF (PARALLEL)	R/RINF (PERP)	R/RINF (IN-PLANE)	R-ANGLE (IN-PLANE)	R/RINF (NORMAL)	R/RINF (RESULTANT)	R/RINF (RESULTANT)	R/RINF (RESULTANT)
1	1.3751	1.1528	7.2744	4.3070	-1.584384	9.8832	-2.7526	-1.4433	6.9743
2	1.4194	1.1000	6.1878	2.7805	-1.497024	8.1788	-1.6788	-1.0988	4.9894
3	1.4830	1.0282	4.0940	1.9044	-1.443821	4.9481	-1.1392	-0.6215	3.4938
4	1.5604	1.0000	3.3557	1.4888	-1.433224	4.2713	-0.8042	-0.513	3.0024
5	1.6429	1.0129	2.6994	1.0271	-1.330939	3.5895	-0.5872	-0.400	2.7381
6	1.7297	1.0000	2.1249	0.715	-1.250942	3.5204	-0.471	-0.352	2.6020
7	1.8199	1.0180	1.8355	0.477	-1.190724	3.4504	-0.354	-0.237	2.4840
8	1.9127	1.0574	1.5740	0.235	-1.130942	3.3805	-0.231	-0.160	2.4040
9	2.0083	1.0977	1.3355	0.078	-1.084893	3.3207	-0.108	-0.087	2.3519
10	2.1067	1.1380	1.1040	0.029	-1.040109	3.2705	-0.023	-0.018	2.3114
11	2.2079	1.1804	0.8980	0.009	-1.000078	3.2273	0.007	-0.014	2.2821
12	2.3119	1.2254	0.7130	0.001	-0.964898	3.1900	0.016	-0.018	2.2634
13	2.4183	1.2724	0.5497	0.000	-0.933210	3.1578	0.029	-0.022	2.2500
14	2.5271	1.3224	0.4080	0.000	-0.904445	3.1300	0.045	-0.030	2.2400
15	2.6383	1.3754	0.2869	0.000	-0.878210	3.1064	0.061	-0.045	2.2303
16	2.7519	1.4324	0.1919	0.000	-0.854930	3.0867	0.078	-0.078	2.2205
17	2.8683	1.4934	0.1247	0.000	-0.834200	3.0705	0.094	-0.094	2.2105
18	2.9871	1.5584	0.0800	0.000	-0.815930	3.0577	0.110	-0.110	2.2003
19	3.1083	1.6274	0.0497	0.000	-0.800200	3.0485	0.127	-0.127	2.1905

ADDITIONAL AXIAL LOCATION NO. 3, AT R/D = -0.3339

I	R/D	R/RINF (PARALLEL)	R/RINF (PERP)	R/RINF (IN-PLANE)	R-ANGLE (IN-PLANE)	R/RINF (NORMAL)	R/RINF (RESULTANT)	R/RINF (RESULTANT)	R/RINF (RESULTANT)
1	1.7891	1.0402	6.4000	4.4723	-1.780804	2.6548	-1.6412	-0.1217	1.8771
2	1.9174	1.0000	5.2782	3.9977	-1.700802	1.7587	-0.9708	-0.2230	1.2438
3	2.0694	0.9104	4.0400	3.1767	-1.647808	1.4424	-0.2253	-0.1421	0.6196
4	2.2449	0.8002	2.8951	2.2100	-1.617105	1.1097	-0.1203	-0.0847	0.2861
5	2.4449	0.6700	1.8900	1.2933	-1.600920	1.2506	-0.0528	-0.0206	0.0895
6	2.6694	0.5301	1.1249	0.8041	-1.600308	1.2483	-0.0102	-0.0098	0.0027
7	2.9189	0.3871	0.6037	0.3809	-1.600494	1.2757	0.0497	-0.0041	0.0011
8	3.1927	0.2417	0.2102	0.2277	-1.600440	1.3389	0.0947	-0.0035	0.0011
9	3.4914	0.0904	0.0000	0.0007	-1.600380	1.4328	0.1472	-0.0023	0.0000
10	3.8149	0.0000	0.0000	0.0000	-1.600340	1.5589	0.2010	-0.0000	0.0000
11	4.1649	0.0000	0.0000	0.0000	-1.600215	1.6844	0.2641	-0.0000	0.0000
12	4.5497	0.0000	0.0000	0.0000	-1.600077	1.8084	0.3394	-0.0001	0.0000
13	4.9691	0.0000	0.0000	0.0000	-1.600000	1.9401	0.4270	-0.0000	0.0000
14	5.4244	0.0000	0.0000	0.0000	-1.600000	2.0804	0.5237	-0.0000	0.0000
15	5.9169	0.0000	0.0000	0.0000	-1.600000	2.2304	0.6389	-0.0000	0.0000
16	6.4469	0.0000	0.0000	0.0000	-1.600000	2.3904	0.7682	-0.0000	0.0000
17	7.0149	0.0000	0.0000	0.0000	-1.600000	2.5604	0.9082	-0.0000	0.0000
18	7.6291	0.0000	0.0000	0.0000	-1.600000	2.7404	1.0582	-0.0000	0.0000
19	8.2891	0.0000	0.0000	0.0000	-1.600000	2.9304	1.2182	-0.0000	0.0000

ADDITIONAL AXIAL LOCATION NO. 4, AT R/D = -0.3373

I	R/D	R/RINF (PARALLEL)	R/RINF (PERP)	R/RINF (IN-PLANE)	R-ANGLE (IN-PLANE)	R/RINF (NORMAL)	R/RINF (RESULTANT)	R/RINF (RESULTANT)	R/RINF (RESULTANT)
1	1.7740	1.0001	6.4000	4.5020	-1.780802	2.5820	-1.6870	0.1228	1.8203
2	1.9174	0.9104	5.2782	3.9985	-1.700802	1.7189	-0.9196	-0.2279	1.2140
3	2.0694	0.8002	4.0400	3.1767	-1.647808	1.4095	-0.2383	-0.1398	0.6097
4	2.2449	0.6700	2.8951	2.2100	-1.617105	1.1010	-0.1383	-0.0800	0.2800
5	2.4449	0.5301	1.8900	1.2933	-1.600920	1.2507	-0.0504	-0.0202	0.0897
6	2.6694	0.3871	1.1249	0.8041	-1.600308	1.2481	-0.0121	-0.0098	0.0027
7	2.9189	0.2417	0.6037	0.3809	-1.600494	1.2757	0.0497	-0.0041	0.0011
8	3.1927	0.0904	0.2102	0.2277	-1.600440	1.3389	0.0947	-0.0035	0.0011
9	3.4914	0.0000	0.0000	0.0007	-1.600380	1.4328	0.1472	-0.0023	0.0000
10	3.8149	0.0000	0.0000	0.0000	-1.600340	1.5589	0.2010	-0.0000	0.0000
11	4.1649	0.0000	0.0000	0.0000	-1.600215	1.6844	0.2641	-0.0000	0.0000
12	4.5497	0.0000	0.0000	0.0000	-1.600077	1.8084	0.3394	-0.0001	0.0000
13	4.9691	0.0000	0.0000	0.0000	-1.600000	1.9401	0.4270	-0.0000	0.0000
14	5.4244	0.0000	0.0000	0.0000	-1.600000	2.0804	0.5237	-0.0000	0.0000
15	5.9169	0.0000	0.0000	0.0000	-1.600000	2.2304	0.6389	-0.0000	0.0000
16	6.4469	0.0000	0.0000	0.0000	-1.600000	2.3904	0.7682	-0.0000	0.0000
17	7.0149	0.0000	0.0000	0.0000	-1.600000	2.5604	0.9082	-0.0000	0.0000
18	7.6291	0.0000	0.0000	0.0000	-1.600000	2.7404	1.0582	-0.0000	0.0000
19	8.2891	0.0000	0.0000	0.0000	-1.600000	2.9304	1.2182	-0.0000	0.0000

Figure A.2(j) - continued

VELOCITY AND TEMPERATURE CONTOURS *****

12 VELOCITY (TEMPERATURE) CONTOUR LINES FOUND

11 POINTS IN CONTOUR LINE OF VELOCITY * 0.000 TOTAL * 22.120

X	Y
0.000	0.000
0.000	0.000
0.000	0.000
0.000	0.000
0.000	0.000
0.000	0.000
0.000	0.000
0.000	0.000
0.000	0.000
0.000	0.000
0.000	0.000
0.000	0.000
0.000	0.000
0.000	0.000
0.000	0.000

11 POINTS IN CONTOUR LINE OF VELOCITY * 0.000 TOTAL * 22.120

X	Y
0.000	0.000
0.000	0.000
0.000	0.000
0.000	0.000
0.000	0.000
0.000	0.000
0.000	0.000
0.000	0.000
0.000	0.000
0.000	0.000
0.000	0.000
0.000	0.000
0.000	0.000
0.000	0.000
0.000	0.000

DENSITY CONTOURS *****

14 DENSITY CONTOUR LINES FOUND

9 POINTS IN CONTOUR LINE OF DENSITY * 0.000

X	Y
0.000	0.000
0.000	0.000
0.000	0.000
0.000	0.000
0.000	0.000
0.000	0.000
0.000	0.000
0.000	0.000
0.000	0.000

**MICROFILMED FROM
BEST AVAILABLE COPY**

APPENDIX A

24 POINTS IN CONTOUR LINE OF $\rho H_0 / \rho H_0 \sin \theta = 4.000$

X/D	Y/D
.9483	.3072
.94817	.3078
.9704	.3776
.9885	.4881
1.0039	.5932
1.0189	.6983
1.0344	.74.47
1.0500	.8476
1.0651	.9477
1.0807	.9886
1.1071	.9777
1.1184	.9828
1.1298	.9458
1.1518	.8882
1.1559	.8281
1.1785	.718
1.1874	.6441
1.1939	.5755
1.2111	.5019
1.2205	.4250

MAGNETIC FIELD CONTOURS *****

12 MAGNETIC FIELD CONTOUR LINES FOUND
(FROM COMPONENT ALONG FIELD LINES PARALLEL TO FLOW IN FREESTREAM)

13 POINTS IN CONTOUR LINE OF $\rho H_0 / \rho H_0 \sin \theta$ (PARALLEL) = .500

X/D	Y/D
.9786	.2183
.9954	.2228
1.0173	.2344
1.0298	.2433
1.0473	.2692
1.0714	.2954
.9844	.3189
1.0831	.3405
1.0988	.3713
1.1110	.3983
1.1176	.4191
1.1272	.4448
1.1277	.4671

14 POINTS IN CONTOUR LINE OF $\rho H_0 / \rho H_0 \sin \theta$ (PARALLEL) = .750

X/D	Y/D
.9513	.3484
.9884	.3437
.9885	.3491
1.0141	.3716
1.0122	.3889
1.0222	.3942
1.0403	.3776
1.0589	.3604
1.0781	.3445
1.0911	.3721
1.0973	.3831
1.1188	.3408
1.1384	.3118
1.1427	.2815
1.1788	.2691
1.1744	.2834
1.1767	.3108
1.1883	.3425
1.1832	.3677

Figure A.2(1) - continued

12 MAGNETIC FIELD CONTOUR LINES FOUND
(FOR COMPONENT ALONG FIELD LINES PERPENDICULAR TO FLOW IN FREESTREAM)

49 POINTS IN CONTOUR LINE OF δ/BIN (PERPENDICULAR) = 2.220

X/D	X/D
-1.8978	1.7899
-1.8527	1.7957
-1.7655	1.8142
-1.6250	1.8220
-1.5257	1.8283
-1.4627	1.8243
-1.4035	1.8241
-1.3439	1.8394
-1.2804	1.8434
-1.2087	1.8467
-1.1279	1.8498
-1.0704	1.8425
-0.9803	1.8440
-0.8404	1.8436
-0.7441	1.8469
-0.6105	1.8403
-0.7138	1.8480
-0.6906	1.8460
-0.6514	1.8505
-0.6051	1.8559
-0.5420	1.8621
-0.5626	1.8632
-0.5392	1.8720
-0.4657	1.8877
-0.4830	1.8882
-0.4322	1.8946
-0.4277	1.8920
-0.3885	1.8947
-0.3700	1.8967
-0.3651	1.8969
-0.3555	2.02345
-0.3838	2.0097
-0.3708	2.01363
-0.3845	2.01324
-0.4257	2.0221
-0.4321	2.02404
-0.4344	2.0274
-0.4657	2.0331
-0.4807	2.03974
-0.4392	2.04094
-0.4200	2.04003
-0.4140	2.0517
-0.4081	2.0431
-0.4091	2.0517
-0.7037	2.0567

6 POINTS IN CONTOUR LINE OF δ/BIN (PERPENDICULAR) = 2.000

X/D	X/D
-2.0673	1.0000
-3.4232	1.0113
-4.1710	1.0300
-4.4214	1.0194
-4.6004	1.0701
-4.7775	1.0803

Figure A.2(m) - concluded

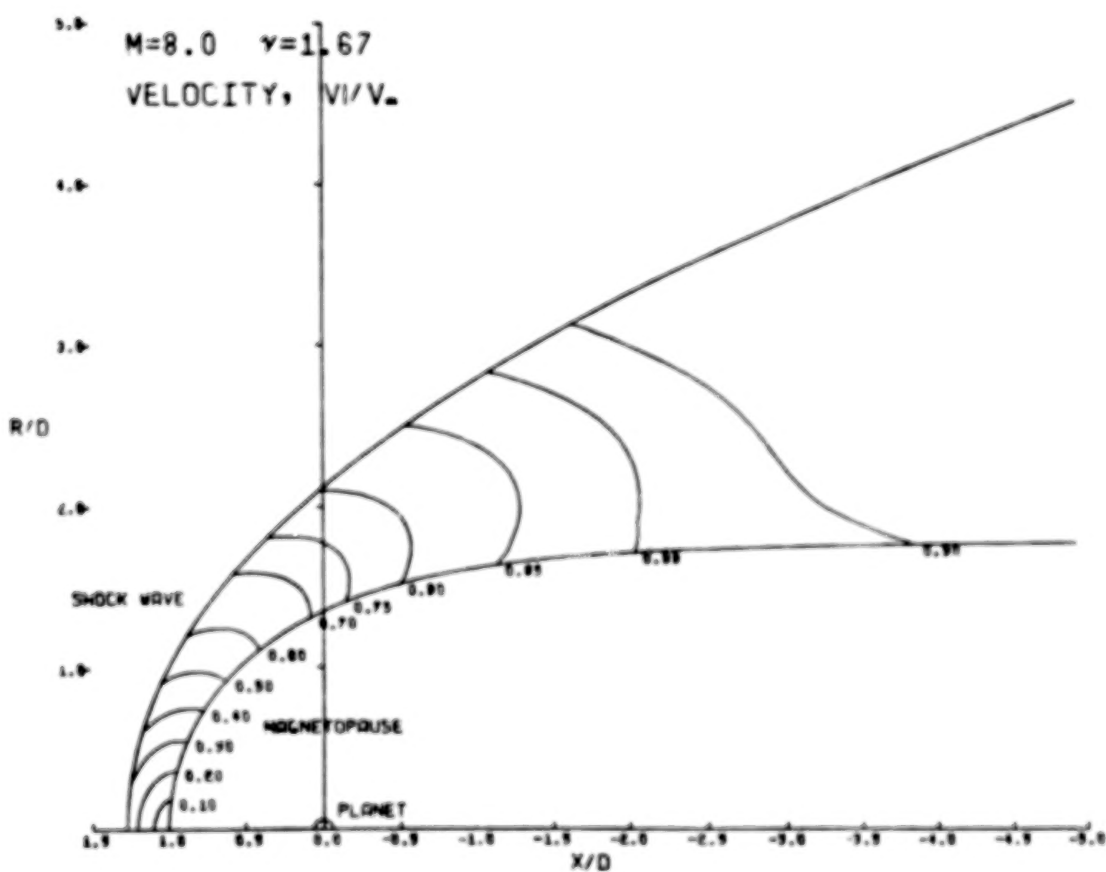
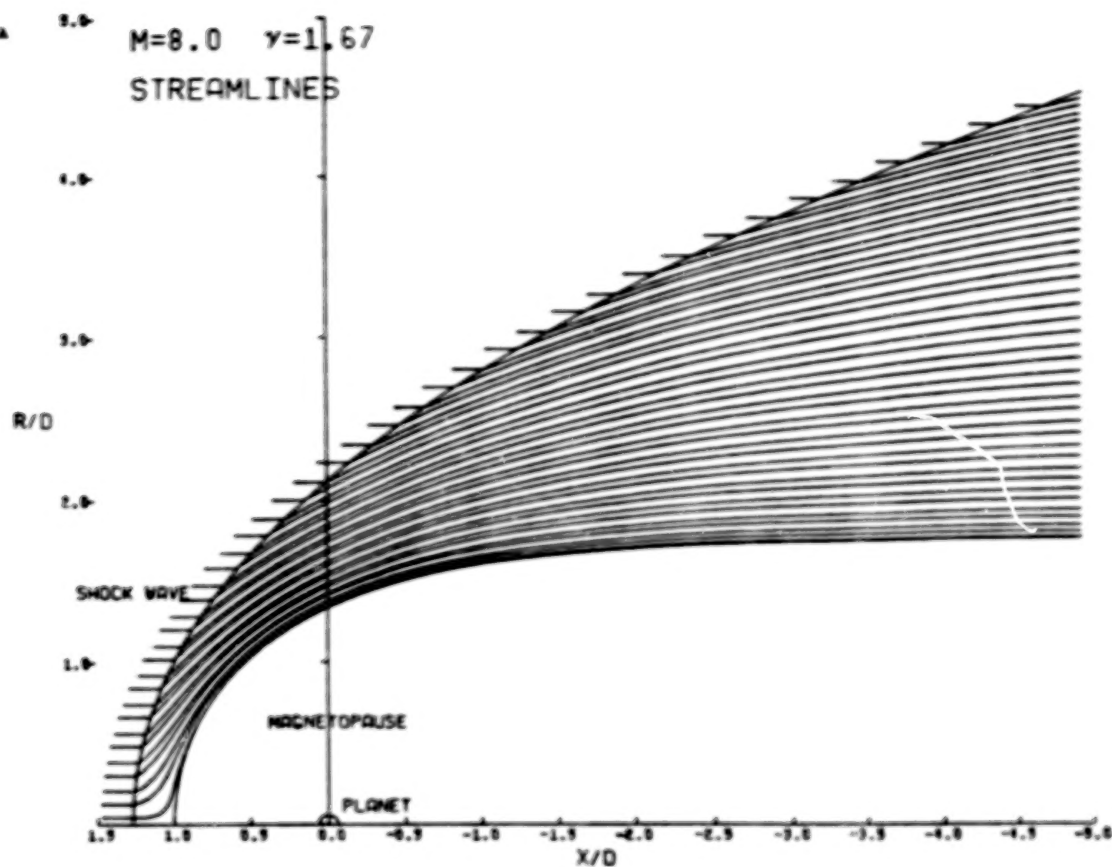


Figure A.3. - Plot output for sample case.

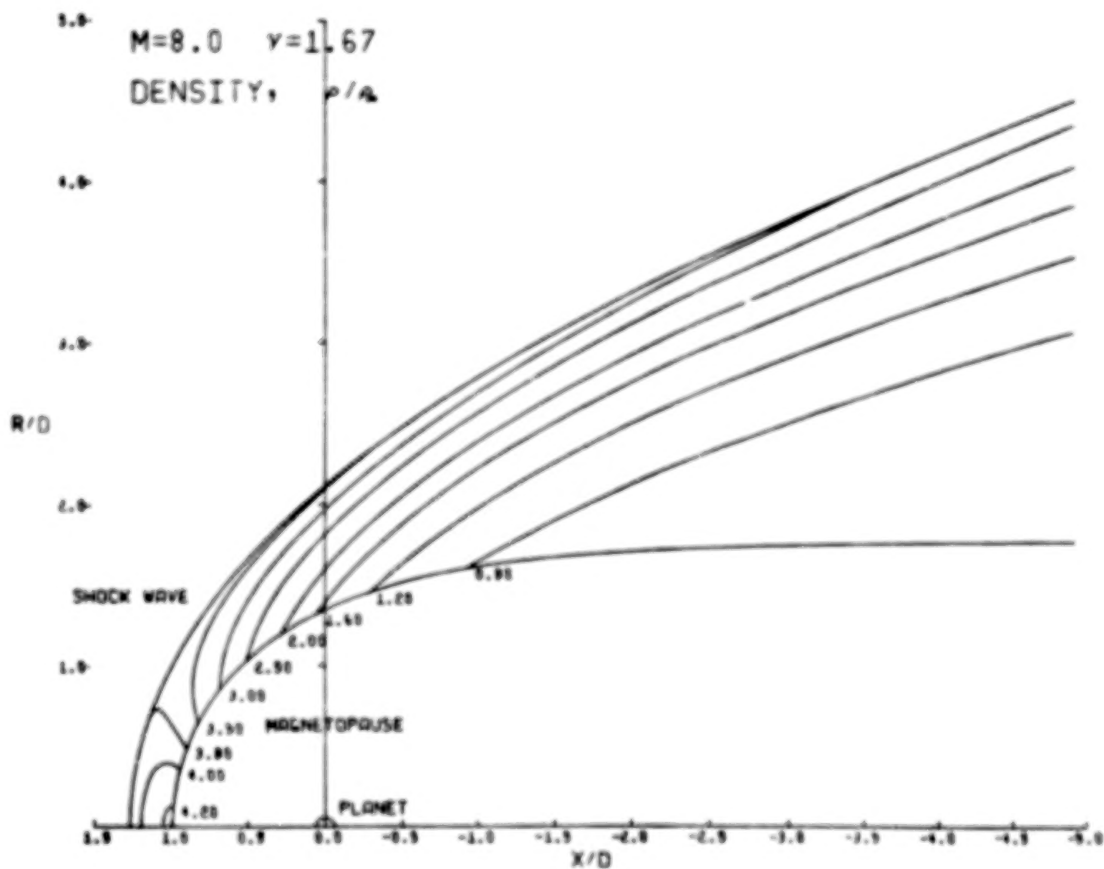
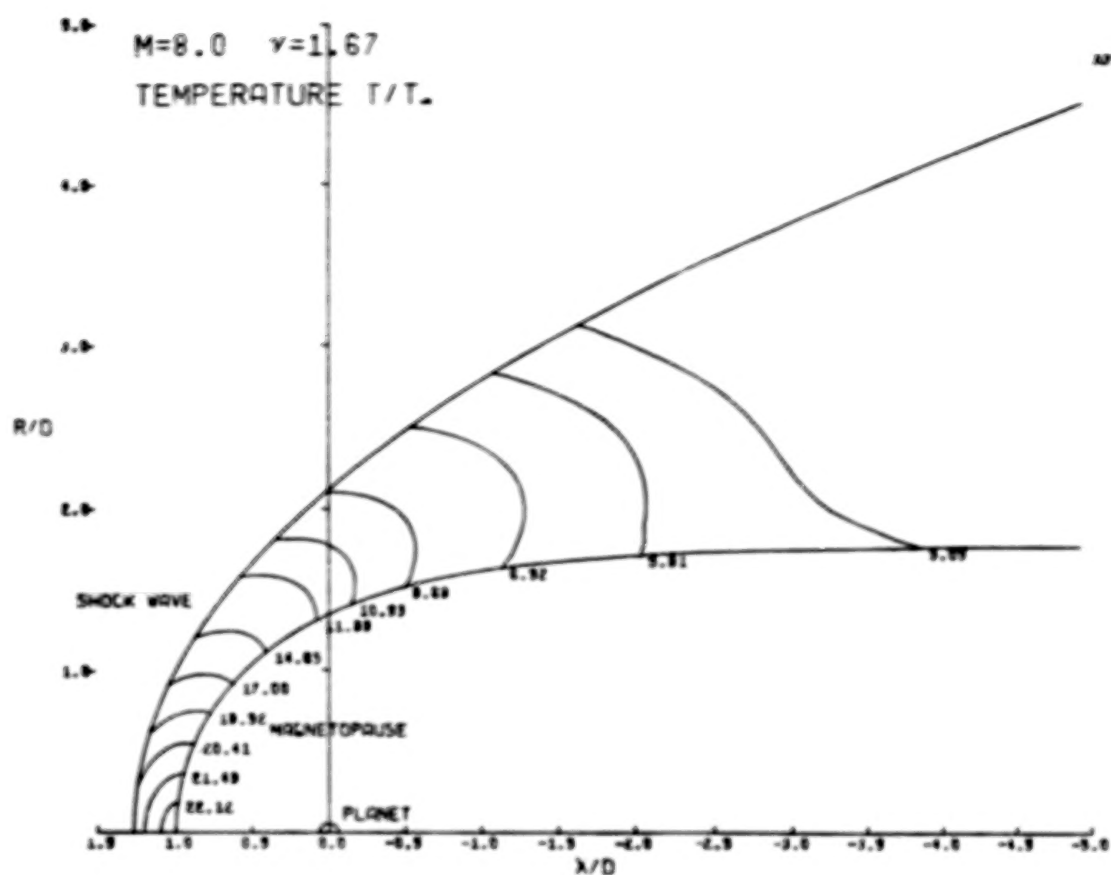


Figure A.3. - Continued.

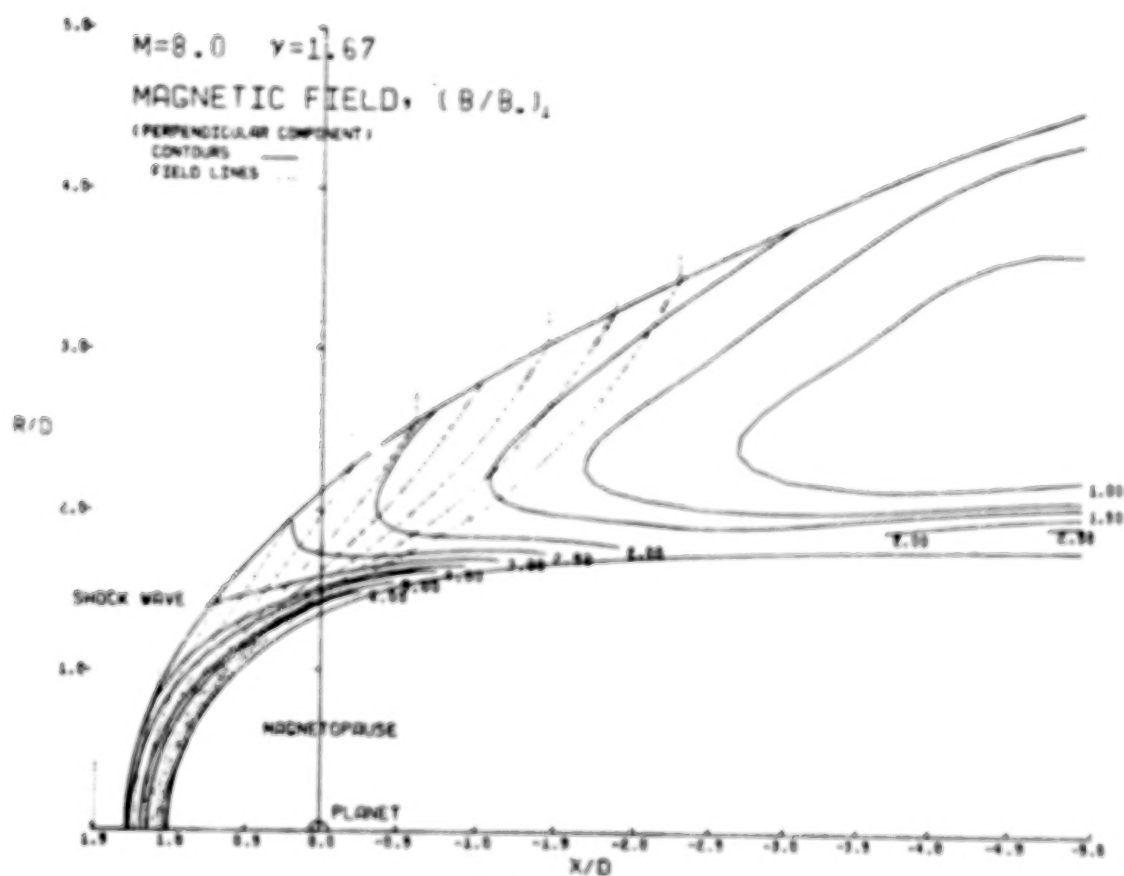
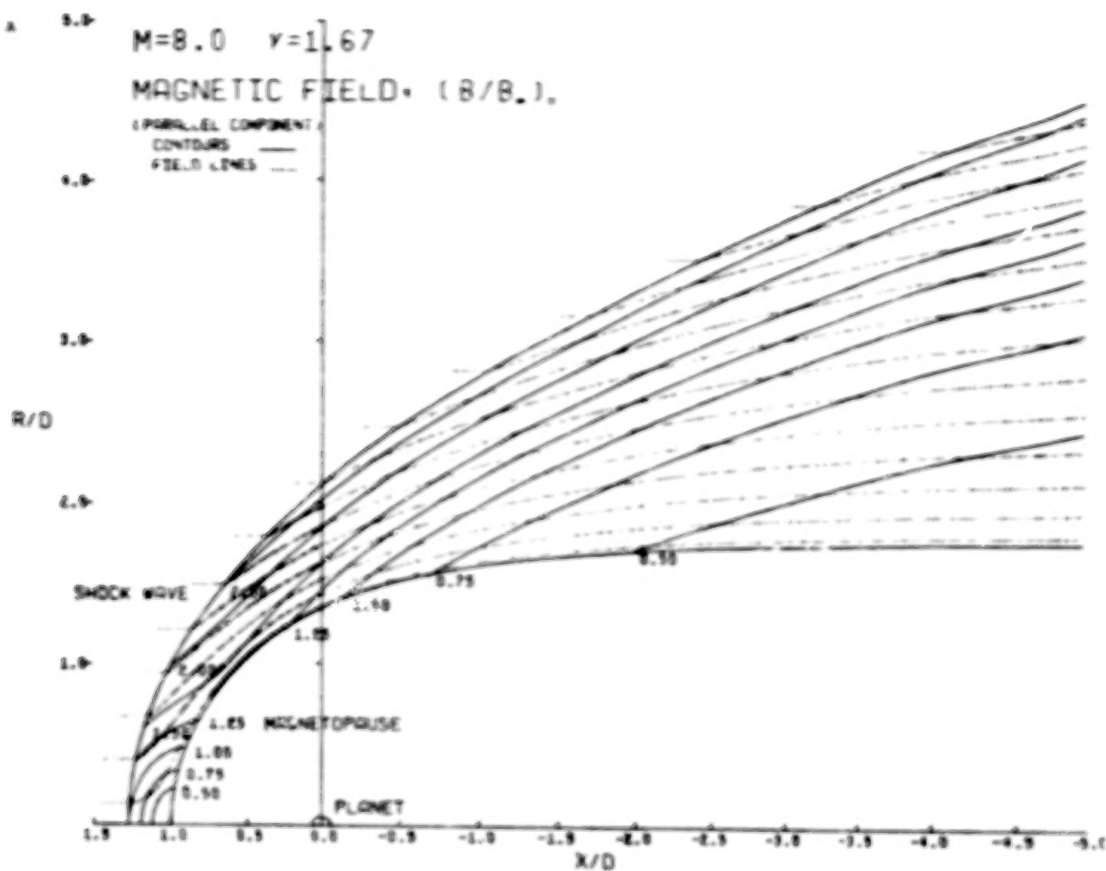


Figure A.3. - Concluded.

BLANK PAGE

BLANK PAGE

LISTING OF COMPUTER PROGRAM

BCOMP	32
BCOMP	33
BCOMP	34
BCOMP	35
BCOMP	36
BCOMP	37
BCOMP	38
BCOMP	39
BCOMP	40
BCOMP	41
BCOMP	42
BCOMP	43
BCOMP	44
BELGAN	2
BVAL	2
BVAL	3
BVAL	4
DISTRN	2
STREAM	2
STREAM	3
S-WCKTS	2
BELGAN	7
BELGAN	8
BELGAN	9
BELGAN	10
BELGAN	11
BELGAN	12
BELGAN	13
BELGAN	14
BELGAN	15
BELGAN	16
BELGAN	17
BELGAN	18
BELGAN	19
BELGAN	20
BELGAN	21
BELGAN	22
BELGAN	23
BELGAN	24
BELGAN	25
BELGAN	26
BELGAN	27
BELGAN	28
BELGAN	29
BELGAN	30
BELGAN	31
BELGAN	32
BELGAN	33
BELGAN	34
BELGAN	35
BELGAN	36
BELGAN	37
BELGAN	38
BELGAN	39
BELGAN	40
BELGAN	41
BELGAN	42
BELGAN	43
BELGAN	44
BELGAN	45
BELGAN	46
BELGAN	47
BELGAN	48
BELGAN	49
BELGAN	50
BELGAN	51
BELGAN	52
BELGAN	53
BELGAN	54
BELGAN	55
BELGAN	56
BELGAN	57
BELGAN	58
BELGAN	59
BELGAN	60
BELGAN	61
BELGAN	62
BELGAN	63
BELGAN	64
BELGAN	65
BELGAN	66
BELGAN	67
BELGAN	68

[illegible][illegible]

BUCHSAL	9
BUCHSAL	10
BUCHSAL	11
BUCHSAL	12
BUCHSAL	13
BUCHSAL	14
BUCHSAL	15
BUCHSAL	16
BUCHSAL	17
BUCHSAL	18
BUCHSAL	19
BUCHSAL	20
BUCHSAL	21
BUCHSAL	22
BUCHSAL	23
BUCHSAL	24
BUCHSAL	25
BUCHSAL	26
BUCHSAL	27
BUCHSAL	28
BUCHSAL	29
BUCHSAL	30
BUCHSAL	31
BUCHSAL	32
BUCHSAL	33
BUCHSAL	34
BUCHSAL	35
BUCHSAL	36
BUCHSAL	37
BUCHSAL	38
BUCHSAL	39
BUCHSAL	40
BUCHSAL	41
BUCHSAL	42
BUCHSAL	43
BUCHSAL	44
BUCHSAL	45
BUCHSAL	46
BUCHSAL	47
BUCHSAL	48
BUCHSAL	49
BUCHSAL	50
BUCHSAL	51
BUCHSAL	52
BUCHSAL	53
BUCHSAL	54
BUCHSAL	55
BUCHSAL	56
BUCHSAL	57
BUCHSAL	58
BUCHSAL	59
BUCHSAL	60
BUCHSAL	61
BUCHSAL	62
BUCHSAL	63
BUCHSAL	64
BUCHSAL	65
BUCHSAL	66
BUCHSAL	67
BUCHSAL	68
BUCHSAL	69
BUCHSAL	70
BUCHSAL	71
BUCHSAL	72
BUCHSAL	73
BUCHSAL	74
BUCHSAL	75
BUCHSAL	76
BUCHSAL	77
BUCHSAL	78
BUCHSAL	79
BUCHSAL	80
BUCHSAL	81
BUCHSAL	82
BUCHSAL	83
BUCHSAL	84
BUCHSAL	85
BUCHSAL	86
BUCHSAL	87
BUCHSAL	88
BUCHSAL	89
BUCHSAL	90
BUCHSAL	91
BUCHSAL	92
BUCHSAL	93
BUCHSAL	94
BUCHSAL	95
BUCHSAL	96
BUCHSAL	97
BUCHSAL	98
BUCHSAL	99
BUCHSAL	100
BUCHSAL	101
BUCHSAL	102
BUCHSAL	103
BUCHSAL	104
BUCHSAL	105
BUCHSAL	106
BUCHSAL	107
BUCHSAL	108
BUCHSAL	109
BUCHSAL	110
BUCHSAL	111
BUCHSAL	112
BUCHSAL	113
BUCHSAL	114
BUCHSAL	115
BUCHSAL	116
BUCHSAL	117
BUCHSAL	118
BUCHSAL	119
BUCHSAL	120
BUCHSAL	121
BUCHSAL	122
BUCHSAL	123
BUCHSAL	124
BUCHSAL	125
BUCHSAL	126
BUCHSAL	127
BUCHSAL	128
BUCHSAL	129
BUCHSAL	130
BUCHSAL	131
BUCHSAL	132
BUCHSAL	133
BUCHSAL	134
BUCHSAL	135
BUCHSAL	136
BUCHSAL	137
BUCHSAL	138
BUCHSAL	139
BUCHSAL	140
BUCHSAL	141
BUCHSAL	142
BUCHSAL	143
BUCHSAL	144
BUCHSAL	145
BUCHSAL	146
BUCHSAL	147
BUCHSAL	148
BUCHSAL	149
BUCHSAL	150
BUCHSAL	151
BUCHSAL	152
BUCHSAL	153
BUCHSAL	154
BUCHSAL	155
BUCHSAL	156
BUCHSAL	157
BUCHSAL	158
BUCHSAL	159
BUCHSAL	160
BUCHSAL	161
BUCHSAL	162
BUCHSAL	163
BUCHSAL	164
BUCHSAL	165
BUCHSAL	166
BUCHSAL	167
BUCHSAL	168
BUCHSAL	169
BUCHSAL	170
BUCHSAL	171
BUCHSAL	172
BUCHSAL	173
BUCHSAL	174
BUCHSAL	175
BUCHSAL	176
BUCHSAL	177
BUCHSAL	178
BUCHSAL	179
BUCHSAL	180
BUCHSAL	181
BUCHSAL	182
BUCHSAL	183
BUCHSAL	184
BUCHSAL	185
BUCHSAL	186
BUCHSAL	187
BUCHSAL	188
BUCHSAL	189
BUCHSAL	190
BUCHSAL	191
BUCHSAL	192
BUCHSAL	193
BUCHSAL	194
BUCHSAL	195
BUCHSAL	196
BUCHSAL	197
BUCHSAL	198

COWT#	110
COWT#	111
COWT#	112
COWT#	113
COWT#	114
COWT#	115
COWT#	116
COWT#	117
COWT#	118
COWT#	119
COWT#	120
COWT#	121
COWT#	122
COWT#	123
COWT#	124
COWT#	125
COWT#	126
COWT#	127
COWT#	128
COWT#	129
COWT#	130
COWT#	131
COWT#	132
COWT#	133
COWT#	134
COWT#	135
COWT#	136
COWT#	137
COWT#	138
COWT#	139
COWT#	140
COWT#	141
COWT#	142
COWT#	143
COWT#	144
COWT#	145
COWT#	146
COWT#	147
COWT#	148
COWT#	149
COWT#	150
COWT#	151
COWT#	152
COWT#	153
COWT#	154
COWT#	155
COWT#	156
COWT#	157
COWT#	158
COWT#	159
COWT#	160
COWT#	161
COWT#	162
COWT#	163
COWT#	164
COWT#	165
COWT#	166
COWT#	167
COWT#	168
COWT#	169
COWT#	170
COWT#	171
COWT#	172
COWT#	173
COWT#	174
COWT#	175
COWT#	176
COWT#	177
COWT#	178
COWT#	179
COWT#	180
COWT#	181
COWT#	182
COWT#	183
COWT#	184
COWT#	185
COWT#	186
COWT#	187
COWT#	188
COWT#	189
COWT#	190
COWT#	191
COWT#	192
COWT#	193
COWT#	194
COWT#	195
COWT#	196
COWT#	197
COWT#	198
COWT#	199
COWT#	200

[illegible][illegible][illegible]

CUNTOR	1
CUNTOR	1
CUNTOR	1
CUNTOR	1
CUNTOR	1
BIN	1
BCOMPS	1
BCOMPS	1
BCOMPS	1
CUNTOR	1
CUNTOR	1
BVAL	1
NVAL	1
BVAL	1
CUNTOR	1
CUNTOR	1

[illegible]

00000	2
00001	3
00002	4
00003	5
00004	6
00005	7
00006	8
00007	9
00008	10
00009	11
00010	12
00011	13
00012	14
00013	15
00014	16
00015	17
00016	18
00017	19

**MICROFILMED FROM
BEST AVAILABLE COPY**

TABLE OF CONTENTS

<u>Section</u>	<u>Page No.</u>
LIST OF ILLUSTRATIONS	iv 1/A6
LIST OF TABLES	v 1/A7
SUMMARY	1 1/A8
INTRODUCTION	1 1/A8
LIST OF SYMBOLS	3 1/A10
ANALYSIS	7 1/A14
General Considerations	7 1/A14
Mathematical Representation of Solar Wind-Magneto/Ionosphere Interaction	8 1/B1
Magnetic Planet - Determination of the Magnetosphere Boundary	11 1/B4
Nonmagnetic Planet - Determination of the Ionosphere Boundary	16 1/B9
Calculation of the Gasdynamic Flow Properties	19 1/B12
Calculation of the Magnetic Field	26 1/C5
RESULTS AND DISCUSSION	29 1/C8
CONCLUDING REMARKS	32 1/C11
APPENDIX A - COMPUTER PROGRAM USER'S MANUAL	34 1/C13
APPENDIX B - LISTING OF COMPUTER PROGRAM	73 1/G1
REFERENCES	107 2/G1
TABLE 1	110 2/E4
FIGURES 1 THROUGH 15	113 2/E10

TRANSF1	2
TRANSF1	3
TRANSF1	4
TRANSF1	5
TRANSF1	6
FLOW	12
DUSTM	2
FLOW	14
FLOW	15
FLOW	17
FLOW	18
FLOW	19
FLOW	24
FLOW	26
FLOW	27
FLOW	28
FLOW	29
FLOW	30
FLOW	31
FLOW	32
FLOW	33
FLOW	34
FLOW	35
FLOW	36
FLOW	37
FLOW	38
FLOW	39
FLOW	40
FLOW	41
FLOW	42
FLOW	43
FLOW	44
FLOW	45
FLOW	46
FLOW	47
FLOW	48
FLOW	49
FLOW	50
FLOW	51
FLOW	52
FLOW	53
FLOW	54
FLOW	55
FLOW	56
FLOW	57
FLOW	58
FLOW	59
FLOW	60
FLOW	61
FLOW	62
FLOW	63
FLOW	64
FLOW	65
FLOW	66
FLOW	67
FLOW	68
FLOW	69
FLOW	70
FLOW	71
FLOW	72
FLOW	73
FLOW	74
FLOW	75
FLOW	76
FLOW	77
FLOW	78
FLOW	79
FLOW	80
FLOW	81
FLOW	82
FLOW	83
FLOW	84
FLOW	85
FLOW	86
FLOW	87
FLOW	88
FLOW	89
FLOW	90

FLOWB	91
FLOWB	92
FLOWB	93
FLOWB	94
FLOWB	97
FLOWB	96
FLOWB	97
FLOWM	2
FLOWM	3
FLOWM	4
FLOWM	5
FLOWM	8
FLOWM	8
TRANSF	2
TRANSF1	3
TRANSF1	4
TRANSF1	5
TRANSF1	5
FLOWM	10
DNSTAM	2
FLOWM	12
FLOWM	13
FLOWM	14
FLOWM	15
FLOWM	16
FLOWM	17
FLOWM	18
FLOWM	19
FLOWM	20
FLOWM	21
FLOWM	22
FLOWM	23
FLOWM	24
FLOWM	25
FLOWM	26
FLOWM	27
FLOWM	28
FLOWM	29
FLOWM	29
FLOWM	31
FLOWM	32
FLOWM	33
FLOWM	34
FLOWM	35
FLOWM	36
FLOWM	38
FLOWM	37
FLOWM	39
FLOWM	40
FLOWM	41
FLOWM	42
FLOWM	43
FLOWM	44
FLOWM	45
FLOWM	46
FLOWM	47
FLOWM	48
FLOWM	49
FLOWM	50
FLOWM	51
FLOWM	52
FLOWM	53
FLOWM	54
FLOWM	55
FLOWM	56
FLOWM	57
FLOWM	58
FLOWM	59
FLOWM	60
FLOWM	61
FLOWM	62
FLOWM	63
FLOWM	64
FLOWM	65
FLOWM	66
FLOWM	67
FLOWM	68
FLOWM	69
FLOWM	70
FLOWM	71
FLOWM	72
FLOWM	72

WITH OUT INPUT AND DEFAULT VALUES TO BE USED

```

100 FORMAT(3A11)
110 FORMAT(4F10.0,2I10,F4.0,3I10)
120 FORMAT(3A11)
130 FORMAT(3F10.0)
140 FORMAT(11C)
150 FORMAT(11L/(2F10.))
160 FORMAT(4F10.0)

C
730 FORMAT(1M//25A,3A10////5A,10M//1P V#7 /45L//25A,10I10//)

```

INPUT	52
INPUT	53
INPUT	54
INPUT	55
INPUT	56
INPUT	57
INPUT	58
INPUT	59
INPUT	60
INPUT	61
INPUT	62
INPUT	63
INPUT	64
INPUT	65
INPUT	66
INPUT	67
INPUT	68
INPUT	69
INPUT	70
INPUT	71
INPUT	72
INPUT	73
INPUT	74
INPUT	75
INPUT	76
INPUT	77
INPUT	78
INPUT	79
INPUT	80
INPUT	81
INPUT	82
INPUT	83
INPUT	84
INPUT	85

```

SUBROUTINE LAB1
  THIS ROUTINE ELIMINATES OVERLAP IN PLOTTING A
  SET OF CONTOUR LABELS.

  COMMON /LABLS/ XLAB(50),YLAB(50),CX(50),CY(50),LAB(50),LAB
  COMMON /DCAL/ XSF,YSF,XMAX,YMAX,XLNGTH,YLNGTH

  SORT THE ARRAY LAB INTO ASCENDING ORDER. CHANGE
  THE ORDER OF LAB AND CY TO CORRESPOND.

  CALL BUBBL

  FIND FIRST LABEL FROM SORTED ARRAY THAT IS ABOVE X=XB(0)
  DO I=XB(0),NEL
    IF(YLAB(I).LT.Y) GO TO 3
    XMIN=X
    GO TO 4
  3 CONTINUE

  NO LABELS FOUND ABOVE X-AXIS. BAD SET OF CONTOUR VALUES
  SPECIFIED. STOP PROGRAM.

  WRITE(X,ZL)
  DO FORMAT(1=2,10+*****),10X,UNREASONABLE TO LABEL CONTOUR LINES BEC
  CAUSE OF OVERLAP,10X,10+*****
  STOP

10 LAB(I)=XMIN
  LAB=I
  IF(NEL=0) RETURN

  EXAMINE ALL LABELS BEYOND LABEL XMIN FOR OVERLAP.

  X=J
  XMIN=XMIN+1
  DO IS=1+XMIN,NEL
    IF(YLAB(IS).LT.YLAB(XMIN)+.77YSF,AND(XLAB(IS).LT.XLAB(XMIN)
    +.4XSF) GO TO 15

  SAVE ARRAY INDEX FOR LABEL TO BE PLOTTED.

  XMIN=I
  ILM(I)=I
  NLAB=N
  X=X+1
20 CONTINUE

  INSURE THAT THE LAST LABEL IS PLOTTED.

  ILM(NLAB)=NEL

```

△△△△△	2
△△△△△	3
△△△△△	4
△△△△△	5
△△△△△	6
△△△△△	7
△△△△△	8
△△△△△	9
△△△△△	10
△△△△△	11
△△△△△	12
△△△△△	13
△△△△△	14
△△△△△	15
△△△△△	16
△△△△△	17
△△△△△	18
△△△△△	19
△△△△△	20
△△△△△	21
△△△△△	22
△△△△△	23
△△△△△	24
△△△△△	25
△△△△△	26
△△△△△	27
△△△△△	28
△△△△△	29
△△△△△	30
△△△△△	31
△△△△△	32
△△△△△	33
△△△△△	34
△△△△△	35
△△△△△	36
△△△△△	37
△△△△△	38
△△△△△	39
△△△△△	40
△△△△△	41
△△△△△	42
△△△△△	43
△△△△△	44
△△△△△	45
△△△△△	46
△△△△△	47
△△△△△	48
△△△△△	49
△△△△△	50
△△△△△	51
△△△△△	52
△△△△△	53
△△△△△	54

**MICROFILMED FROM
BEST AVAILABLE COPY**

BLANK PAGE

BLANK PAGE

MAR	163
MAR	165
MAR	176
MAR	171
MAR	172
MAR	173
MAR	174
MAR	175
MAR	176
MAR	177
MAR	178
MAR	179
MAR	180
MAR	181
MAR	182
MAR	183
MAR	184
MAR	185
MAR	186
MAR	187
MAR	188
MAR	189
MAR	190
MAR	191
MAR	192
MAR	193
MAR	194
MAR	195
MAR	196
MAR	197
MAR	198
MAR	199
MAR	200
MAR	201
MAR	202
MAR	203
MAR	204
MAR	205
MAR	206
MAR	207
MAR	208
MAR	209
MAR	210
MAR	211
MAR	212
MAR	213
MAR	214
MAR	215
MAR	216
MAR	217
MAR	218
MAR	219
MAR	220
MAR	221
MAR	222
MAR	223
MAR	224
MAR	225
MAR	226
MAR	227
MAR	228
MAR	229
MAR	230
MAR	231
MAR	232
MAR	233
MAR	234
MAR	235
MAR	236
MAR	237
MAR	238
MAR	239
MAR	240
MAR	241
MAR	242
MAR	243
MAR	244
MAR	245
MAR	246
MAR	247
MAR	248
MAR	249
MAR	250
MAR	251
MAR	252

```

100 IF (XJDE*ZCZD) GO TO 40
C
C      NO MAX A POINTS. ENTER IT IN THE TABLE.
      NODP=NDP+1
      IF (XJDE*GT*ISIZZ) GO TO 30
      ND(1)=NODP
      CALL -NTRK(KODCZ,ZCZD,XVAL,AL,AZ,DMIN,KMIN,ICM,KOD,X,Y,XY,AC)
      *      ISIZZ)
      IF (XJDE*LCZD) GO TO 70
      NAD(NDP)=NXY
C
C      NO MAX THE LENGTH OF THE LINE.
      NODP=NDP+2
      NODP=2
      NXY51=NXY
      JS=4
      K=K+K
100 CALL -WALKER(BD,ZCZD,XVAL,DMIN,ICM,KMIN,DMAX,KMIN,KMAX,KOD,NXY,
      *      PCNT,KODCZ,X,Y,NXY,ISIZZ)
      IF (XJDE*LCZD) GO TO 70
      IF (XJDE*LCZD) GO TO 30
C
C      IF THIS LINE IS A CLOSED CURVE, CLOSE IT BY ENTERING FIRST
C      POINT AGAIN.
      I1ST=SUBT((X(NXY51)-X(NXY))**2+(Y(NXY51)-Y(NXY))**2)
      IF (I1ST*GT*1e-4) GO TO 40
      NXY=NXY+1
      IF (NXY*GT*ISIZZ) GO TO 60
      X(NXY)=X(NXY51)
      Y(NXY)=Y(NXY51)
      ICM(1,NXY)=ICM(1,NXY51)
      ICM(2,NXY)=ICM(2,NXY51)
      ICM(3,NXY)=ICM(3,NXY51)
      ICM(4,NXY)=ICM(4,NXY51)
C
C      CONTINUE
40 CONTINUE
40 CONTINUE
C
C      ENTER END OF LAST LINE IN BOOKKEEPING ARRAYS.
      NXY=NXY+1
      NEUP=NADP+1
      IF (NEUP*GT*ISIZZ) GO TO 30
      NAD(NEUP)=NXY
      GO TO 30
C
C      WRITE ERROR MESSAGES.
30 WRITE(12,100)
100 FORMAT(7HCONTINUED SEARCH ABORTED - TABLE OVERFLOW IN NAD)
      NAD(1)=ISIZZ
      GO TO 30
C
C      WRITE(12,100)
100 FORMAT(14HCONTINUED SEARCH ABORTED - TABLE OVERFLOW IN (X,Y))
C
C      WRITE(12,100)
GO TO 70
100 FORMAT(14HCONTINUED SEARCH ABORTED - TABLE OVERFLOW IN (X,Y))
C
C      RETURN
END
C
SUBROUTINE PLOTCH
C
C      THIS ROUTINE CONTROLS THE DRAWING OF THE PLOTS
C      OCC PLOT SUBROUTINES CALLED ARE
C      DASHENPLT,PLOT.
C
C      IPLOT = 1 FOR VELOCITY CONTOUR PLOT
C      IPLOT = 2 FOR DENSITY CONTOUR PLOT
C      IPLOT = 3 FOR STREAMLINE PLOT
C
C      LEVEL Z,X,Y,YUT,NUM,NST
C      COMMON/COMMON/ XOD(100),YOD(100),XSHK(100),YSHK(100),NMAX,
1      *      NMIN,AMAX,AMIN,AMAX,AMIN,NMIN
C      COMMON/PLUTCH/ X(100),Y(100),CVAL(30),NAD(30),IPLOT
C      COMMON /SCALE/ XSF,YSF,XMAX,YMAX,XLENGTH,YLENGTH
C      COMMON/STRAFM/ XST(30),YST(30),YST(30),NUM(50),NST
C
C      * PLOT STREAMLINES
C      THE FIRST CALL TO PLOT INITIALIZES THE PLOT.
C      SCALE FACTORS ARE EQUAL TO 1.

```

MAP	253
MAP	254
MAP	255
MAP	256
MAP	257
MAP	258
MAP	259
MAP	260
MAP	261
MAP	262
MAP	263
MAP	264
MAP	265
MAP	266
MAP	267
MAP	268
MAP	269
MAP	270
MAP	271
MAP	272
MAP	273
MAP	274
MAP	275
MAP	276
MAP	277
MAP	278
MAP	279
MAP	280
MAP	281
MAP	282
MAP	283
MAP	284
MAP	285
MAP	286
MAP	287
MAP	288
MAP	289
MAP	290
MAP	291
MAP	292
MAP	293
MAP	294
MAP	295
MAP	296
MAP	297
MAP	298
MAP	299
MAP	300
MAP	301
MAP	302
MAP	303
MAP	304
MAP	305
MAP	306
MAP	307
MAP	308
MAP	309
MAP	310
MAP	311
MAP	312
MAP	313
MAP	314
MAP	315
PLOTCH	2
PLOTCH	3
PLOTCH	4
PLOTCH	5
PLOTCH	6
PLOTCH	7
PLOTCH	8
PLOTCH	9
PLOTCH	10
PLOTCH	11
PLOTCH	12
PLOTCH	13
PLOTCH	14
PLOTCH	15
SCALE	2
PLOTCH	17
PLOTCH	18
PLOTCH	19
PLOTCH	20
PLOTCH	21
PLOTCH	22


```

30 CONTINUE
  AZERO=AZIDE
  CALL XTRF
  RETURN

PRINT LWRUP MSG: IF TAPE4 IS NOT THE SAME CASE AS
SPECIFIED IN CARD INPUT - PROGRAM IS STOPPED

100 WRITE (10,1000) AMAC,LCAM,HK0,AMACH,LCAM,HK0
100 FORMAT(1H1,1X,14H*,2X,20HEX:CUION TERMINATED 2X,14H*/2X,1
  * 34H*RUN DATA ON TAPE4 DOES NOT AGREE/2X,20HEX:ITH CASE
  * 24H*SPECIFIED ON CARD INPUT/2X,14H*NO DATA SINGARMA,5X
  * 4H*/H//42X,14H*JM CARD//14X,F4.4/12X,14H*FROM TAPE4
  * 24X,F4.4//
  .
STOP
END

```

```

FUNCTION RINF(I,J)
C
C THIS ROUTINE CALCULATES R/RINF AT THE (I,J) GRID POINT
C
COMMON/EGGUP/ XMOD(100),YMOD(100),XSMK(100),YSMK(100),NXMAX,
1      NZMAX,AMACM,GAM,MWU,NHINDX
COMMON/LCUT/ KVCJN,VCON(20),KCLUP,KCON(20),ACIZU,100,YCIZU,100,
*  YFIZC,100,XKFIZC,100)
      LEVIL 20 XJ1=KSTXNUM,NST
COMMON /STR/LM/ XJ1(50,100),RST(50,100),NUM(50),N01
C
C IF POINT IS ON SHOCK BOUNDARY R/RINF=1.0
C
      IF (I.EQ.1) NXMAX .AND. J.GT.1) GO TO 10
      RINF=1.0
      RETURN
C
C BACK:1 POINT BY TWO STREAMLINES
C
10 CONTINUE
  X=XC(I,J)
  Y=YC(I,J)
  RZ=0.0
  DO 20 JST=J,NST
    NR=NUM(JST)
    DO 30 K=1,NR
      IF (XST(JST,K).GT. X) GO TO 40
30 CONTINUE
      K=NR
40 CONTINUE
      J2=JST
      J1=JST-1
      R1=R2
      IF (X.EQ.1) R2=XST(J2,1)
      IF (Y.GT.1) R2=XJ1(J2,K-1)*(X-XST(J2,K-1))/(XST(J2,K)-
*  XST(J2,K-1))+XST(J2,K-1)
      IF (R2.GT. Y) GO TO 60
20 CONTINUE
60 IF (J2.EQ.1) GO TO 100
C
C INTERPOLATE FOR R/RINF
C
      RINF1=XST(J1,1)
70 RINF2=XST(J2,1)
      RRINF=Y/(RINF1*(RINF2-RINF1)+(Y-R1)/(R2-K1))
      RETURN
C
C USE SYMMETRY AXIS AND BODY FOR ZERO-TH STREAMLINE
C
100 CONTINUE
  IF (X.GT. -1.0) GO TO 110
  RRINF=1.0+Y/(K2*(K2/XST(1,1)-1.0))
  RETURN
110 DO 120 K=2,NZMAX
  IF (X.LT. XC(1,K)) GO TO 130
120 CONTINUE
130 K2=YC(1,K-1)*(X-XC(1,K-1))/(YC(1,K)-YC(1,K-1))/(XC(1,K)-XC(1,K-1))
  RINF1=0.0
  GO TO 70
END

```

```

SUBROUTINE SEARCH(J,K,K002,A,J01P,ICLK,NXY,NJ03,NVAL,AL,AZ,ACONT)
C
C   CONTOUR PROGRAMS MAP, WALK, SEARCH, ENTER, AND CHECK

```

K:RUN	97
K:RUN	98
K:RUN	99
K:RUN	100
K:RUN	101
K:RUN	102
K:RUN	103
K:RUN	104
K:RUN	105
K:RUN	106
K:RUN	107
K:RUN	108
K:RUN	109
K:RUN	110
K:RUN	111
K:RUN	112

RRINF	2
RRINF	3
RRINF	4
RRINF	5
RRINF	6
RRINF	7
RRINF	8
RRINF	9
STREAM	2
STREAM	3
RRINF	11
RRINF	12
RRINF	13
RRINF	14
RRINF	15
RRINF	16
RRINF	17
RRINF	18
RRINF	19

RR INF	21
RR INF	22
RR INF	23
RR INF	24
RR INF	25
RR INF	26
RR INF	27
RR INF	28
RR INF	29
RR INF	30
RR INF	31
RR INF	32
RR INF	33
RR INF	34
RR INF	35
RR INF	36
RR INF	37
RR INF	38
RR INF	39
RR INF	40
RR INF	41
RR INF	42
RR INF	43
RR INF	44
RR INF	45
RR INF	46
RR INF	47
RR INF	48
RR INF	49
RR INF	50
RR INF	51
RR INF	52
RR INF	53
RR INF	54
RR INF	55
RR INF	56
RR INF	57
RR INF	58
RR INF	59
RR INF	60

[illegible]

SEARCH	5
SEARCH	6
SEARCH	7
SEARCH	8
SEARCH	10
SEARCH	11
SEARCH	12
SEARCH	13
SEARCH	14
SEARCH	15
SEARCH	16
SEARCH	17
SEARCH	18
SEARCH	19
SEARCH	20
SEARCH	21
SEARCH	23
SEARCH	24
SEARCH	25
SEARCH	26
SEARCH	27
SEARCH	28
SEARCH	29
SEARCH	31
SEARCH	32
SEARCH	33
SEARCH	34
SEARCH	35
SEARCH	36
SEARCH	37
SEARCH	38
SEARCH	39
SEARCH	40
SEARCH	41

SETUP	2
SETUP	3
SETUP	4
SETUP	5
*SETUP	6
SETUP	7
SETUP	8
SETUP	10
SETUP	11
SETUP	12
SCALE	2
SETUP	14
SETUP	15
SETUP	16
SETUP	17
SETUP	18
SETUP	19
SETUP	20
SETUP	21
SETUP	23
SETUP	24
SETUP	25
SETUP	27
SETUP	28
SETUP	29
SETUP	36
SETUP	31
SETUP	32
SETUP	33
SETUP	34
SETUP	35
SETUP	36
SETUP	37
SETUP	39
SETUP	40
SETUP	41
SETUP	42
SETUP	43
SETUP	44
SETUP	45

800Y	59
800Y	60
800Y	61
800Y	62
800Y	63
800Y	64
800Y	65
800Y	66
800Y	67
800Y	68
800Y	69
800Y	70
800Y	71
800Y	72
800Y	73
800Y	74
800Y	75
800Y	76
800Y	77
800Y	78
800Y	79
800Y	80
800Y	81
800Y	82
800Y	83
800Y	84
800Y	85
800Y	86
800Y	87
800Y	88
800Y	89
800Y	90
800Y	91
800Y	92
800Y	93
800Y	94
800Y	95
800Y	96
800Y	97

BTNI	2
BTNI	2
CJMN	2
CJMN	3
ITNI	5
ITNI	6
STNI	7
STNI	8
STNI	9
STNI	10
STNI	11
STNI	12
STNI	13
STNI	14
STNI	15
STNI	16
STNI	17
STNI	18
STNI	19
STNI	20
STNI	21
STNI	22
STNI	23
STNI	24
STNI	25
STNI	26
STNI	27
STNI	28
STNI	29
STNI	30
STNI	31
STNI	32
STNI	33
STNI	34
STNI	35
STNI	36
STNI	37
STNI	38
STNI	39
STNI	40
STNI	41
STNI	42

01551P	2
COR1	2
COR1	3
COR1	4
COR2	4
COR2	4
COR3	2
01551P	6
01551P	7
01551P	8
01551P	9
01551P	10
01551P	11
01551P	12
01551P	13
01551P	14
01551P	15
01551P	16
01551P	17
01551P	18
01551P	19
01551P	20
01551P	21
01551P	22
01551P	23
01551P	24
01551P	25
01551P	26
01551P	27
01551P	28
01551P	29
01551P	30
01551P	31
01551P	32
01551P	33

```
EFCON      2
COM1       4
COM1       3
COM1       4
COM2       2
COM2       3
COM3       2
EFCON      0
```



```

OUTPUT 32
OUTPUT 53
OUTPUT 54
OUTPUT 55
OUTPUT 56
OUTPUT 57
OUTPUT 58
OUTPUT 59
OUTPUT 60
OUTPUT 61
OUTPUT 62
OUTPUT 63
OUTPUT 64
OUTPUT 65
OUTPUT 66
OUTPUT 67
OUTPUT 68
OUTPUT 69
OUTPUT 70
OUTPUT 71
OUTPUT 72
OUTPUT 73
OUTPUT 74
OUTPUT 75
OUTPUT 76
OUTPUT 77
OUTPUT 78
OUTPUT 79

```

RMS	2
CUM	2
CUM1	3
CUM2	4
CUM3	4
RMS	5
RMS	6
RMS	7
RMS	8
RMS	9
RMS	10
RMS	11
RMS	12
RMS	13
RMS	14
RMS	15
RMS	16
RMS	17
RMS	18
RMS	19
RMS	20
RMS	21
RMS	22
RMS	23
RMS	24
RMS	25
RMS	26
RMS	27
RMS	28
RMS	29
RMS	30

SHOCK	2
COM1	2
COM1	3
COM1	4
COM2	2
COM2	3
COM3	2
SHOCK	6
SHOCK	7
SHOCK	8
SHOCK	9
SHOCK	10
SHOCK	11
SHOCK	12
SHOCK	13
SHOCK	14
SHOCK	15
SHOCK	16
SHOCK	17
SHOCK	18
SHOCK	19

97

```

2 CONTINUE
4 CONTINUE
  WRITE(12,
    * 100)
  RETURN
5 CONTINUE
  WRITE(12,
    * 101)
  STOP
102 SUBROUTINE
  * 200-PA
103 SUBROUTINE
  * 300-PA
  * 400-PA
  * 500-PA
  * 600-PA
  * 700-PA
  * 800-PA
  * 900-PA
  * 1000-PA
  * 1100-PA
  * 1200-PA
  * 1300-PA
  * 1400-PA
  * 1500-PA
  * 1600-PA
  * 1700-PA
  * 1800-PA
  * 1900-PA
  * 2000-PA
  * 2100-PA
  * 2200-PA
  * 2300-PA
  * 2400-PA
  * 2500-PA
  * 2600-PA
  * 2700-PA
  * 2800-PA
  * 2900-PA
  * 3000-PA
  * 3100-PA
  * 3200-PA
  * 3300-PA
  * 3400-PA
  * 3500-PA
  * 3600-PA
  * 3700-PA
  * 3800-PA
  * 3900-PA
  * 4000-PA
  * 4100-PA
  * 4200-PA
  * 4300-PA
  * 4400-PA
  * 4500-PA
  * 4600-PA
  * 4700-PA
  * 4800-PA
  * 4900-PA
  * 5000-PA
  * 5100-PA
  * 5200-PA
  * 5300-PA
  * 5400-PA
  * 5500-PA
  * 5600-PA
  * 5700-PA
  * 5800-PA
  * 5900-PA
  * 6000-PA
  * 6100-PA
  * 6200-PA
  * 6300-PA
  * 6400-PA
  * 6500-PA
  * 6600-PA
  * 6700-PA
  * 6800-PA
  * 6900-PA
  * 7000-PA
  * 7100-PA
  * 7200-PA
  * 7300-PA
  * 7400-PA
  * 7500-PA
  * 7600-PA
  * 7700-PA
  * 7800-PA
  * 7900-PA
  * 8000-PA
  * 8100-PA
  * 8200-PA
  * 8300-PA
  * 8400-PA
  * 8500-PA
  * 8600-PA
  * 8700-PA
  * 8800-PA
  * 8900-PA
  * 9000-PA
  * 9100-PA
  * 9200-PA
  * 9300-PA
  * 9400-PA
  * 9500-PA
  * 9600-PA
  * 9700-PA
  * 9800-PA
  * 9900-PA
  * 10000-PA
  * 10100-PA
  * 10200-PA
  * 10300-PA
  * 10400-PA
  * 10500-PA
  * 10600-PA
  * 10700-PA
  * 10800-PA
  * 10900-PA
  * 11000-PA
  * 11100-PA
  * 11200-PA
  * 11300-PA
  * 11400-PA
  * 11500-PA
  * 11600-PA
  * 11700-PA
  * 11800-PA
  * 11900-PA
  * 12000-PA
  * 12100-PA
  * 12200-PA
  * 12300-PA
  * 12400-PA
  * 12500-PA
  * 12600-PA
  * 12700-PA
  * 12800-PA
  * 12900-PA
  * 13000-PA
  * 13100-PA
  * 13200-PA
  * 13300-PA
  * 13400-PA
  * 13500-PA
  * 13600-PA
  * 13700-PA
  * 13800-PA
  * 13900-PA
  * 14000-PA
  * 14100-PA
  * 14200-PA
  * 14300-PA
  * 14400-PA
  * 14500-PA
  * 14600-PA
  * 14700-PA
  * 14800-PA
  * 14900-PA
  * 15000-PA
  * 15100-PA
  * 15200-PA
  * 15300-PA
  * 15400-PA
  * 15500-PA
  * 15600-PA
  * 15700-PA
  * 15800-PA
  * 15900-PA
  * 16000-PA
  * 16100-PA
  * 16200-PA
  * 16300-PA
  * 16400-PA
  * 16500-PA
  * 16600-PA
  * 16700-PA
  * 16800-PA
  * 16900-PA
  * 17000-PA
  * 17100-PA
  * 17200-PA
  * 17300-PA
  * 17400-PA
  * 17500-PA
  * 17600-PA
  * 17700-PA
  * 17800-PA
  * 17900-PA
  * 18000-PA
  * 18100-PA
  * 18200-PA
  * 18300-PA
  * 18400-PA
  * 18500-PA
  * 18600-PA
  * 18700-PA
  * 18800-PA
  * 18900-PA
  * 19000-PA
  * 19100-PA
  * 19200-PA
  * 19300-PA
  * 19400-PA
  * 19500-PA
  * 19600-PA
  * 19700-PA
  * 19800-PA
  * 19900-PA
  * 20000-PA
  * 20100-PA
  * 20200-PA
  * 20300-PA
  * 20400-PA
  * 20500-PA
  * 20600-PA
  * 20700-PA
  * 20800-PA
  * 20900-PA
  * 21000-PA
  * 21100-PA
  * 21200-PA
  * 21300-PA
  * 21400-PA
  * 21500-PA
  * 21600-PA
  * 21700-PA
  * 21800-PA
  * 21900-PA
  * 22000-PA
  * 22100-PA
  * 22200-PA
  * 22300-PA
  * 22400-PA
  * 22500-PA
  * 22600-PA
  * 22700-PA
  * 22800-PA
  * 22900-PA
  * 23000-PA
  * 23100-PA
  * 23200-PA
  * 23300-PA
  * 23400-PA
  * 23500-PA
  * 23600-PA
  * 23700-PA
  * 23800-PA
  * 23900-PA
  * 24000-PA
  * 24100-PA
  * 24200-PA
  * 24300-PA
  * 24400-PA
  * 24500-PA
  * 24600-PA
  * 24700-PA
  * 24800-PA
  * 24900-PA
  * 25000-PA
  * 25100-PA
  * 25200-PA
  * 25300-PA
  * 25400-PA
  * 25500-PA
  * 25600-PA
  * 25700-PA
  * 25800-PA
  * 25900-PA
  * 26000-PA
  * 26100-PA
  * 26200-PA
  * 26300-PA
  * 26400-PA
  * 26500-PA
  * 26600-PA
  * 26700-PA
  * 26800-PA
  * 26900-PA
  * 27000-PA
  * 27100-PA
  * 27200-PA
  * 27300-PA
  * 27400-PA
  * 27500-PA
  * 27600-PA
  * 27700-PA
  * 27800-PA
  * 27900-PA
  * 28000-PA
  * 28100-PA
  * 28200-PA
  * 28300-PA
  * 28400-PA
  * 28500-PA
  * 28600-PA
  * 28700-PA
  * 28800-PA
  * 28900-PA
  * 29000-PA
  * 29100-PA
  * 29200-PA
  * 29300-PA
  * 29400-PA
  * 29500-PA
  * 29600-PA
  * 29700-PA
  * 29800-PA
  * 29900-PA
  * 30000-PA
  * 30100-PA
  * 30200-PA
  * 30300-PA
  * 30400-PA
  * 30500-PA
  * 30600-PA
  * 30700-PA
  * 30800-PA
  * 30900-PA
  * 31000-PA
  * 31100-PA
  * 31200-PA
  * 31300-PA
  * 31400-PA
  * 31500-PA
  * 31600-PA
  * 31700-PA
  * 31800-PA
  * 31900-PA
  * 32000-PA
  * 32100-PA
  * 32200-PA
  * 32300-PA
  * 32400-PA
  * 32500-PA
  * 32600-PA
  * 32700-PA
  * 32800-PA
  * 32900-PA
  * 33000-PA
  * 33100-PA
  * 33200-PA
  * 33300-PA
  * 33400-PA
  * 33500-PA
  * 33600-PA
  * 33700-PA
  * 33800-PA
  * 33900-PA
  * 34000-PA
  * 34100-PA
  * 34200-PA
  * 34300-PA
  * 34400-PA
  * 34500-PA
  * 34600-PA
  * 34700-PA
  * 34800-PA
  * 34900-PA
  * 35000-PA
  * 35100-PA
  * 35200-PA
  * 35300-PA
  * 35400-PA
  * 35500-PA
  * 35600-PA
  * 35700-PA
  * 35800-PA
  * 35900-PA
  * 36000-PA
  * 36100-PA
  * 36200-PA
  * 36300-PA
  * 36400-PA
  * 36500-PA
  * 36600-PA
  * 36700-PA
  * 36800-PA
  * 36900-PA
  * 37000-PA
  * 37100-PA
  * 37200-PA
  * 37300-PA
  * 37400-PA
  * 37500-PA
  * 37600-PA
  * 37700-PA
 
```

SHOCK	103
SHOCK	106
SHOCK	107
SHOCK	108
SHOCK	109
SHOCK	110
SHOCK	111
SHOCK	112
SHOCK	113
SHOCK	114
SHOCK	115
SHOCK	116
SHOCK	117
XIETAD	2
COM1	2
COM1	3
COM2	4
COM3	3
COM3	2
XIETAD	6
XIETAD	7
XIETAD	8
XIETAD	9
XIETAD	10
XIETAD	11
XIETAD	12
XIETAD	13
XIETAD	14
XIETAD	15
XIETAD	16
XIETAD	17
XIETAD	18
XIETAD	19
XIETAD	20
XIETAD	21
XIETAD	22
XIETAD	23
XIETAD	24
XIETAD	25
XIETAD	26
XIETAD	27
XIETAD	28
XIETAD	29
XIETAD	30
XIETAD	31
XIETAD	32
XIETAD	33
XIETAD	34
XIETAD	35
XIETAD	36
XIETAD	37
XIETAD	38
XIETAD	39
XIETAD	40
XIETAD	41
XIETAD	42
XIETAD	43
XIETAD	44
XIETAD	45
XIETAD	46
XIETAD	47
XIETAD	48
XIETAD	49
XIETAD	50
XIETAD	51
XIETAD	52
XIETAD	53
XIETAD	54
XIETAD	55
XIETAD	56
XIETAD	57
XIETAD	58
XIETAD	59
XIETAD	60
XIETAD	61
MARCH	2
CVARS	2
CVARS	3
CVARS	4

APPENDIX

PEARL	4
PEARL	3
PEARL	4
PEARL	5
PEARL	6
PEARL	7
PEARL	8
PEARL	9
PEARL	10
PEARL	11
PEARL	12
PEARL	13
PEARL	14
PEARL	15
PEARL	16
PEARL	17
PEARL	18
PEARL	19
PEARL	20
PEARL	21
PEARL	22
PEARL	23
PEARL	24
PEARL	25
PEARL	26
PEARL	27
PEARL	28
PEARL	29
PEARL	30
PEARL	31
PEARL	32
PEARL	33
PEARL	34
PEARL	35
PEARL	36
PEARL	37
PEARL	38
PEARL	39
PEARL	40
PEARL	41
PEARL	42

合司公限有	2
司公限有	2
司公限有	3
司公限有	4
司公限有	2
司公限有	3
司公限有	4
司公限有	5
司公限有	5
司公限有	7
司公限有	8
司公限有	9
司公限有	11
司公限有	16
司公限有	2
司公限有	3
司公限有	4
司公限有	5
司公限有	6
司公限有	7
司公限有	8
司公限有	9
司公限有	10
司公限有	11

1

[illegible]

MICROFILMED FROM
BEST AVAILABLE COPY


```

C..... CONST(4) = LAX DAMPING
C..... CONST(4) = 0, NO DAMPING
C..... CONST(4) = 0, 4TH ORDER DAMPING
C
C IFICONST(4) = 0, 2, 3, 11
C..... DISSIPATION TERM IN THE RADIAL DIRECTION
21 IF (J.LT.5) GO TO 7
  J = NT
  GO TO 1
7 J = 1
  GO TO 1
C J = J
6 DISSP = CONST(4) * (1.0 + 0.1 * (N,JD+2,K) * 0.1 * (N,JD-2,K) - 0.0 * (N,JD+1,K) -
  * 0.0 * (N,JD-1,K) + 0.0 * (N,JD,K))
  GO TO 2
21 CONTINUE
  IF (J.LT.4) AND (J.LT.NT) GO TO 5
  IF (J.LT.4) GO TO 7
  J = NT
  GO TO 1
7 J = 4
  GO TO 1
C J = J
5C DISSP = CONST(4) * (1.0 + 0.1 * (N,JD+2,K) * 0.1 * (N,JD-2,K) - 0.25 * (N,JD,K))
  GO TO 7
  DISSP = 0
C
C..... CONST(4) = LAX DAMPING
C..... CONST(4) = 0, NO DAMPING
C..... CONST(4) = 0, 4TH ORDER DAMPING
C
C IFICONST(4) = 0, 3, 11
C..... DISSIPATION TERM IN THE MERIDIONAL DIRECTION
31 CONTINUE
  IF (K.LT.4) AND (K.LT.NPH) GO TO 10
  IF (K.LT.4) GO TO 100
  K = NPH
  GO TO 1
10 K = 4
  GO TO 1
C K = K
5C DISSP = CONST(4) * (1.0 + 0.1 * (N,KD+1) * 0.1 * (N,KD-1) - 0.25 * (N,KD))
  GO TO 4
11 CONTINUE
  IF (K.LT.3) P(1,1) = P(1,3)
  IF (K.LT.3) P(1,2) = P(1,4)
  PF1 = ABS(P(1,K+2) - 2.0 * P(1,K+1) + P(1,K)) / (P(1,K+2) + 2.0 * P(1,K+1) + P(1,K))
  PF2 = ABS(P(1,K+1) - 2.0 * P(1,K) + P(1,K-1)) / (P(1,K+1) + 2.0 * P(1,K) + P(1,K-1))
  PF3 = ABS(P(1,K) - 2.0 * P(1,K-1) + P(1,K-2)) / (P(1,K) + 2.0 * P(1,K-1) + P(1,K-2))
  DISSP = 0.5 * (TA * (PF1 + PF2) * (N,JD+1) - 0.0 * (N,JD,K))
  * (PF2 + PF3) * (N,JD,K) - 1.0 * (N,JD,K-1)) * CONST(5)
  GO TO 4
3 DISSP = 0
4 DISSP = DISSP * DISSP
  RETURN
  END

SUBROUTINE EIGENM
  LEVEL 2, ETAMP, X0, F0, G0, MD
  COMMON /LAKU/ ET, PP(4,4,4), CD(4,2,4,4),
  * FU(4,2,4,4), G(4,2,4,4), H(4,2,4,4)
  LEVEL 2, PH0, P, U, V, W, R, Q, DZ, VINF, WINF, RDBP, RB, RBZ, RBPH, OTOP,
  * ACT, OTOT, OTOR, ACT, ICONST, GAM, CONST, NREGON, RS, RSZ, RSPH, RST, RSTZ,
  * RSPH1
  COMMON /PVARB/ RH0(2,4,4), P(2,4,4), U(2,4,4), V(2,4,4), W(2,4,4)
  * RH0(4,4), RH0Z(4,4), VINF(4,4), WINF(4,4),
  * RDBP(4,4), RB(4,4), RBZ(4,4), RBPH(4,4),
  * OTOP(2,4,4), ACT(4,4), OTOT(2,4,4), OTOR(4,4), ACT(4,4),
  * ICONST(4,4), GAM(4,4), CONST(4,4), NREGON, RS(4,4),
  * RSZ(4,4), RSPH1(4,4), RST(4,4), RSTZ(4,4), RSPH1(4,4)
  COMMON /ICVARB/ RH, ZTA(4,4), PHIP(4,4), DTIL(4,4), OTIL(4,4), UETA, TP(2,4)
  COMMON /SVARB/ T, Z, P4, D1, D2, UPHI, ZIN,
  * ZENL, P1, ALPHA, GAMMA, SIGMA, APACH, TAPE1,
  * TAPE2, DISK1, ALPH, DISK2, SIGM, NPHNT, DZDT,
  * DZDPH, ZM, THWD, TMLD, THW, TML, TTM,

```

```

DISSPM 27 * TTPL = Z, DZ, NPHI, N1, NPHI, N1TER,
DISSPM 28 * NPH1, NPH11, NPH12, NPH13, NPH14, NPH15, NPH16, NPH17,
DISSPM 29 * N1, N11, N12, N13, N14, N15, N16, N17,
DISSPM 30 * PHIF, MET400, LAG, N6C, PINT, N6JH, JINF,
DISSPM 31 * CINF, CASCOS, NPH1, NPH11,
DISSPM 32 INTOT = DISK1, DISK2, TAPE1, TAPE2,
DISSPM 33 COMMON /CLUST/ CLUST(4,4), DTIL(4,4), DTIL(4,4),
DISSPM 34 DIMENSION CLUST(4,4), DTIL(4,4),
DISSPM 35 * K4 = 1, 2, 3, 4, 5, 6, 7, 8, 9, 10, 11, 12, 13, 14, 15, 16, 17, 18, 19, 20, 21, 22, 23, 24, 25, 26, 27, 28, 29, 30, 31, 32, 33, 34, 35, 36, 37, 38, 39, 40, 41, 42, 43, 44, 45, 46, 47, 48, 49, 50, 51, 52, 53, 54, 55, 56, 57, 58, 59, 60, 61, 62, 63, 64, 65, 66, 67, 68, 69, 70, 71, 72, 73, 74, 75, 76, 77, 78, 79, 80, 81, 82, 83, 84, 85, 86, 87, 88, 89, 90, 91, 92, 93, 94, 95, 96, 97, 98, 99, 100, 101, 102, 103, 104, 105, 106, 107, 108, 109, 110, 111, 112, 113, 114, 115, 116, 117, 118, 119, 120, 121, 122, 123, 124, 125, 126, 127, 128, 129, 130, 131, 132, 133, 134, 135, 136, 137, 138, 139, 140, 141, 142, 143, 144, 145, 146, 147, 148, 149, 150, 151, 152, 153, 154, 155, 156, 157, 158, 159, 160, 161, 162, 163, 164, 165, 166, 167, 168, 169, 170, 171, 172, 173, 174, 175, 176, 177, 178, 179, 180, 181, 182, 183, 184, 185, 186, 187, 188, 189, 190, 191, 192, 193, 194, 195, 196, 197, 198, 199, 200, 201, 202, 203, 204, 205, 206, 207, 208, 209, 210, 211, 212, 213, 214, 215, 216, 217, 218, 219, 220, 221, 222, 223, 224, 225, 226, 227, 228, 229, 230, 231, 232, 233, 234, 235, 236, 237, 238, 239, 240, 241, 242, 243, 244, 245, 246, 247, 248, 249, 250, 251, 252, 253, 254, 255, 256, 257, 258, 259, 260, 261, 262, 263, 264, 265, 266, 267, 268, 269, 270, 271, 272, 273, 274, 275, 276, 277, 278, 279, 280, 281, 282, 283, 284, 285, 286, 287, 288, 289, 290, 291, 292, 293, 294, 295, 296, 297, 298, 299, 300, 301, 302, 303, 304, 305, 306, 307, 308, 309, 310, 311, 312, 313, 314, 315, 316, 317, 318, 319, 320, 321, 322, 323, 324, 325, 326, 327, 328, 329, 330, 331, 332, 333, 334, 335, 336, 337, 338, 339, 340, 341, 342, 343, 344, 345, 346, 347, 348, 349, 350, 351, 352, 353, 354, 355, 356, 357, 358, 359, 360, 361, 362, 363, 364, 365, 366, 367, 368, 369, 370, 371, 372, 373, 374, 375, 376, 377, 378, 379, 380, 381, 382, 383, 384, 385, 386, 387, 388, 389, 390, 391, 392, 393, 394, 395, 396, 397, 398, 399, 400, 401, 402, 403, 404, 405, 406, 407, 408, 409, 410, 411, 412, 413, 414, 415, 416, 417, 418, 419, 420, 421, 422, 423, 424, 425, 426, 427, 428, 429, 430, 431, 432, 433, 434, 435, 436, 437, 438, 439, 440, 441, 442, 443, 444, 445, 446, 447, 448, 449, 450, 451, 452, 453, 454, 455, 456, 457, 458, 459, 460, 461, 462, 463, 464, 465, 466, 467, 468, 469, 470, 471, 472, 473, 474, 475, 476, 477, 478, 479, 480, 481, 482, 483, 484, 485, 486, 487, 488, 489, 490, 491, 492, 493, 494, 495, 496, 497, 498, 499, 500, 501, 502, 503, 504, 505, 506, 507, 508, 509, 510, 511, 512, 513, 514, 515, 516, 517, 518, 519, 520, 521, 522, 523, 524, 525, 526, 527, 528, 529, 530, 531, 532, 533, 534, 535, 536, 537, 538, 539, 540, 541, 542, 543, 544, 545, 546, 547, 548, 549, 550, 551, 552, 553, 554, 555, 556, 557, 558, 559, 560, 561, 562, 563, 564, 565, 566, 567, 568, 569, 570, 571, 572, 573, 574, 575, 576, 577, 578, 579, 580, 581, 582, 583, 584, 585, 586, 587, 588, 589, 590, 591, 592, 593, 594, 595, 596, 597, 598, 599, 600, 601, 602, 603, 604, 605, 606, 607, 608, 609, 610, 611, 612, 613, 614, 615, 616, 617, 618, 619, 620, 621, 622, 623, 624, 625, 626, 627, 628, 629, 630, 631, 632, 633, 634, 635, 636, 637, 638, 639, 640, 641, 642, 643, 644, 645, 646, 647, 648, 649, 650, 651, 652, 653, 654, 655, 656, 657, 658, 659, 660, 661, 662, 663, 664, 665, 666, 667, 668, 669, 670, 671, 672, 673, 674, 675, 676, 677, 678, 679, 680, 681, 682, 683, 684, 685, 686, 687, 688, 689, 690, 691, 692, 693, 694, 695, 696, 697, 698, 699, 700, 701, 702, 703, 704, 705, 706, 707, 708, 709, 710, 711, 712, 713, 714, 715, 716, 717, 718, 719, 720, 721, 722, 723, 724, 725, 726, 727, 728, 729, 730, 731, 732, 733, 734, 735, 736, 737, 738, 739, 740, 741, 742, 743, 744, 745, 746, 747, 748, 749, 750, 751, 752, 753, 754, 755, 756, 757, 758, 759, 760, 761, 762, 763, 764, 765, 766, 767, 768, 769, 770, 771, 772, 773, 774, 775, 776, 777, 778, 779, 780, 781, 782, 783, 784, 785, 786, 787, 788, 789, 790, 791, 792, 793, 794, 795, 796, 797, 798, 799, 800, 801, 802, 803, 804, 805, 806, 807, 808, 809, 810, 811, 812, 813, 814, 815, 816, 817, 818, 819, 820, 821, 822, 823, 824, 825, 826, 827, 828, 829, 830, 831, 832, 833, 834, 835, 836, 837, 838, 839, 840, 841, 842, 843, 844, 845, 846, 847, 848, 849, 850, 851, 852, 853, 854, 855, 856, 857, 858, 859, 860, 861, 862, 863, 864, 865, 866, 867, 868, 869, 870, 871, 872, 873, 874, 875, 876, 877, 878, 879, 880, 881, 882, 883, 884, 885, 886, 887, 888, 889, 890, 891, 892, 893, 894, 895, 896, 897, 898, 899, 900, 901, 902, 903, 904, 905, 906, 907, 908, 909, 910, 911, 912, 913, 914, 915, 916, 917, 918, 919, 920, 921, 922, 923, 924, 925, 926, 927, 928, 929, 930, 931, 932, 933, 934, 935, 936, 937, 938, 939, 940, 941, 942, 943, 944, 945, 946, 947, 948, 949, 950, 951, 952, 953, 954, 955, 956, 957, 958, 959, 960, 961, 962, 963, 964, 965, 966, 967, 968, 969, 970, 971, 972, 973, 974, 975, 976, 977, 978, 979, 980, 981, 982, 983, 984, 985, 986, 987, 988, 989, 990, 991, 992, 993, 994, 995, 996, 997, 998, 999, 1000, 1001, 1002, 1003, 1004, 1005, 1006, 1007, 1008, 1009, 1010, 1011, 1012, 1013, 1014, 1015, 1016, 1017, 1018, 1019, 1020, 1021, 1022, 1023, 1024, 1025, 1026, 1027, 1028, 1029, 1030, 1031, 1032, 1033, 1034, 1035, 1036, 1037, 1038, 1039, 1040, 1041, 1042, 1043, 1044, 1045, 1046, 1047, 1048, 1049, 1050, 1051, 1052, 1053, 1054, 1055, 1056, 1057, 1058, 1059, 1060, 1061, 1062, 1063, 1064, 1065, 1066, 1067, 1068, 1069, 1070, 1071, 1072, 1073, 1074, 1075, 1076, 1077, 1078, 1079, 1080, 1081, 1082, 1083, 1084, 1085, 1086, 1087, 1088, 1089, 1090, 1091, 1092, 1093, 1094, 1095, 1096, 1097, 1098, 1099, 1100, 1101, 1102, 1103, 1104, 1105, 1106, 1107, 1108, 1109, 1110, 1111, 1112, 1113, 1114, 1115, 1116, 1117, 1118, 1119, 1120, 1121, 1122, 1123, 1124, 1125, 1126, 1127, 1128, 1129, 1130, 1131, 1132, 1133, 1134, 1135, 1136, 1137, 1138, 1139, 1140, 1141, 1142, 1143, 1144, 1145, 1146, 1147, 1148, 1149, 1150, 1151, 1152, 1153, 1154, 1155, 1156, 1157, 1158, 1159, 1160, 1161, 1162, 1163, 1164, 1165, 1166, 1167, 1168, 1169, 1170, 1171, 1172, 1173, 1174, 1175, 1176, 1177, 1178, 1179, 1180, 1181, 1182, 1183, 1184, 1185, 1186, 1187, 1188, 1189, 1190, 1191, 1192, 1193, 1194, 1195, 1196, 1197, 1198, 1199, 1200, 1201, 1202, 1203, 1204, 1205, 1206, 1207, 1208, 1209, 1210, 1211, 1212, 1213, 1214, 1215, 1216, 1217, 1218, 1219, 1220, 1221, 1222, 1223, 1224, 1225, 1226, 1227, 1228, 1229, 1230, 1231, 1232, 1233, 1234, 1235, 1236, 1237, 1238, 1239, 1240, 1241, 1242, 1243, 1244, 1245, 1246, 1247, 1248, 1249, 1250, 1251, 1252, 1253, 1254, 1255, 1256, 1257, 1258, 1259, 1260, 1261, 1262, 1263, 1264, 1265, 1266, 1267, 1268, 1269, 1270, 1271, 1272, 1273, 1274, 1275, 1276, 1277, 1278, 1279, 1280, 1281, 1282, 1283, 1284, 1285, 1286, 1287, 1288, 1289, 1290, 1291, 1292, 1293, 1294, 1295, 1296, 1297, 1298, 1299, 1300, 1301, 1302, 1303, 1304, 1305, 1306, 1307, 1308, 1309, 1310, 1311, 1312, 1313, 1314, 1315, 1316, 1317, 1318, 1319, 1320, 1321, 1322, 1323, 1324, 1325, 1326, 1327, 1328, 1329, 1330, 1331, 1332, 1333, 1334, 1335, 1336, 1337, 1338, 1339, 1340, 1341, 1342, 1343, 1344, 1345, 1346, 1347, 1348, 1349, 1350, 1351, 1352, 1353, 1354, 1355, 1356, 1357, 1358, 1359, 1360, 1361, 1362, 1363, 1364, 1365, 1366, 1367, 1368, 1369, 1370, 1371, 1372, 1373, 1374, 1375, 1376, 1377, 1378, 1379, 1380, 1381, 1382, 1383, 1384, 1385, 1386, 1387, 1388, 1389, 1390, 1391, 1392, 1393, 1394, 1395, 1396, 1397, 1398, 1399, 1400, 1401, 1402, 1403, 1404, 1405, 1406, 1407, 1408, 1409, 1410, 1411, 1412, 1413, 1414, 1415, 1416, 1417, 1418, 1419, 1420, 1421, 1422, 1423, 1424, 1425, 1426, 1427, 1428, 1429, 1430, 1431, 1432, 1433, 1434, 1435, 1436, 1437, 1438, 1439, 1440, 1441, 1442, 1443, 1444, 1445, 1446, 1447, 1448, 1449, 1450, 1451, 1452, 1453, 1454, 1455, 1456, 1457, 1458, 1459, 1460, 1461, 1462, 1463, 1464, 1465, 1466, 1467, 1468, 1469, 1470, 1471, 1472, 1473, 1474, 1475, 1476, 1477, 1478, 1479, 1480, 1481, 1482, 1483, 1484, 1485, 1486, 1487, 1488, 1489, 1490, 1491, 1492, 1493, 1494, 1495, 1496, 1497, 1498, 1499, 1500, 1501, 1502, 1503, 1504, 1505, 1506, 1507, 1508, 1509, 1510, 1511, 1512, 1513, 1514, 1515, 1516, 1517, 1518, 1519, 1520, 1521, 1522, 1523, 1524, 1525, 1526, 1527, 1528, 1529, 1530, 1531, 1532, 1533, 1534, 1535, 1536, 1537, 1538, 1539, 1540, 1541, 1542, 1543, 1544, 1545, 1546, 1547, 1548, 1549, 1550, 1551, 1552, 1553, 1554, 1555, 1556, 1557, 1558, 1559, 1560, 1561, 1562, 1563, 1564, 1565, 1566, 1567, 1568, 1569, 1570, 1571, 1572, 1573, 1574, 1575, 1576, 1577, 1578, 1579, 1580, 1581, 1582, 1583, 1584, 1585, 1586, 1587, 1588, 1589, 1590, 1591, 1592, 1593, 1594, 1595, 1596, 1597, 1598, 1599, 1600, 1601, 1602, 1603, 1604, 1605, 1606, 1607, 1608, 1609, 1610, 1611, 1612, 1613, 1614, 1615, 1616, 1617, 1618, 1619, 1620, 1621, 1622, 1623, 1624, 1625, 1626, 1627, 1628, 1629, 1630, 1631, 1632, 1633, 1634, 1635, 1636, 1637, 1638, 1639, 1640, 1641, 1642, 1643, 1644, 1645, 1646, 1647, 1648, 1649, 1650, 1651, 1652, 1653, 1654, 1655, 1656, 1657, 1658, 1659, 1660, 1661, 1662, 1663, 1664, 1665, 1666, 1667, 1668, 1669, 1670, 1671, 1672, 1673, 1674, 1675, 1676, 1677, 1678, 1679, 1680, 1681, 1682, 1683, 1684, 1685, 1686, 1687, 1688, 1689, 1690, 1691, 1692, 1693, 1694, 1695, 1696, 1697, 1698, 1699, 1700, 1701, 1702, 1703, 1704, 1705, 1706, 1707, 1708, 1709, 1710, 1711, 1712, 1713, 1714, 1715, 1716, 1717, 1718, 1719, 1720, 1721, 1722, 1723, 1724, 1725, 1726, 1727, 1728, 1729, 1730, 1731, 1732, 1733, 1734, 1735, 1736, 1737, 1738, 1739, 1740, 1741, 1742, 1743, 1744, 1745, 1746, 1747, 1748, 1749, 1750, 1751, 1752, 1753, 1754, 1755, 1756, 1757, 1758, 1759, 1760, 1761, 1762, 1763, 1764, 1765, 1766, 1767, 1768, 1769, 1770, 1771, 1772, 1773, 1774, 1775, 1776, 1777, 1778, 1779, 1780, 1781, 1782, 1783, 1784, 1785, 1786, 1787, 1788, 1789, 1790, 1791, 1792, 1793, 1794, 1795, 1796, 1797, 1798, 1799, 1800, 1801, 1802, 1803, 1804, 1805, 1806, 1807, 1808, 1809, 1810, 1811, 1812, 1813, 1814, 1815, 1816, 1817, 1818, 1819, 1820, 1821, 1822, 1823, 1824, 1825, 1826, 1827, 1828, 1829, 1830, 1831, 1832, 1833, 1834, 1835, 1836, 1837, 1838, 1839, 1840, 1841, 1842, 1843, 1844, 1845, 1846, 1847, 1848, 1849, 1850, 1851, 1852, 1853, 1854, 1855, 1856, 1857, 1858, 1859, 1860, 1861, 1862, 1863, 1864, 1865, 1866, 1867, 1868, 1869, 1870, 1871, 1872, 1873, 1874, 1875, 1876, 1877, 1878, 1879, 1880, 1881, 1882, 1883, 1884, 1885, 1886, 1887, 1888, 1889, 1890, 1891, 1892, 1893, 1894, 1895, 1896, 1897, 1898, 1899, 1900, 1901, 1902, 1903, 1904, 1905, 1906, 1907, 1908, 1909, 1910, 1911, 1912, 1913, 1914, 1915, 1916, 1917, 1918, 1919, 1920, 1921, 1922, 1923, 1924, 1925, 1926, 1927, 1928, 1929, 1930, 1931, 1932, 1933, 1934, 1935, 1936, 1937, 1938, 1939, 1940, 1941, 1942, 19
```



```

      A=PSZ(K)-T*(HUBZ(K)-RSZ(K))
      B=KSPH(K)-T*(RJP(K)-RSPH(K))
      C=RCB(K)-RB(K)
      D=RCBZ(K)-RBZ(K)
      E=ROBPH(K)-RBP(K)
      DTG(1)=A/C
      LTRPH(1)=B/C
      CDT(1)=1.0/1.0
      ACT(K)=D/C
      PCT(K)=1/C
      K=CM(K)*B(K)
      X=KSPH(K)*B(K)
      Y=ROBPH(K)*B(K)
      CONTINUE
    CONTINUE
  RETURN
END

```

```

SUBROUTINE GEOMZ(K)
  LEVEL 7, ETMP, CD, FJ, GD, H7
  COMMON/LARGE/TEMP(4,24,41),L3(4,24,41),
    * FQ(4,24,41), G(4,24,41), MC(4,24,41)
  LEVEL 7, RMU, P, U, V, W, R0B, R0BZ, VIN, WIN, R0BPH, R0BZ, RBP, DTG(4),
    * BCT, DTGZ, DTGZ, ACT, ICNST, GAM, CONST, NREGON, RS, RSZ, RSPH, RST, RSZT,
    * RSPHIT
  COMMON /PVARR/RH0(24,41), P1(24,41), U1(24,41), V1(24,41), W1(24,41),
    * I1,
    * R0B(41), R0BZ(41), VIN(41), WIN(41),
    * R0BPH(41), R0BZ(41), RBP(41),
    * DTGPH(24,41), BCT(41), DTGZ(24,41), DTGZ(41), ACT(41),
    * ICNST(150), GAM(24), CONST(150), NREGON, RS(41),
    * RSZ(41), RSPH(41), RST(41), RSZT(41), RSPHIT(41)
  COMMON /IDLARR/RK,ETA(41),PHI(41),DTIL(41),DTIL(41),DTA,TF(24)
  COMMON /SVARR/SV, Z, PHI, DT, DZ, DP41, ZINT,
    * ZEND, P1, ALPHA, GAMMA, SIGMA, XACH, TAP1,
    * TAP12, DISK1, ALPH, DISK2, SIGN, NPRINT, DOUT,
    * DZDPH, ZM, TMD, TMD, TMD, TMD, TMD,
    * TPL, KZ, KZ, NIPHI, NIT, KPHI, NITER,
    * NPH1, NPH11, NPH12, NPH13, NPH1, NPH12, NPH13,
    * NT, NT1, NT2, NT3, PHIF, NCONL, RAD1,
    * PHIF, MET400, LAG, NBC, PINF, RHUIN, UINF,
    * GINF, GASCON, NRECAL, NPLNCH
  INTEGER DISK1, DISK2, TAP1, TAP12
  DO 1 K=1,NPH12
    PH=PHI(K)
    GO TO (3,2),K3
  CONTINUE
  R0B(K)=AS(K)
  R0BZ(K)=RSZ(K)
  R0BPH(K)=RSPH(K)
  GO TO 4
  CONTINUE
  R0B(K)=RST(K)
  R0BZ(K)=RSZT(K)
  R0BPH(K)=RSPHIT(K)
  CONTINUE
  RETURN
END

```

```

SUBROUTINE GEOM3(K7,PHI,P,NPH1,Z,RB,RBZ,RBP,IPRNT)
  COMMON/JDI/ZL1,CF1,CF2,ZLF,ZTRAN,DZTRAN
  COMMON /ACCT/NRECA(151)
  COMMON/INIL/YY, AMACH, GAMF, KM2, P1INF, R1INF, V1INF, P0U(20,3),
    * RH0(120,3), UR0(120,3), V0(120,3), W0(120,3), RS0(13),
    * RS2(1013), RSPH(13), RH0, R0B
  LEVEL 2, RB, RBP, RBZ
  DIMENSION R0(41), R0BPH(41), R0BZ(41), PHIP(41)
  DIMENSION ZSTA(120), URU(120), RZ(120)
  C
  C.....CONSTANTS
  C
  IF (7,NE,0) GO TO 1
  CF2=1.0
  ANG=89.5
  NST=1
  H=HPO
  RH0SE=1.0
  CALL GEOM1(ANG,RZ,URDZ,ZSTA,H,R0)
  RETURN

```

```

C
C.....FIND CORRECT Z INTERVAL
C
  1 CONTINUE

```

```

GEOM1 17
GEOM1 18
GEOM1 19
GEOM1 20
GEOM1 21
GEOM1 22
GEOM1 23
GEOM1 24
GEOM1 25
GEOM1 26
GEOM1 27
GEOM1 28
GEOM1 29
GEOM1 30
GEOM1 31
GEOM1 32
GEOM1 33

```

```

GEOM2 2
GEOM2 3
GEOM2 4
GEOM2 5
GEOM2 6
GEOM2 7
GEOM2 8
GEOM2 9
GEOM2 10
GEOM2 11
GEOM2 12
GEOM2 13
GEOM2 14
GEOM2 15
GEOM2 16
GEOM2 17
GEOM2 18
GEOM2 19
GEOM2 20
GEOM2 21
GEOM2 22

```

```

GEOM3 2
JDE 2
ACCT 2
TRANSF 2
TRANSF 3
TRANSF 4
GEOM3 6
GEOM3 7
GEOM3 8
GEOM3 9
GEOM3 10
GEOM3 11
GEOM3 12
GEOM3 13
GEOM3 14
GEOM3 15
GEOM3 16
GEOM3 17
GEOM3 18
GEOM3 19
GEOM3 20
GEOM3 21
GEOM3 22
GEOM3 23

```

```

  A=NST
  IF (1Z,GE, ZSTAEN) AND, (Z,LE, ZSTAEN) GO TO 20
  A=0.1
  GO TO 10
  CONTINUE
  NST=0
  PRODY=Z(EN)+PZEN(1)-RZEN(1)/(ZSTAEN(1)-ZSTAEN(1))
  PRODYZ=L0(1)+E0(1)/(ZSTAEN(1)-ZSTAEN(1))
  R0BPH=L0
  DO 10 K=1,NPH1
    R0B(K)=R0BPH
    R0BPH(K)=R0BPH
    R0BZ(K)=R0BZ
  CONTINUE
  DO 30 K=1,N
    R0B(K)=R0B
    R0BZ(K)=R0BZ
  CONTINUE
  END

```

```

SUBROUTINE INITA
  LEVEL 7, ETMP, CD, FJ, GD, H7
  COMMON/LARGE/TEMP(4,24,41),L3(4,24,41),
    * FQ(4,24,41), G(4,24,41), MC(4,24,41)
  LEVEL 2, RMU, P, U, V, W, R0B, R0BZ, VIN, WIN, R0BPH, R0BZ, RBP, DTG(4),
    * BCT, DTGZ, DTGZ, ACT, ICNST, GAM, CONST, NREGON, RS, RSZ, RSPH, RST, RSZT,
    * RSPHIT
  COMMON /PVARR/RH0(24,41), P1(24,41), U1(24,41), V1(24,41), W1(24,41),
    * I1,
    * R0B(41), R0BZ(41), VIN(41), WIN(41),
    * R0BPH(41), R0BZ(41), RBP(41),
    * DTGPH(24,41), BCT(41), DTGZ(24,41), DTGZ(41), ACT(41),
    * ICNST(150), GAM(24), CONST(150), NREGON, RS(41),
    * RSZ(41), RSPH(41), RST(41), RSZT(41), RSPHIT(41)
  COMMON /IDLARR/RK,ETA(41),PHI(41),DTIL(41),DTIL(41),DTA,TF(24)
  COMMON /SVARR/SV, Z, PHI, DT, DZ, DP41, ZINT,
    * ZEND, P1, ALPHA, GAMMA, SIGMA, XACH, TAP1,
    * TAP12, DISK1, ALPH, DISK2, SIGN, NPRINT, DOUT,
    * DZDPH, ZM, TMD, TMD, TMD, TMD, TMD,
    * TPL, KZ, KZ, NIPHI, NIT, KPHI, NITER,
    * NPH1, NPH11, NPH12, NPH13, NPH1, NPH12, NPH13,
    * NT, NT1, NT2, NT3, PHIF, NCONL, RAD1,
    * PHIF, MET400, LAG, NBC, PINF, RHUIN, UINF,
    * GINF, GASCON, NRECAL, NPLNCH
  INTEGER DISK1, DISK2, TAP1, TAP12
  COMMON/JDI/ZL1,CF1,CF2,ZLF,ZTRAN,DZTRAN
  COMMON/INIL/YY, Z0S, ZF0, ITPH, ITPH, NCASE, NTDSUS
  COMMON/CLUSTR/RJ, K1(24), TRIT(24)
  COMMON/INIL/YY, AMACH, GAMF, KM2, P1INF, R1INF, V1INF, P0U(20,3),
    * RH0(120,3), UR0(120,3), V0(120,3), W0(120,3), RS0(13),
    * RS2(1013), RSPH(13), RH0, R0B
  RAD1=37.24570
  P1=3.14159265
  ZINT=1.0
  Z=ZINT
  ZEND=ZLF+1.0
  ALPH=0.0
  NIPHI=2
  NIT=KM2
  XACH=AMACH
  (APPA=GAMF
  ALPH=ALPH/RAD1
  SIGN=SIGN/RAD1
  PHIF=180.0/RAD1
  NPH1=NPH1+3
  NPH12=NPH1+1
  NPH13=NPH1+2
  NPH14=NPH1-1
  NPH15=NPH1-2
  NT=NIT+2
  NT1=NT+1
  NT2=NT+2
  ICNST(1)=1
  ICNST(10)=1
  IPRINT=ICNST(4)
  IF (ICNST(10),NE,1) ICNST(10)=0
  LAG=1

```

```

GEOM3 24
GEOM3 25
GEOM3 26
GEOM3 27
GEOM3 28
GEOM3 29
GEOM3 30
GEOM3 31
GEOM3 32
GEOM3 33
GEOM3 34
GEOM3 35
GEOM3 36
GEOM3 37
GEOM3 38
GEOM3 39
GEOM3 40
GEOM3 41
GEOM3 42
GEOM3 43
GEOM3 44
GEOM3 45
GEOM3 46
GEOM3 47
GEOM3 48
GEOM3 49
GEOM3 50

```

```

INITA 2
GEOM3 2
GEOM3 3
GEOM3 4
GEOM3 5
GEOM3 6
GEOM3 7
GEOM3 8
GEOM3 9
GEOM3 10
GEOM3 11
GEOM3 12
GEOM3 13
GEOM3 14
GEOM3 15
GEOM3 16
GEOM3 17
GEOM3 18
GEOM3 19
GEOM3 20
GEOM3 21
GEOM3 22
GEOM3 23
GEOM3 24
GEOM3 25
GEOM3 26
GEOM3 27
GEOM3 28
GEOM3 29
GEOM3 30
GEOM3 31
GEOM3 32
GEOM3 33
GEOM3 34
GEOM3 35
GEOM3 36
GEOM3 37
GEOM3 38
GEOM3 39
GEOM3 40
GEOM3 41
GEOM3 42
GEOM3 43
GEOM3 44
GEOM3 45
GEOM3 46
GEOM3 47
GEOM3 48
GEOM3 49
GEOM3 50

```


MICROFILMED FROM
BEST AVAILABLE COPY

```

C...:T CONStantive VARIAbles AT M
DO 2, N=2,4
  C(1,N)=C(1,N)+1
  C(2,N)=C(2,N)+1
  C(3,N)=C(3,N)+1
  C(4,N)=C(4,N)+1
  C(5,N)=C(5,N)+1
  C(6,N)=C(6,N)+1
  C(7,N)=C(7,N)+1
  C(8,N)=C(8,N)+1
  C(9,N)=C(9,N)+1
  C(10,N)=C(10,N)+1
  C(11,N)=C(11,N)+1
  C(12,N)=C(12,N)+1
  C(13,N)=C(13,N)+1
  C(14,N)=C(14,N)+1
  C(15,N)=C(15,N)+1
  C(16,N)=C(16,N)+1
  C(17,N)=C(17,N)+1
  C(18,N)=C(18,N)+1
  C(19,N)=C(19,N)+1
  C(20,N)=C(20,N)+1
  C(21,N)=C(21,N)+1
  C(22,N)=C(22,N)+1
  C(23,N)=C(23,N)+1
  C(24,N)=C(24,N)+1
  C(25,N)=C(25,N)+1
  C(26,N)=C(26,N)+1
  C(27,N)=C(27,N)+1
  C(28,N)=C(28,N)+1
  C(29,N)=C(29,N)+1
  C(30,N)=C(30,N)+1
  C(31,N)=C(31,N)+1
  C(32,N)=C(32,N)+1
  C(33,N)=C(33,N)+1
  C(34,N)=C(34,N)+1
  C(35,N)=C(35,N)+1
  C(36,N)=C(36,N)+1
  C(37,N)=C(37,N)+1
  C(38,N)=C(38,N)+1
  C(39,N)=C(39,N)+1
  C(40,N)=C(40,N)+1
  C(41,N)=C(41,N)+1
  C(42,N)=C(42,N)+1
  C(43,N)=C(43,N)+1
  C(44,N)=C(44,N)+1
  C(45,N)=C(45,N)+1
  C(46,N)=C(46,N)+1
  C(47,N)=C(47,N)+1
  C(48,N)=C(48,N)+1
  C(49,N)=C(49,N)+1
  C(50,N)=C(50,N)+1
  C(51,N)=C(51,N)+1
  C(52,N)=C(52,N)+1
  C(53,N)=C(53,N)+1
  C(54,N)=C(54,N)+1
  C(55,N)=C(55,N)+1
  C(56,N)=C(56,N)+1
  C(57,N)=C(57,N)+1
  C(58,N)=C(58,N)+1
  C(59,N)=C(59,N)+1
  C(60,N)=C(60,N)+1
  C(61,N)=C(61,N)+1
  C(62,N)=C(62,N)+1
  C(63,N)=C(63,N)+1
  C(64,N)=C(64,N)+1
  C(65,N)=C(65,N)+1
  C(66,N)=C(66,N)+1
  C(67,N)=C(67,N)+1
  C(68,N)=C(68,N)+1
  C(69,N)=C(69,N)+1
  C(70,N)=C(70,N)+1
  C(71,N)=C(71,N)+1
  C(72,N)=C(72,N)+1
  C(73,N)=C(73,N)+1
  C(74,N)=C(74,N)+1
  C(75,N)=C(75,N)+1
  C(76,N)=C(76,N)+1
  C(77,N)=C(77,N)+1
  C(78,N)=C(78,N)+1
  C(79,N)=C(79,N)+1
  C(80,N)=C(80,N)+1
  C(81,N)=C(81,N)+1
  C(82,N)=C(82,N)+1
  C(83,N)=C(83,N)+1
  C(84,N)=C(84,N)+1
  C(85,N)=C(85,N)+1
  C(86,N)=C(86,N)+1
  C(87,N)=C(87,N)+1
  C(88,N)=C(88,N)+1
  C(89,N)=C(89,N)+1
  C(90,N)=C(90,N)+1
  C(91,N)=C(91,N)+1
  C(92,N)=C(92,N)+1
  C(93,N)=C(93,N)+1
  C(94,N)=C(94,N)+1
  C(95,N)=C(95,N)+1
  C(96,N)=C(96,N)+1
  C(97,N)=C(97,N)+1
  C(98,N)=C(98,N)+1
  C(99,N)=C(99,N)+1
  C(100,N)=C(100,N)+1
  C(101,N)=C(101,N)+1
  C(102,N)=C(102,N)+1
  C(103,N)=C(103,N)+1
  C(104,N)=C(104,N)+1
  C(105,N)=C(105,N)+1
  C(106,N)=C(106,N)+1
  C(107,N)=C(107,N)+1
  C(108,N)=C(108,N)+1
  C(109,N)=C(109,N)+1
  C(110,N)=C(110,N)+1
  C(111,N)=C(111,N)+1
  C(112,N)=C(112,N)+1
  C(113,N)=C(113,N)+1
  C(114,N)=C(114,N)+1
  C(115,N)=C(115,N)+1
  C(116,N)=C(116,N)+1
  C(117,N)=C(117,N)+1
  C(118,N)=C(118,N)+1
  C(119,N)=C(119,N)+1
  C(120,N)=C(120,N)+1
  C(121,N)=C(121,N)+1
  C(122,N)=C(122,N)+1
  C(123,N)=C(123,N)+1
  C(124,N)=C(124,N)+1
  C(125,N)=C(125,N)+1
  C(126,N)=C(126,N)+1
  C(127,N)=C(127,N)+1
  C(128,N)=C(128,N)+1
  C(129,N)=C(129,N)+1
  C(130,N)=C(130,N)+1
  C(131,N)=C(131,N)+1
  C(132,N)=C(132,N)+1
  C(133,N)=C(133,N)+1
  C(134,N)=C(134,N)+1
  C(135,N)=C(135,N)+1
  C(136,N)=C(136,N)+1
  C(137,N)=C(137,N)+1
  C(138,N)=C(138,N)+1
  C(139,N)=C(139,N)+1
  C(140,N)=C(140,N)+1
  C(141,N)=C(141,N)+1
  C(142,N)=C(142,N)+1
  C(143,N)=C(143,N)+1
  C(144,N)=C(144,N)+1
  C(145,N)=C(145,N)+1
  C(146,N)=C(146,N)+1
  C(147,N)=C(147,N)+1
  C(148,N)=C(148,N)+1
  C(149,N)=C(149,N)+1
  C(150,N)=C(150,N)+1
  C(151,N)=C(151,N)+1
  C(152,N)=C(152,N)+1
  C(153,N)=C(153,N)+1
  C(154,N)=C(154,N)+1
  C(155,N)=C(155,N)+1
  C(156,N)=C(156,N)+1
  C(157,N)=C(157,N)+1
  C(158,N)=C(158,N)+1
  C(159,N)=C(159,N)+1
  C(160,N)=C(160,N)+1
  C(161,N)=C(161,N)+1
  C(162,N)=C(162,N)+1
  C(163,N)=C(163,N)+1
  C(164,N)=C(164,N)+1
  C(165,N)=C(165,N)+1
  C(166,N)=C(166,N)+1
  C(167,N)=C(167,N)+1
  C(168,N)=C(168,N)+1
  C(169,N)=C(169,N)+1
  C(170,N)=C(170,N)+1
  C(171,N)=C(171,N)+1
  C(172,N)=C(172,N)+1
  C(173,N)=C(173,N)+1
  C(174,N)=C(174,N)+1
  C(175,N)=C(175,N)+1
  C(176,N)=C(176,N)+1
  C(177,N)=C(177,N)+1
  C(178,N)=C(178,N)+1
  C(179,N)=C(179,N)+1
  C(180,N)=C(180,N)+1
  C(181,N)=C(181,N)+1
  C(182,N)=C(182,N)+1
  C(183,N)=C(183,N)+1
  C(184,N)=C(184,N)+1
  C(185,N)=C(185,N)+1
  C(186,N)=C(186,N)+1
  C(187,N)=C(187,N)+1
  C(188,N)=C(188,N)+1
  C(189,N)=C(189,N)+1
  C(190,N)=C(190,N)+1
  C(191,N)=C(191,N)+1
  C(192,N)=C(192,N)+1
  C(193,N)=C(193,N)+1
  C(194,N)=C(194,N)+1
  C(195,N)=C(195,N)+1
  C(196,N)=C(196,N)+1
  C(197,N)=C(197,N)+1
  C(198,N)=C(198,N)+1
  C(199,N)=C(199,N)+1
  C(200,N)=C(200,N)+1
  C(201,N)=C(201,N)+1
  C(202,N)=C(202,N)+1
  C(203,N)=C(203,N)+1
  C(204,N)=C(204,N)+1
  C(205,N)=C(205,N)+1
  C(206,N)=C(206,N)+1
  C(207,N)=C(207,N)+1
  C(208,N)=C(208,N)+1
  C(209,N)=C(209,N)+1
  C(210,N)=C(210,N)+1
  C(211,N)=C(211,N)+1
  C(212,N)=C(212,N)+1
  C(213,N)=C(213,N)+1
  C(214,N)=C(214,N)+1
  C(215,N)=C(215,N)+1
  C(216,N)=C(216,N)+1
  C(217,N)=C(217,N)+1
  C(218,N)=C(218,N)+1
  C(219,N)=C(219,N)+1
  C(220,N)=C(220,N)+1
  C(221,N)=C(221,N)+1
  C(222,N)=C(222,N)+1
  C(223,N)=C(223,N)+1
  C(224,N)=C(224,N)+1
  C(225,N)=C(225,N)+1
  C(226,N)=C(226,N)+1
  C(227,N)=C(227,N)+1
  C(228,N)=C(228,N)+1
  C(229,N)=C(229,N)+1
  C(230,N)=C(230,N)+1
  C(231,N)=C(231,N)+1
  C(232,N)=C(232,N)+1
  C(233,N)=C(233,N)+1
  C(234,N)=C(234,N)+1
  C(235,N)=C(235,N)+1
  C(236,N)=C(236,N)+1
  C(237,N)=C(237,N)+1
  C(238,N)=C(238,N)+1
  C(239,N)=C(239,N)+1
  C(240,N)=C(240,N)+1
  C(241,N)=C(241,N)+1
  C(242,N)=C(242,N)+1
  C(243,N)=C(243,N)+1
  C(244,N)=C(244,N)+1
  C(245,N)=C(245,N)+1
  C(246,N)=C(246,N)+1
  C(247,N)=C(247,N)+1
  C(248,N)=C(248,N)+1
  C(249,N)=C(249,N)+1
  C(250,N)=C(250,N)+1
  C(251,N)=C(251,N)+1
  C(252,N)=C(252,N)+1
 
```

IOCCN	100
IOCCN	100
IOCCN	107
IOCCN	108
IOCCN	109
IOCCN	110
IOCCN	111
IOCCN	117
IOCCN	113
IOCCN	114
IOCCN	115
IOCCN	116
IOCCN	117
IOCCN	118
IOCCN	119
IOCCN	120
IOCCN	121
IOCCN	122
IOCCN	123
IOCCN	124
IOCCN	125
IOCCN	126
IOCCN	127
IOCCN	128
IOCCN	129
IOCCN	130
IOCCN	131
IOCCN	132
IOCCN	133
IOCCN	134
IOCCN	135
IOCCN	136
IOCCN	137
IOCCN	138
IOCCN	139
IOCCN	140
IOCCN	141
IOCCN	142
IOCCN	143
IOCCN	144
IOCCN	145
IOCCN	146
IOCCN	147
IOCCN	148
IOCCN	149
IOCCN	150
OUTPTM	2
CVARS	2
CVARS	2
CVARS	4
PVARS	2
PVARS	3
PVARS	4
PVARS	5
PVARS	6
PVARS	7
PVARS	8
PVARS	10
PVARS	11
IDVARS	2
SVARS	2
SVARS	3
SVARS	4
SVARS	5
SVARS	7
SVARS	8
SVARS	9
SVARS	10
SVARS	11
ENTRO	2
CLUSTM	2
DUSTM	2
TRANSF1	2
TRANSF1	3
TRANSF1	4
TRANSF1	5
TRANSF1	6
SHOCKS	3
OUTPTM	12
OUTPTM	13
OUTPTM	13

105

547041	98
547043	99
547045	100
547047	101
547049	102
547051	103

[illegible]

540C RM	38
540C RM	39
540C RM	40
540C RM	41
540C RM	43
540C RM	44
540C RM	45
540C RM	46
540C RM	47
540C RM	48
540C RM	49
540C RM	50
540C RM	51
540C RM	52
540C RM	53
540C RM	54
540C RM	55
540C RM	56
540C RM	57
540C RM	58
540C RM	59
540C RM	60
540C RM	61
540C RM	62
540C RM	63
540C RM	64
540C RM	65
540C RM	66
540C RM	67
540C RM	68
540C RM	69
540C RM	70
540C RM	71
540C RM	72
540C RM	73
540C RM	74
540C RM	75
540C RM	76
540C RM	77
540C RM	78
540C RM	79
540C RM	80
540C RM	81
540C RM	82
540C RM	83
540C RM	84
540C RM	85
540C RM	86
540C RM	87
540C RM	88
540C RM	89
540C RM	90
540C RM	91
540C RM	92
540C RM	93
540C RM	94
540C RM	95
540C RM	96
540C RM	97
540C RM	98
540C RM	99
540C RM	100
540C RM	101
540C RM	102
540C RM	103
540C RM	104
540C RM	105
540C RM	106
540C RM	107
540C RM	108
540C RM	109
540C RM	110
540C RM	111
540C RM	112

[illegible]

項目	金額
1. 現金	100.00
2. 有価証券	0.00
3. 債権	0.00
4. 貸倒引当金	0.00
5. 前払金	0.00
6. 前払金	0.00
7. 前払金	0.00
8. 前払金	0.00
9. 前払金	0.00
10. 前払金	0.00
11. 前払金	0.00
12. 前払金	0.00
13. 前払金	0.00
14. 前払金	0.00
15. 前払金	0.00
16. 前払金	0.00
17. 前払金	0.00
18. 前払金	0.00
19. 前払金	0.00
20. 前払金	0.00
21. 前払金	0.00
22. 前払金	0.00
23. 前払金	0.00
24. 前払金	0.00
25. 前払金	0.00
26. 前払金	0.00
27. 前払金	0.00
28. 前払金	0.00
29. 前払金	0.00
30. 前払金	0.00
31. 前払金	0.00
32. 前払金	0.00
33. 前払金	0.00
34. 前払金	0.00
35. 前払金	0.00
36. 前払金	0.00
37. 前払金	0.00
38. 前払金	0.00
39. 前払金	0.00
40. 前払金	0.00
41. 前払金	0.00
42. 前払金	0.00
43. 前払金	0.00
44. 前払金	0.00
45. 前払金	0.00
46. 前払金	0.00
47. 前払金	0.00
48. 前払金	0.00
49. 前払金	0.00
50. 前払金	0.00
51. 前払金	0.00
52. 前払金	0.00
53. 前払金	0.00
54. 前払金	0.00
55. 前払金	0.00
56. 前払金	0.00
57. 前払金	0.00
58. 前払金	0.00
59. 前払金	0.00
60. 前払金	0.00
61. 前払金	0.00
62. 前払金	0.00
63. 前払金	0.00
64. 前払金	0.00
65. 前払金	0.00
66. 前払金	0.00
67. 前払金	0.00
68. 前払金	0.00
69. 前払金	0.00
70. 前払金	0.00
71. 前払金	0.00
72. 前払金	0.00
73. 前払金	0.00
74. 前払金	0.00
75. 前払金	0.00
76. 前払金	0.00
77. 前払金	0.00
78. 前払金	0.00
79. 前払金	0.00
80. 前払金	0.00
81. 前払金	0.00
82. 前払金	0.00
83. 前払金	0.00
84. 前払金	0.00
85. 前払金	0.00
86. 前払金	0.00
87. 前払金	0.00
88. 前払金	0.00
89. 前払金	0.00
90. 前払金	0.00
91. 前払金	0.00
92. 前払金	0.00
93. 前払金	0.00
94. 前払金	0.00
95. 前払金	0.00
96. 前払金	0.00
97. 前払金	0.00
98. 前払金	0.00
99. 前払金	0.00
100. 前払金	0.00

```

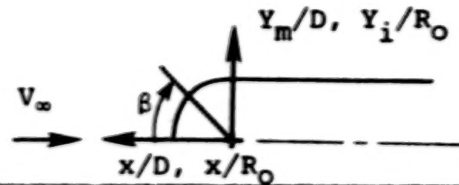
1  A[1] := 0
2  C := 0
3  W := 0
4  D := 0
5  E := 0
6  F := 0
7  G := 0
8  H := 0
9  I := 0
10 J := 0
11 K := 0
12 L := 0
13 M := 0
14 N := 0
15 O := 0
16 P := 0
17 Q := 0
18 R := 0
19 S := 0
20 T := 0
21 U := 0
22 V := 0
23 W := 0
24 X := 0
25 Y := 0
26 Z := 0
27 A[2] := 0
28 A[3] := 0
29 A[4] := 0
30 A[5] := 0
31 A[6] := 0
32 A[7] := 0
33 A[8] := 0
34 A[9] := 0
35 A[10] := 0
36 A[11] := 0
37 A[12] := 0
38 A[13] := 0
39 A[14] := 0
40 A[15] := 0
41 A[16] := 0
42 A[17] := 0
43 A[18] := 0
44 A[19] := 0
45 A[20] := 0
46 A[21] := 0
47 A[22] := 0
48 A[23] := 0
49 A[24] := 0
50 A[25] := 0
51 A[26] := 0
52 A[27] := 0
53 A[28] := 0
54 A[29] := 0
55 A[30] := 0
56 A[31] := 0
57 A[32] := 0
58 A[33] := 0
59 A[34] := 0
60 A[35] := 0
61 A[36] := 0
62 A[37] := 0
63 A[38] := 0
64 A[39] := 0
65 A[40] := 0
66 A[41] := 0
67 A[42] := 0
68 A[43] := 0
69 A[44] := 0
70 A[45] := 0
71 A[46] := 0
72 A[47] := 0
73 A[48] := 0
74 A[49] := 0
75 A[50] := 0
76 A[51] := 0
77 A[52] := 0
78 A[53] := 0
79 A[54] := 0
80 A[55] := 0
81 A[56] := 0
82 A[57] := 0
83 A[58] := 0
84 A[59] := 0
85 A[60] := 0
86 A[61] := 0
87 A[62] := 0
88 A[63] := 0
89 A[64] := 0
90 A[65] := 0
91 A[66] := 0
92 A[67] := 0
93 A[68] := 0
94 A[69] := 0
95 A[70] := 0
96 A[71] := 0
97 A[72] := 0
98 A[73] := 0
99 A[74] := 0
100 A[75] := 0
101 A[76] := 0
102 A[77] := 0
103 A[78] := 0
104 A[79] := 0
105 A[80] := 0
106 A[81] := 0
107 A[82] := 0
108 A[83] := 0
109 A[84] := 0
110 A[85] := 0
111 A[86] := 0
112 A[87] := 0
113 A[88] := 0
114 A[89] := 0
115 A[90] := 0
116 A[91] := 0
117 A[92] := 0
118 A[93] := 0
119 A[94] := 0
120 A[95] := 0
121 A[96] := 0
122 A[97] := 0
123 A[98] := 0
124 A[99] := 0
125 A[100] := 0
126 A[101] := 0
127 A[102] := 0
128 A[103] := 0
129 A[104] := 0
130 A[105] := 0
131 A[106] := 0
132 A[107] := 0
133 A[108] := 0
134 A[109] := 0
135 A[110] := 0
136 A[111] := 0
137 A[112] := 0
138 A[113] := 0
139 A[114] := 0
140 A[115] := 0
141 A[116] := 0
142 A[117] := 0
143 A[118] := 0
144 A[119] := 0
145 A[120] := 0
146 A[121] := 0
147 A[122] := 0
148 A[123] := 0
149 A[124] := 0
150 A[125] := 0
151 A[126] := 0
152 A[127] := 0
153 A[128] := 0
154 A[129] := 0
155 A[130] := 0
156 A[131] := 0
157 A[132] := 0
158 A[133] := 0
159 A[134] := 0
160 A[135] := 0
161 A[136] := 0
162 A[137] := 0
163 A[138] := 0
164 A[139] := 0
165 A[140] := 0
166 A[141] := 0
167 A[142] := 0
168 A[143] := 0
169 A[144] := 0
170 A[145] := 0
171 A[146] := 0
172 A[147] := 0
173 A[148] := 0
174 A[149] := 0
175 A[150] := 0
176 A[151] := 0
177 A[152] := 0
178 A[153] := 0
179 A[154] := 0
180 A[155] := 0
181 A[156] := 0
182 A[157] := 0
183 A[158] := 0
184 A[159] := 0
185 A[160] := 0
186 A[161] := 0
187 A[162] := 0
188 A[163] := 0
189 A[164] := 0
190 A[165] := 0
191 A[166] := 0
192 A[167] := 0
193 A[168] := 0
194 A[169] := 0
195 A[170] := 0
196 A[171] := 0
197 A[172] := 0
198 A[173] := 0
199 A[174] := 0
200 A[175] := 0
201 A[176] := 0
202 A[177] := 0
203 A[178] := 0
204 A[179] := 0
205 A[180] := 0
206 A[181] := 0
207 A[182] := 0
208 A[183] := 0
209 A[184] := 0
210 A[185] := 0
211 A[186] := 0
212 A[187] := 0
213 A[188] := 0
214 A[189] := 0
215 A[190] := 0
216 A[191] := 0
217 A[192] := 0
218 A[193] := 0
219 A[194] := 0
220 A[195] := 0
221 A[196] := 0
222 A[197] := 0
223 A[198] := 0
224 A[199] := 0
225 A[200] := 0
226 A[201] := 0
227 A[202] := 0
228 A[203] := 0
229 A[204] := 0
230 A[205] := 0
231 A[206] := 0
232 A[207] := 0
233 A[208] := 0
234 A[209] := 0
235 A[210] := 0
236 A[211] := 0
237 A[212] := 0
238 A[213] := 0
239 A[214] := 0
240 A[215] := 0
241 A[216] := 0
242 A[217] := 0
243 A[218] := 0
244 A[219] := 0
245 A[220] := 0
246 A[221] := 0
247 A[222] := 0
248 A[223] := 0
249 A[224] := 0
250 A[225] := 0
251 A[226] := 0
252 A[227] := 0
253 A[228] := 0
254 A[229] := 0
255 A[230] := 0
256 A[231] := 0
257 A[232] := 0
258 A[233] := 0
259 A[234] := 0
260 A[235] := 0
261 A[236] := 0
262 A[237] := 0
263 A[238] := 0
264 A[239] := 0
265 A[240] := 0
266 A[241] := 0
267 A[242] := 0
268 A[243] := 0
269 A[244] := 0
270 A[245] := 0
271 A[246] := 0
272 A[247] := 0
273 A[248] := 0
274 A[249] := 0
275 A[250] := 0
276 A[251] := 0
277 A[252] := 0
278 A[253] := 0
279 A[254] := 0
280 A[255] := 0
281 A[256] := 0
282 A[257] := 0
283 A[258] := 0
284 A[259] := 0
285 A[260] := 0
286 A[261] := 0
287 A[262] := 0
288 A[263] := 0
289 A[264] := 0
290 A[265] := 0
291 A[266] := 0
292 A[267] := 0
293 A[268] := 0
294 A[269] := 0
295 A[270] := 0
296 A[271] := 0
297 A[272] := 0
298 A[273] := 0
299 A[274] := 0
300 A[275] := 0
301 A[276] := 0
302 A[277] := 0
303 A[278] := 0
304 A[279] := 0
305 A[280] := 0
306 A[281] := 0
307 A[282] := 0
308 A[283] := 0
309 A[284] := 0
310 A[285] := 0
311 A[286] := 0
312 A[287] := 0
313 A[288] := 0
314 A[289] := 0
315 A[290] := 0
316 A[291] := 0
317 A[292] := 0
318 A[293] := 0
319 A[294] := 0
320 A[295] := 0
321 A[296] := 0
322 A[297] := 0
323 A[298] := 0
324 A[299] := 0
325 A[300] := 0
326 A[301] := 0
327 A[302] := 0
328 A[303] := 0
329 A[304] := 0
330 A[305] := 0
331 A[306] := 0
332 A[307] := 0
333 A[308] := 0
334 A[309] := 0
335 A[310] := 0
336 A[311] := 0
337 A[312] := 0
338 A[313] := 0
339 A[314] := 0
340 A[315] := 0
341 A[
```

REFERENCES

1. Spreiter, J. R. and Jones, W. P.: On the Effect of a Weak Interplanetary Magnetic Field on the Interaction Between the Solar Wind and the Geomagnetic Field. *Jour. Geophy. Res.*, vol. 68, 1963, pp. 3555-3564.
2. Spreiter, J. R., Alksne, A. Y., and Summers, A. L.: Hydromagnetic Flow Around the Magnetopause. *Plan. & Space Sci.*, vol. 14, 1966, pp. 223-253.
3. Spreiter, J. R., Alksne, A. Y., and Summers, A. L.: External Aerodynamics of the Magnetosphere. *Physics of the Magnetosphere* (Ed. R. L. Carovillano, J. F. McClay, and H. R. Radoski), D. Reidel Pub. Co., 1968, pp. 304-378 (also NASA TN 4482, 1968).
4. Spreiter, J. R. and Alksne, A. Y.: Plasma Flow Around the Magnetosphere. *Rev. Geophys.*, vol. 7, 1969, pp. 11-50.
5. Spreiter, J. R., Summers, A. L., and Rizzi, A. W.: Solar Wind Flow Past Nonmagnetic Planets - Venus and Mars. *Plan. & Space Sci.*, vol. 18, 1970, pp. 1281-1289.
6. Spreiter, J. R. and Alksne, A. Y.: Solar Wind Flow Past Objects in the Solar System. *Ann. Rev. Fluid Mech.*, vol. 2, pp. 313-354 (Ed. W. R. Sears, M. D. Van Dyke, and W. G. Vincenti), Annual Review, Inc., Palo Alto, CA, 1970.
7. Spreiter, J. R., March, C. M., Summers, A.: Hydromagnetic Aspects of Solar Wind Flow Past the Moon. *Cosmic Electrodynamics*, vol. 1, no. 1, 1970, pp. 5-50.
8. Spreiter, J. R. and Rizzi, A. W.: Aligned Magnetohydrodynamics Solution for Solar Wind Flow Past the Earth's Magnetosphere. *Acta Astronautica*, vol. 1, 1974, pp. 15-35.
9. Briggs, B. R. and Spreiter, J. R.: Theoretical Determination of the Boundary and Distortion of the Geomagnetic Field in a Steady Solar Wind. NASA TR R-178, 1963.
10. Chapman, S. and Ferraro, V. C. A.: An Outline of a Theory of Magnetic Storms. *Terrest. Magnetism Atmospheric Elec.*, vol. 36, 1931, pp. 77-97, 171-186.
11. Midgley, J. E. and Davis, Jr., L.: Calculation by a Moment Technique of the Perturbation of the Geomagnetic Field by the Solar Wind. *Jour. Geophy. Res.*, vol. 68, 1963, pp. 5111-5123.
12. Mead, G. D. and Beard, D. B.: Shape of the Geomagnetic Field Solar Wind Boundary. *Jour. Geophy. Res.*, vol. 69, 1964, pp. 1169-1179.
13. Olsen, W. P.: The Shape of the Titled Magnetopause. *Jour. Geophy. Res.*, Vol. 74, 1969, pp. 5642-5651.

14. Beard, D. B.: The Interaction of the Terrestrial Magnetic Field with the Solar Corpuscular Radiation. Jour. Geophys. Res., vol. 65, 1960, pp. 3559-3568.
15. Spreiter, J. R. and Briggs, B. R.: Theoretical Determination of the Form of the Hollow Produced in the Solar Corpuscular Stream by Interaction with the Magnetic Dipole Field of the Earth. NASA TR R-120, 1961.
16. Spreiter, J. R. and Briggs, B. R.: Theoretical Determination of the Form of the Boundary of the Solar Corpuscular Stream Produced by Interaction with the Magnetic Dipole Field of the Earth. Jour. Geophys. Res., vol. 67, no. 1, Jan. 1962, pp. 37-51.
17. Spreiter, J. R. and Briggs, B. R.: On the Choice of Condition to Apply at the Boundary of the Geomagnetic Field in the Steady-State Chapman-Ferraro Problem. Jour. Geophys. Res., vol. 67, no. 7, Jul. 1962, pp. 2983-2985.
18. Davis, Jr., L. and Beard, D. B.: A Correction to the Approximate Condition for Locating the Boundary Between a Magnetic Field and a Plasma. Jour. Geophys. Res., vol. 67, 1962, pp. 4505-4507.
19. Spreiter, J. R. and Summers, A. L.: On Conditions Near the Neutral Points on the Magnetosphere Boundary. Plan. & Space Sci., vol. 15, 1967, pp. 787-798.
20. Kuhn, G. D., Goodwin, F. K., and Perkins, Jr., S. C.: User's Manual for Space-Shuttle Computer Programs. NEAR TR 110, Apr. 1976.
21. Chaussee, D. S., Stahara, S. S., and Spreiter, J. R.: Application of an Axisymmetric Implicit Blunt Body Procedure: Computation of Solar Wind Flows Past Terrestrial Planets. AIAA Paper No. 77-700, Jun. 1977.
22. Beam, R. M. and Warming, R. F.: An Implicit Finite-Difference Algorithm for Hyperbolic Systems in Conservation-Law Form. J. Comp. Phys., vol. 22, no. 1, Sep. 1976.
23. Kutler, P., Reinhardt, W. A., and Warming, R. F.: Multi-Shocked, Three-Dimensional Supersonic Flow Fields with Real Gas Effects. AIAA Journal, vol. 11, May 1973, pp. 657-664.
24. Kutler, P., Reinhardt, W. A., and Warming, R. F.: Numerical Computations of Multi-Shocked Three-Dimensional Supersonic Flow Fields with Real Gas Effects. AIAA Paper No. 72-702, Jun. 1972.
25. Chaussee, D. S., Holtz, T., and Kutler, P.: Inviscid Supersonic/Hypersonic Body Flow Fields and Aerodynamics from Shock-Capturing Technique Calculations. AIAA Paper No. 75-837, Jun. 1975.
26. McCormack, R. W.: The Effect of Viscosity in Hypervelocity Impact Cratering. AIAA Paper No. 69-354, 1969.
27. Alksne, A. Y. and Webster, D. L.: Magnetic and Electric Fields in the Magnetosheath. Plan. & Space Sci., vol. 18, 1970, pp. 1203-1212.

28. Grad, H.: **Reducible Problems in Magneto-Fluid Dynamics Steady Flows.**
Rev. Mod. Phys., vol. 32, 1960, pp. 830-847.
29. Imai, I.: **On Flows of Conducting Fluids Past Bodies.** Rev. Mod.
Phys., vol. 32, 1960, pp. 992-999.
30. Inouye, M. and Lomax, H.: **Comparison of Experimental and Numerical
Results for the Flow of a Perfect Gas About Blunt-Nosed Bodies.**
NASA TD-1426, Sep. 1962.



β	MAGNETOPAUSE		IONOPAUSE		IONOPAUSE		IONOPAUSE		IONOPAUSE	
	Equatorial Trace		$H/R_O = 0.01$		$H/R_O = 0.1$		$H/R_O = 0.2$		$H/R_O = 0.5$	
	x/D	Y_m/D	x/R_O	Y_i/R_O	x/R_O	Y_i/R_O	x/R_O	Y_i/R_O	x/R_O	Y_i/R_O
0°	1.0	0.0	1.0	0.0	1.0	0.0	1.0	0.0	1.0	0.0
2°	0.9995	0.0349	0.9994	0.0348	0.9995	0.0348	0.9995	0.0349	0.9996	0.0349
6°	0.9957	0.1046	0.9946	0.1045	0.9954	0.1046	0.9958	0.1047	0.9966	0.1047
10°	0.9879	0.1742	0.9851	0.1737	0.9870	0.1740	0.9883	0.1743	0.9906	0.1747
14°	0.9764	0.2434	0.9709	0.2421	0.9745	0.2430	0.9771	0.2436	0.9814	0.2447
18°	0.9610	0.3122	0.9520	0.3093	0.9580	0.3113	0.9621	0.3126	0.9692	0.3149
22°	0.9417	0.3805	0.9285	0.3751	0.9373	0.3787	0.9434	0.3812	0.9537	0.3853
26°	0.9185	0.4480	0.9006	0.4393	0.9125	0.4451	0.9209	0.4491	0.9349	0.4560
30°	0.8915	0.5147	0.8684	0.5014	0.8838	0.5103	0.8945	0.5164	0.9127	0.5269
34°	0.8607	0.5805	0.8320	0.5612	0.8510	0.5740	0.8643	0.5830	0.8869	0.5982
38°	0.8260	0.6453	0.7916	0.6185	0.8143	0.6362	0.8302	0.6486	0.8573	0.6698
42°	0.7874	0.7089	0.7473	0.6729	0.7738	0.6967	0.7921	0.7132	0.8238	0.7418
46°	0.7448	0.7713	0.6995	0.7243	0.7293	0.7553	0.7501	0.7767	0.7862	0.8141
50°	0.6984	0.8323	0.6481	0.7724	0.6811	0.8118	0.7040	0.8390	0.7441	0.8868
54°	0.6480	0.8919	0.5936	0.8171	0.6292	0.8660	0.6538	0.8999	0.6974	0.9598
58°	0.5935	0.9499	0.5362	0.8581	0.5736	0.9180	0.5995	0.9593	0.6456	1.0332
62°	0.5350	1.0062	0.4760	0.8953	0.5144	0.9675	0.5408	1.0172	0.5885	1.1068
66°	0.4723	1.0609	0.4134	0.9285	0.4516	1.0143	0.4778	1.0733	0.5256	1.1806
70°	0.4054	1.1137	0.3486	0.9578	0.3852	1.0585	0.4104	1.1275	0.4566	1.2546
74°	0.3340	1.1648	0.2819	0.9829	0.3154	1.0998	0.3383	1.1797	0.3809	1.3285

Table 1.- Ordinates of Various Magneto/Ionopause Shapes

β	MAGNETOPAUSE		IONOPAUSE		IONOPAUSE		IONOPAUSE		IONOPAUSE	
	Equatorial Trace		$H/R_0 = 0.01$		$H/R_0 = 0.1$		$H/R_0 = 0.2$		$H/R_0 = 0.5$	
	x/D	y_m/D	x/R_0	y_i/R_0	x/R_0	y_i/R_0	x/R_0	y_i/R_0	x/R_0	y_i/R_0
78°	0.2580	1.2138	0.2134	1.0041	0.2419	1.1382	0.2614	1.2298	0.2981	1.4024
82°	0.1772	1.2610	0.1435	1.0212	0.1650	1.1737	0.1796	1.2777	0.2074	1.4759
86°	0.0913	1.3060	0.0723	1.0345	0.0843	1.2062	0.0925	1.3232	0.1083	1.5491
90°	0.0	1.3491	0.0	1.0442	0.0	1.2356	0.0	1.3661	0.0	1.6216
94°	-0.0972	1.3900	-0.0735	1.0507	-0.0882	1.2620	-0.0983	1.4065	-0.1184	1.6932
98°	-0.2008	1.4289	-0.1482	1.0547	-0.1806	1.2854	-0.2029	1.4441	-0.2479	1.7636
102°	-0.3115	1.4656	-0.2246	1.0568	-0.2776	1.3058	-0.3143	1.4788	-0.3895	1.8325
106°	-0.4302	1.5002	-0.3033	1.0577	-0.3795	1.3233	-0.4332	1.5106	-0.5447	1.8997
110°	-0.5578	1.5327	-0.3851	1.0580	-0.4870	1.3380	-0.5603	1.5394	-0.7150	1.9646
114°	-0.6959	1.5630	-0.4711	1.0581	-0.6011	1.3501	-0.6968	1.5651	-0.9024	2.0269
118°	-0.8461	1.5913	-0.5626	1.0581	-0.7230	1.3598	-0.8442	1.5877	-1.1092	2.0861
122°	-0.0107	1.6175	-0.6612	1.0581	-0.8543	1.3672	-1.0043	1.6072	-1.3384	2.1419
126°	-1.1927	1.6416	-0.7688	1.0581	-0.9973	1.3727	-1.1797	1.6237	-1.5938	2.1936
130°	-1.3961	1.6638	-0.8879	1.0581	-1.1550	1.3765	-1.3737	1.6371	-1.8803	2.2409
134°	-1.6262	1.6840	-1.0218	1.0581	-1.3317	1.3790	-1.5911	1.6476	-2.2048	2.2832
138°	-1.8905	1.7022	-1.1752	1.0581	-1.5332	1.3805	-1.8387	1.6555	-2.5767	2.3200
142°	-2.1997	1.7186	-1.3544	1.0581	-1.7679	1.3812	-2.1261	1.6611	-3.0093	2.3511
146°	-2.5696	1.7332	-1.5688	1.0581	-2.0483	1.3816	-2.4679	1.6646	-3.5226	2.3761
150°	-3.0242	1.7460	-1.8328	1.0581	-2.3932	1.3817	-2.8866	1.6666	-4.1480	2.3948
154°	-3.6026	1.7571	-2.1695	1.0581	-2.8330	1.3817	-3.4189	1.6675	-4.9365	2.4077

Table 1 (Continued)

β	MAGNETOPAUSE		IONOPAUSE		IONOPAUSE		IONOPAUSE		IONOPAUSE	
	Equatorial Trace		$H/R_0 = 0.01$		$H/R_0 = 0.1$		$H/R_0 = 0.2$		$H/R_0 = 0.5$	
	x/D	Y_m/D	x/R_0	Y_i/R_0	x/R_0	Y_i/R_0	x/R_0	Y_i/R_0	x/R_0	Y_i/R_0
158°	-4.3723	1.7665	-2.6190	1.0581	-3.4199	1.3817	-4.1281	1.6678	-5.9779	2.4152
162°	-5.4608	1.7743	-3.2567	1.0582	-4.2526	1.3817	-5.1333	1.6679	-7.4439	2.4187
166°	-7.1412	1.7805	-4.2440	1.0582	-5.5419	1.3817	-6.6897	1.6679	-9.7048	2.4197
170°	-10.1239	1.7851	-6.0011	1.0582	-7.8363	1.3818	-9.4594	1.6679	-13.7235	2.4198
174°	-17.0135	1.7882	-10.0678	1.0582	-13.1466	1.3818	-15.8695	1.6680	-23.0232	2.4198

Table 1 (Concluded)

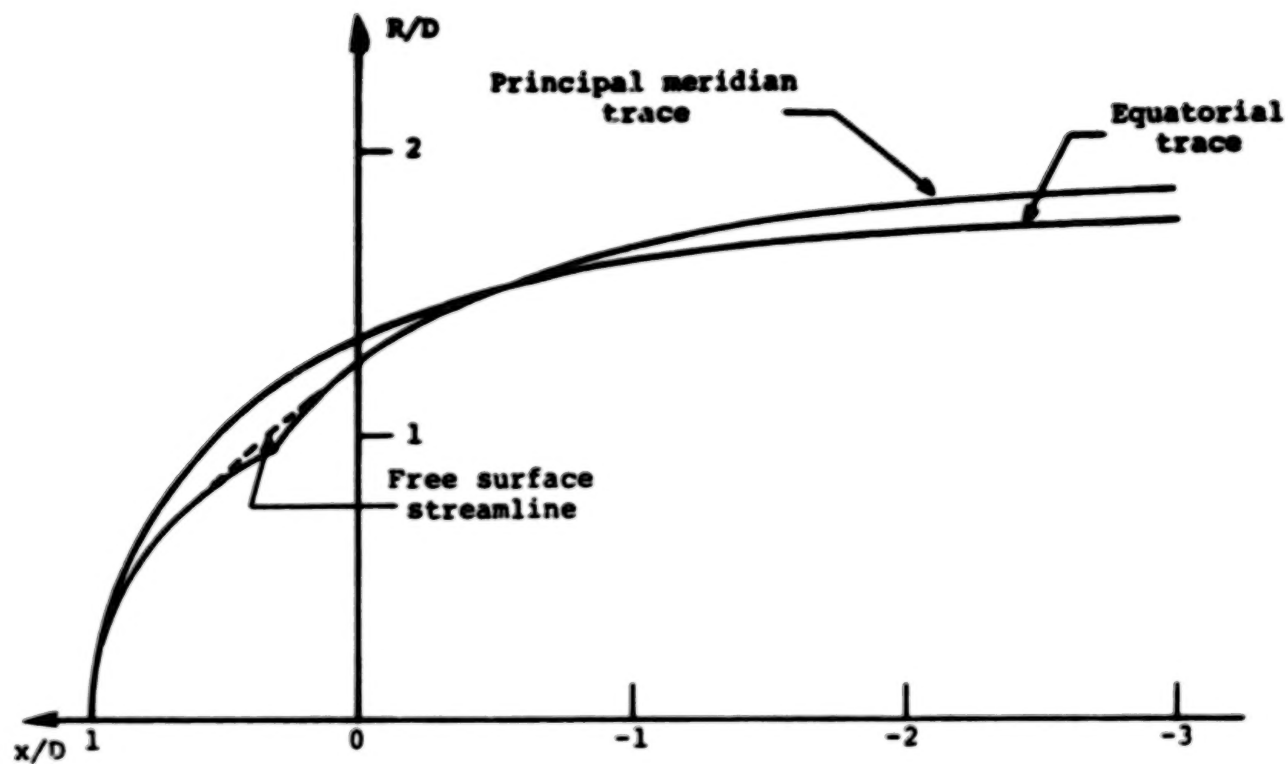


Figure 1. - Comparison of the equatorial and principal meridian traces of the magnetosphere boundary as provided by the simplified theory of equation 16.

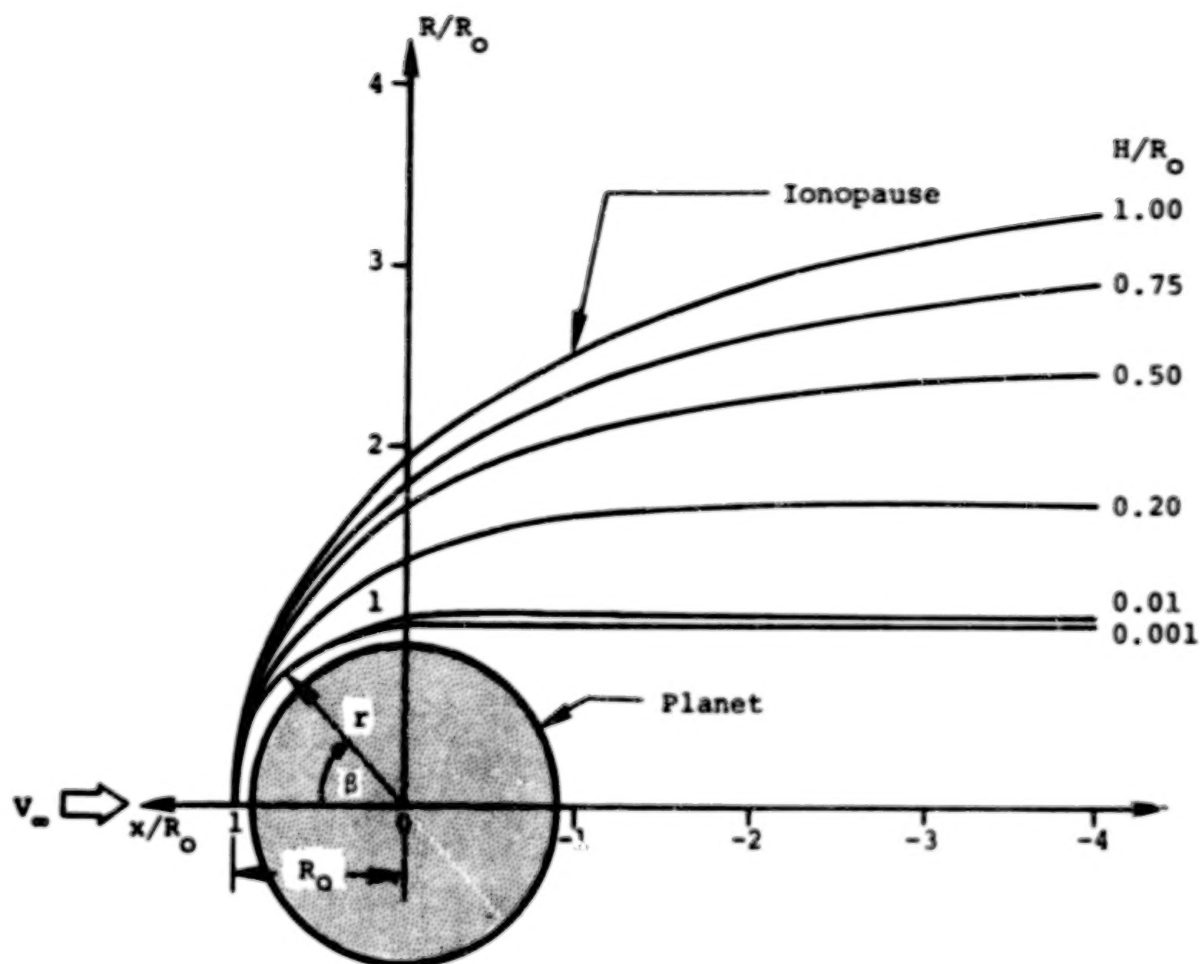


Figure 2. - Illustration of ionopause shapes for various values of the ionosphere scale height to shock standoff distance ratio H/R_0 .

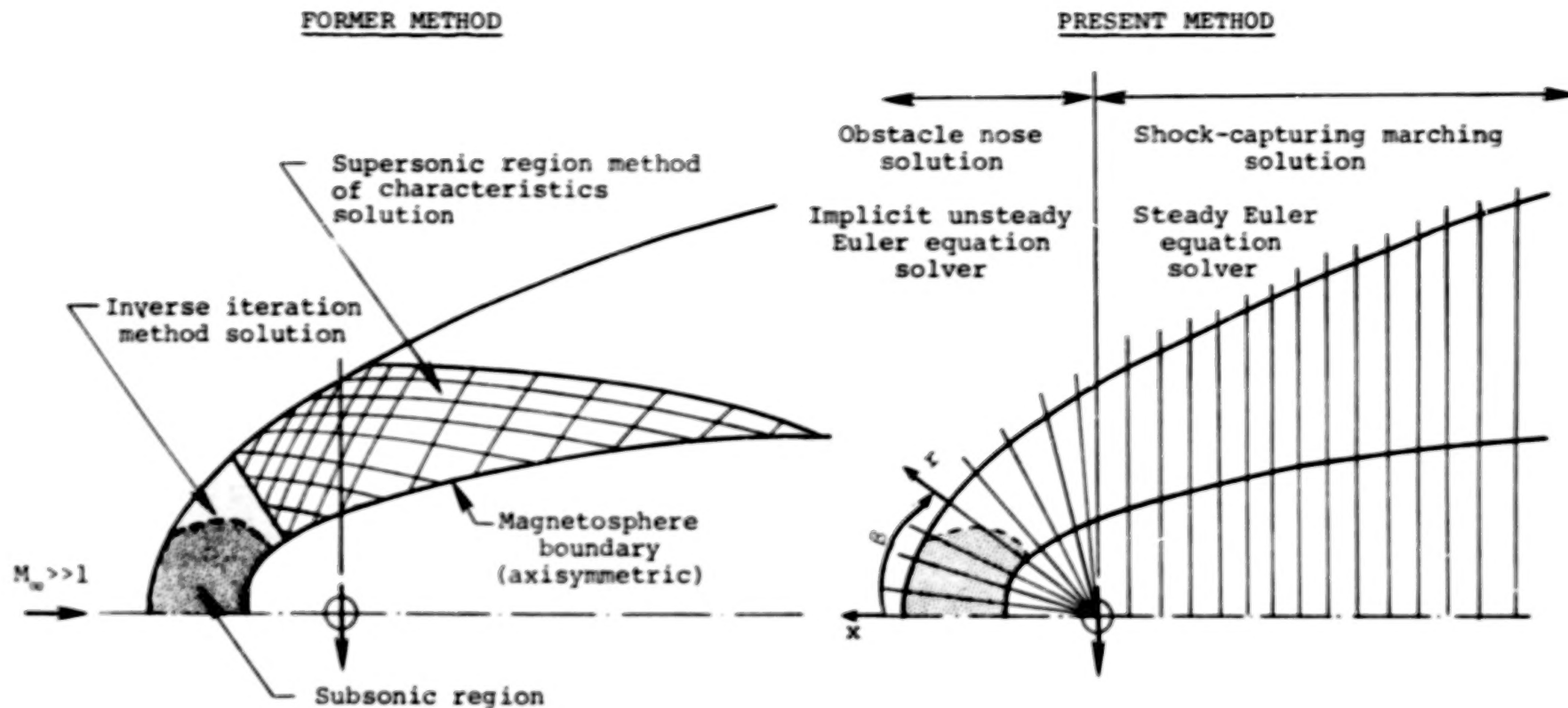


Figure 3. - Comparison of former and present computational procedures for determining the gasdynamic flow properties of solar wind-magneto/ionopause interactions.

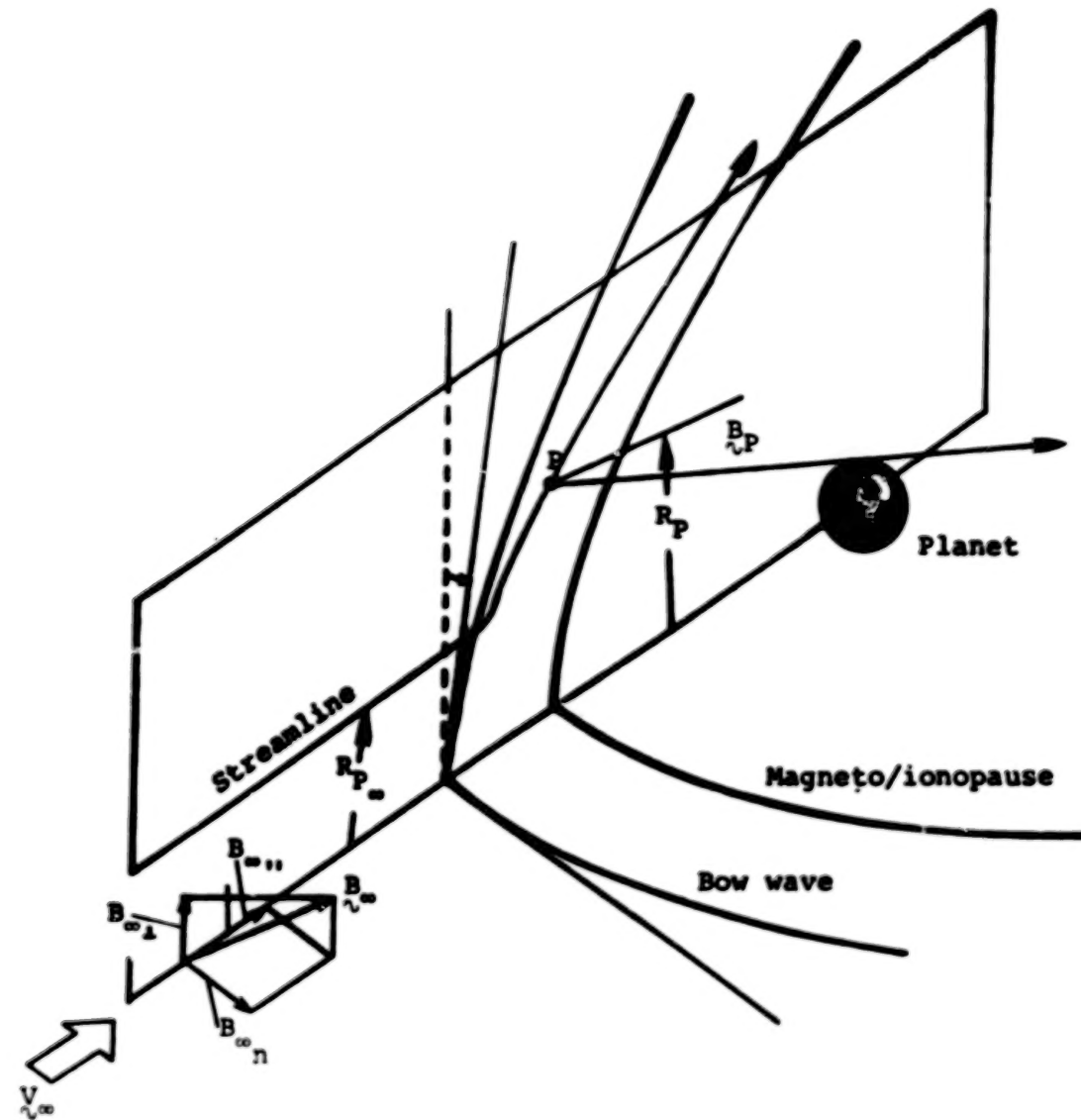


Figure 4. - Illustration of the components of the three-dimensional magnetic field.

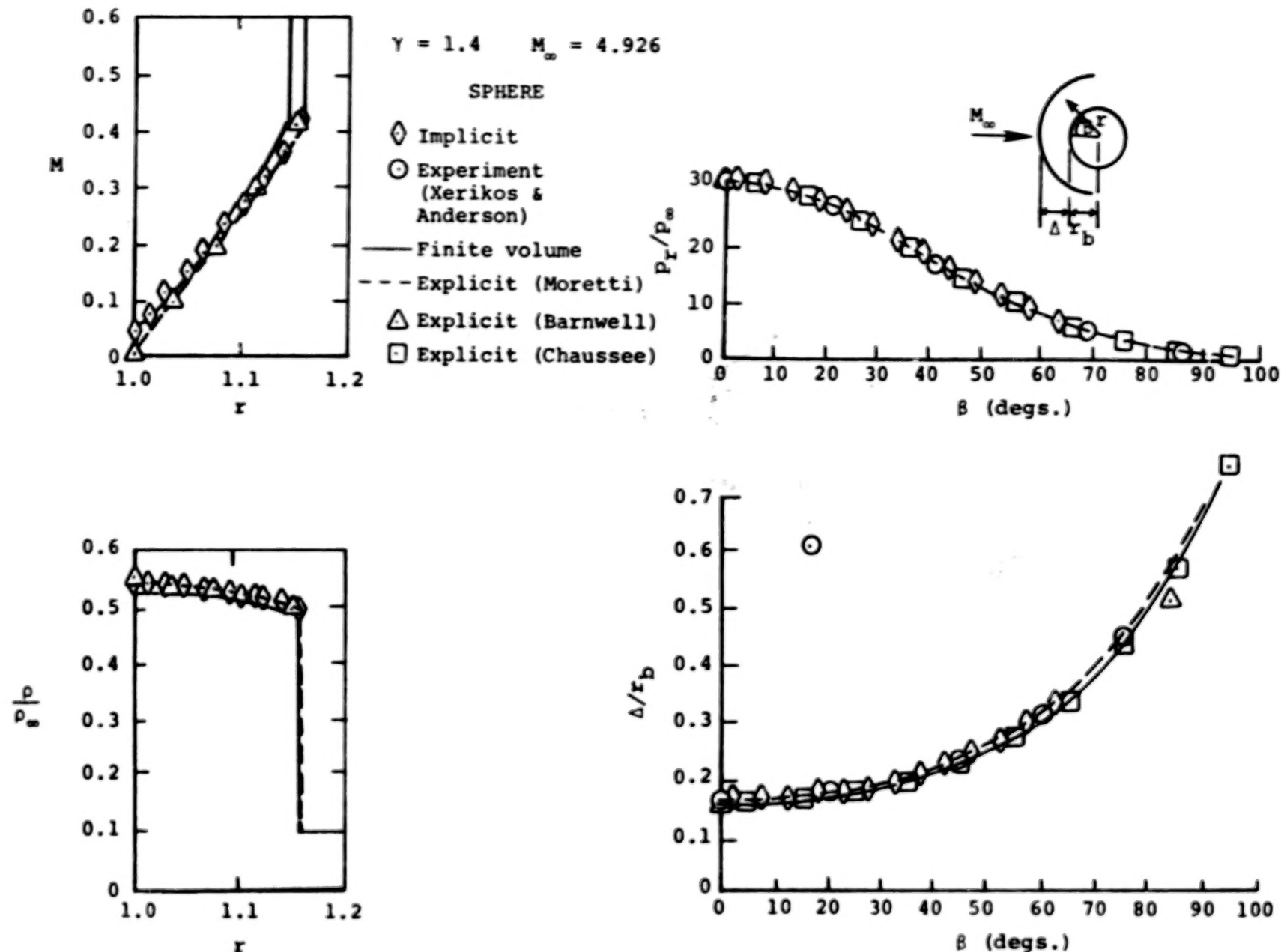
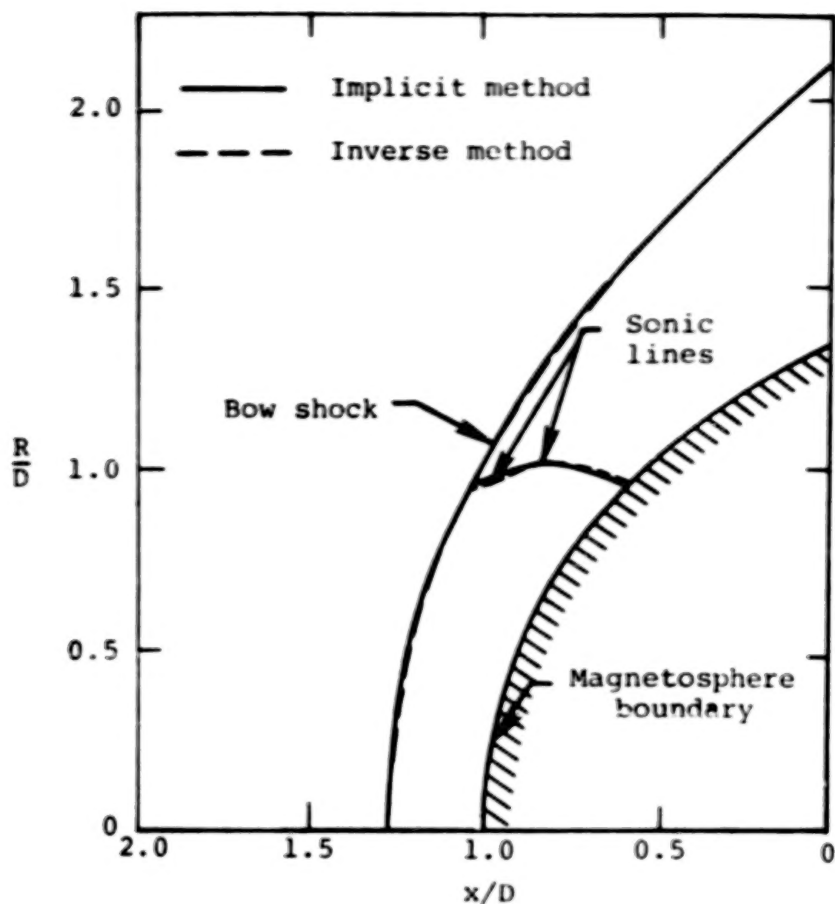
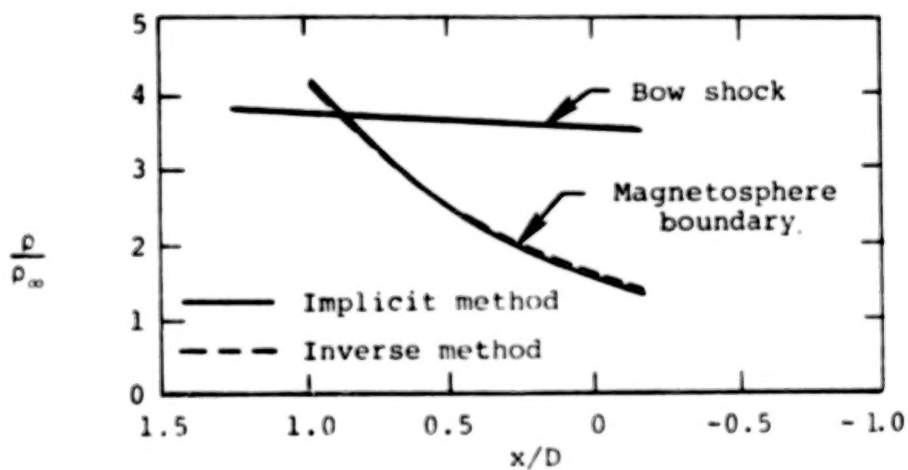


Figure 5. - Comparison of flow properties predicted by the present implicit method with other techniques and experiment for supersonic flow past a sphere; $M_\infty = 4.926$, $\gamma = 1.4$.



(a) Shock shape and sonic line location.



(b) Density distribution.

Figure 6. - Comparison of implicit and inverse methods for shock shape and sonic line location, and density distribution along bow shock and magnetosphere boundary for $M_\infty = 8$, $\gamma = 5/3$ flow past the rotated equatorial trace of the magnetopause.

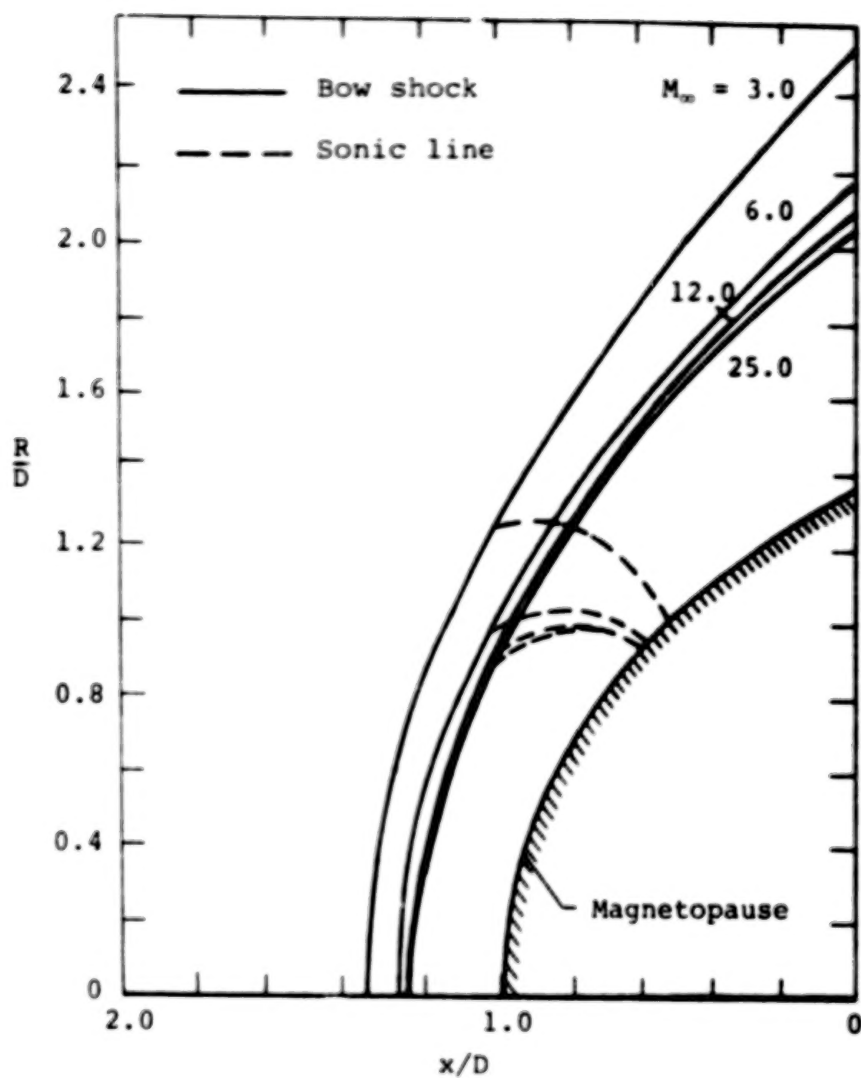


Figure 7. - Bow wave and sonic line locations for various supersonic flows past the rotated equatorial trace of the magnetopause with $\gamma = 5/3$.

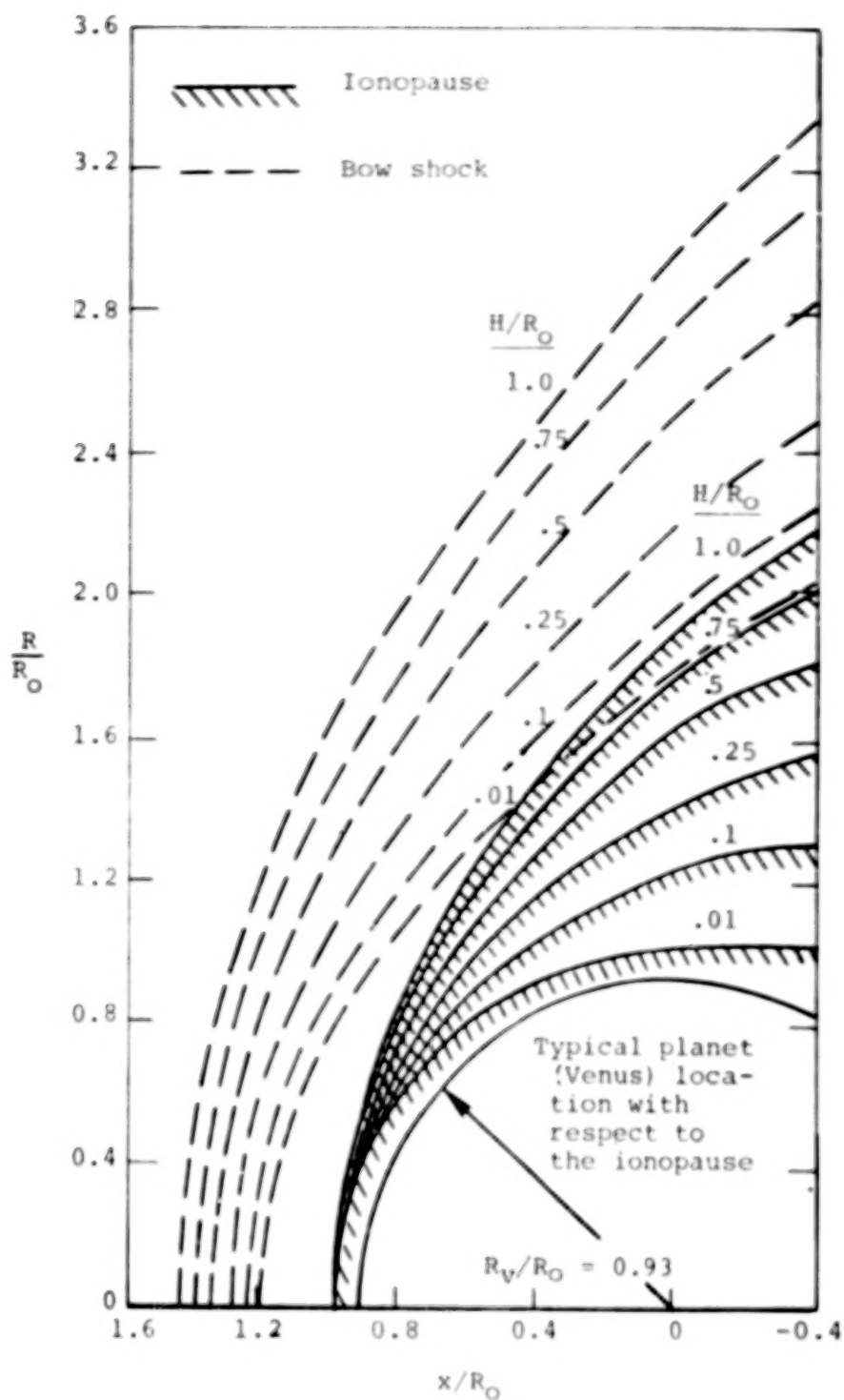


Figure 8. - Bow shock location for solar wind flow with $M_\infty = 8$, $\gamma = 5/3$ past various ionopause shapes.

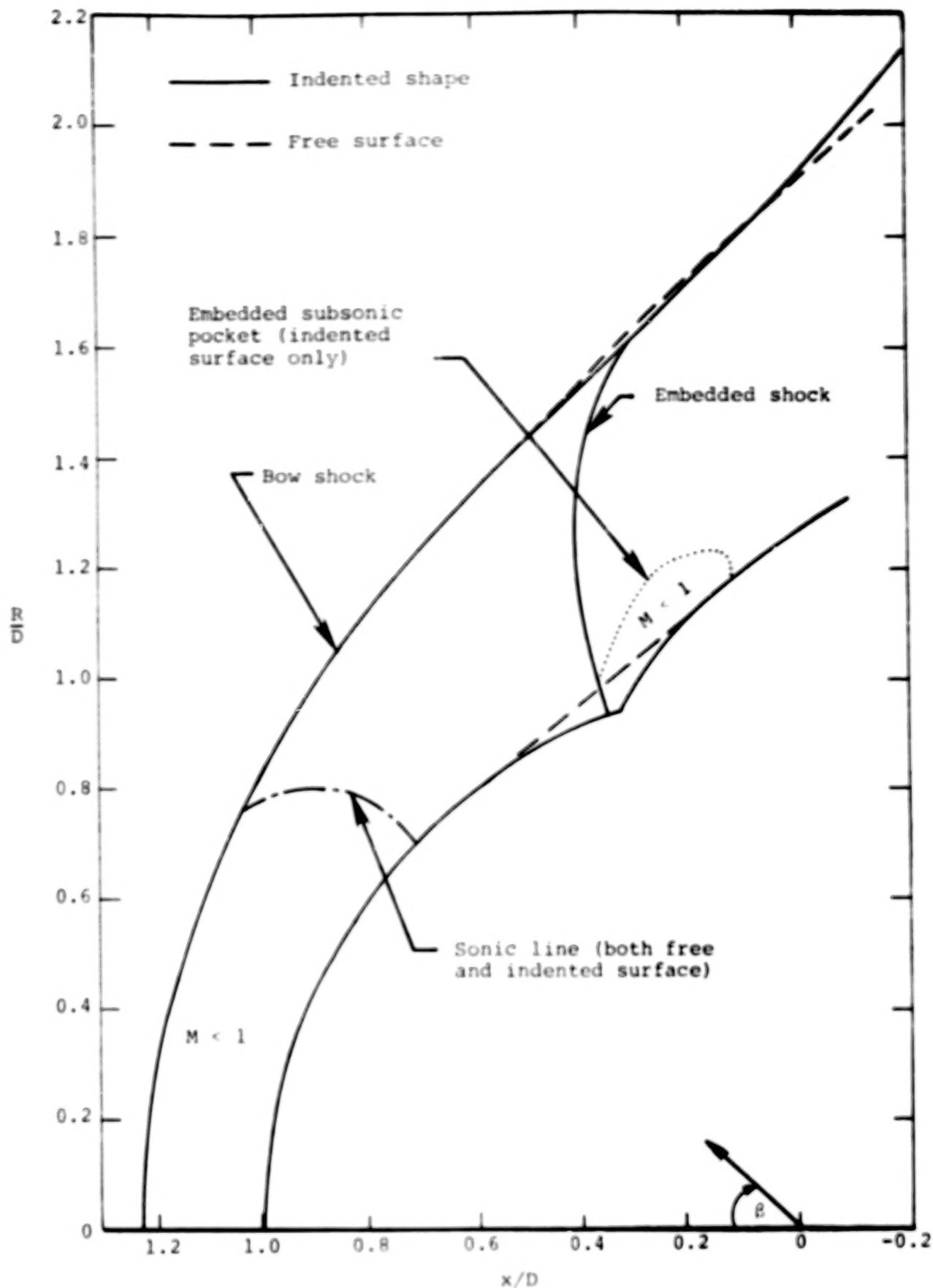


Figure 9. - Bow shock and embedded shock locations for solar wind flow with $M_{\infty} = 5$, $\gamma = 5/3$ past the rotated principal meridian of the magnetosphere.

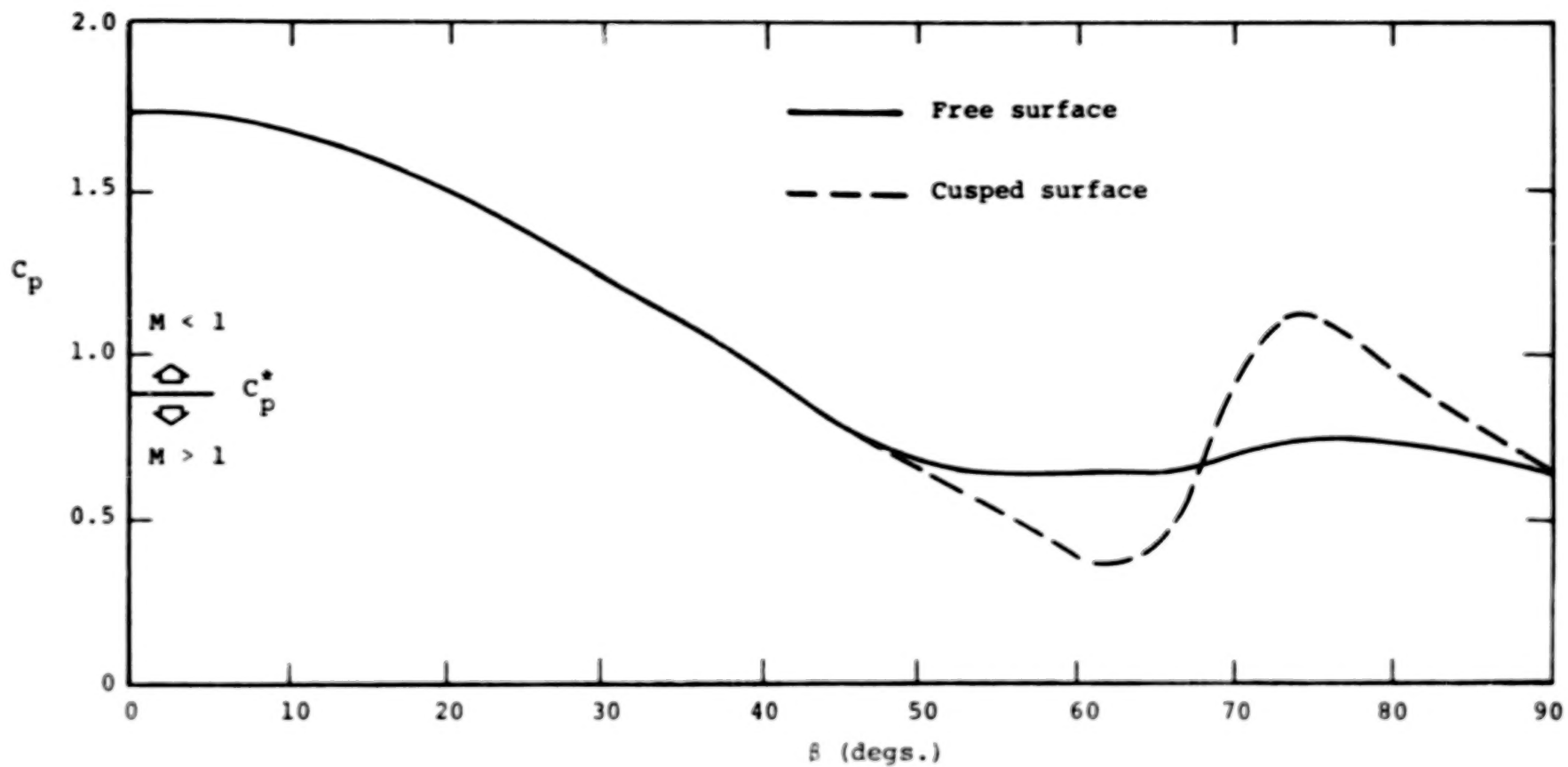
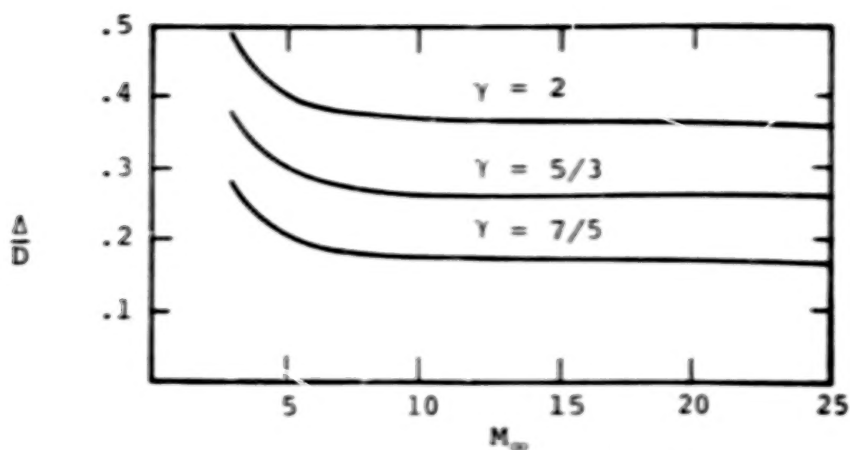
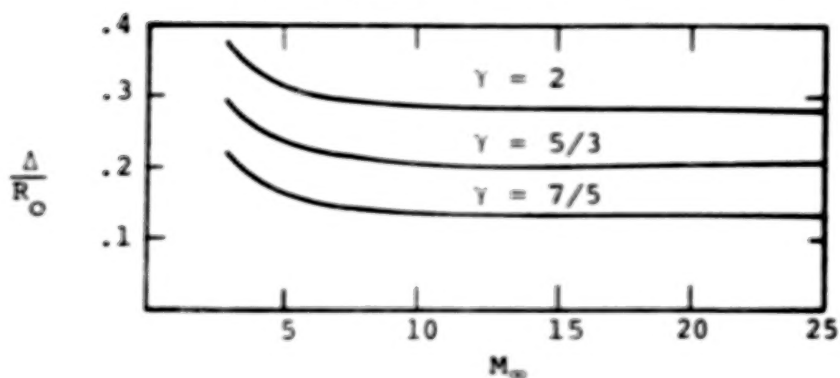


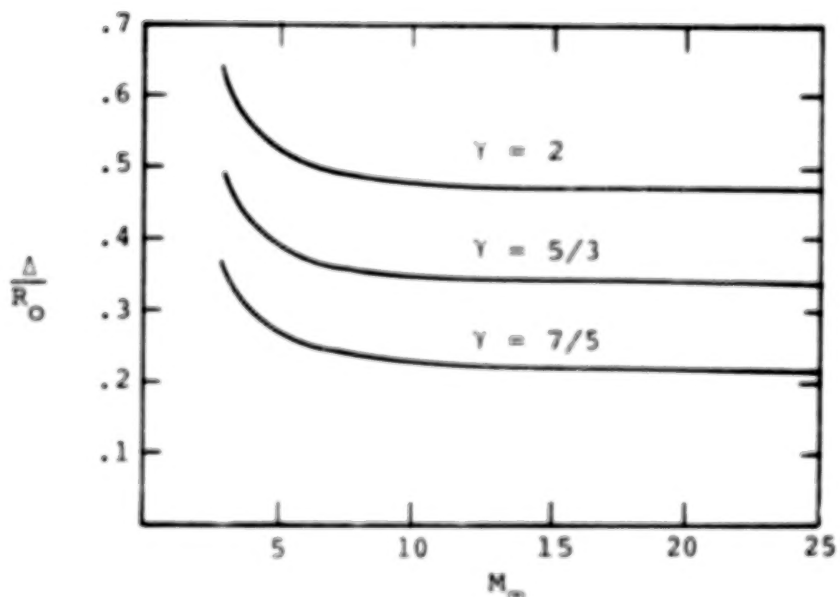
Figure 10. - Magnetopause pressure coefficients for the principal meridian magnetopause shapes shown in figure 9.



(a) Magnetopause equatorial trace



(b) Ionopause trace - $H/R_0 = .01$



(c) Ionopause trace - $H/R_0 = .5$

Figure 11. - Variation of shock stand-off distance with oncoming Mach number and ratio of specific heats for various magneto/ionopause traces as determined by the present implicit procedure.

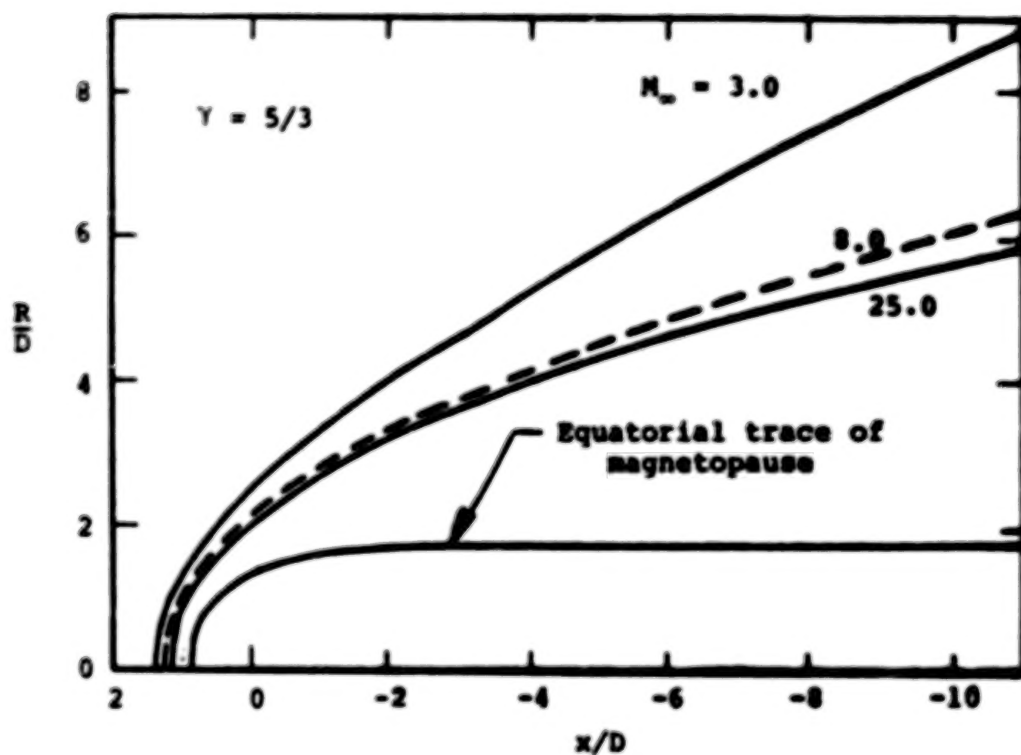


Figure 12. - Shock shapes for various supersonic flows past the rotated equatorial trace of the magnetopause; combined near (blunt body) and far (marching) solutions.

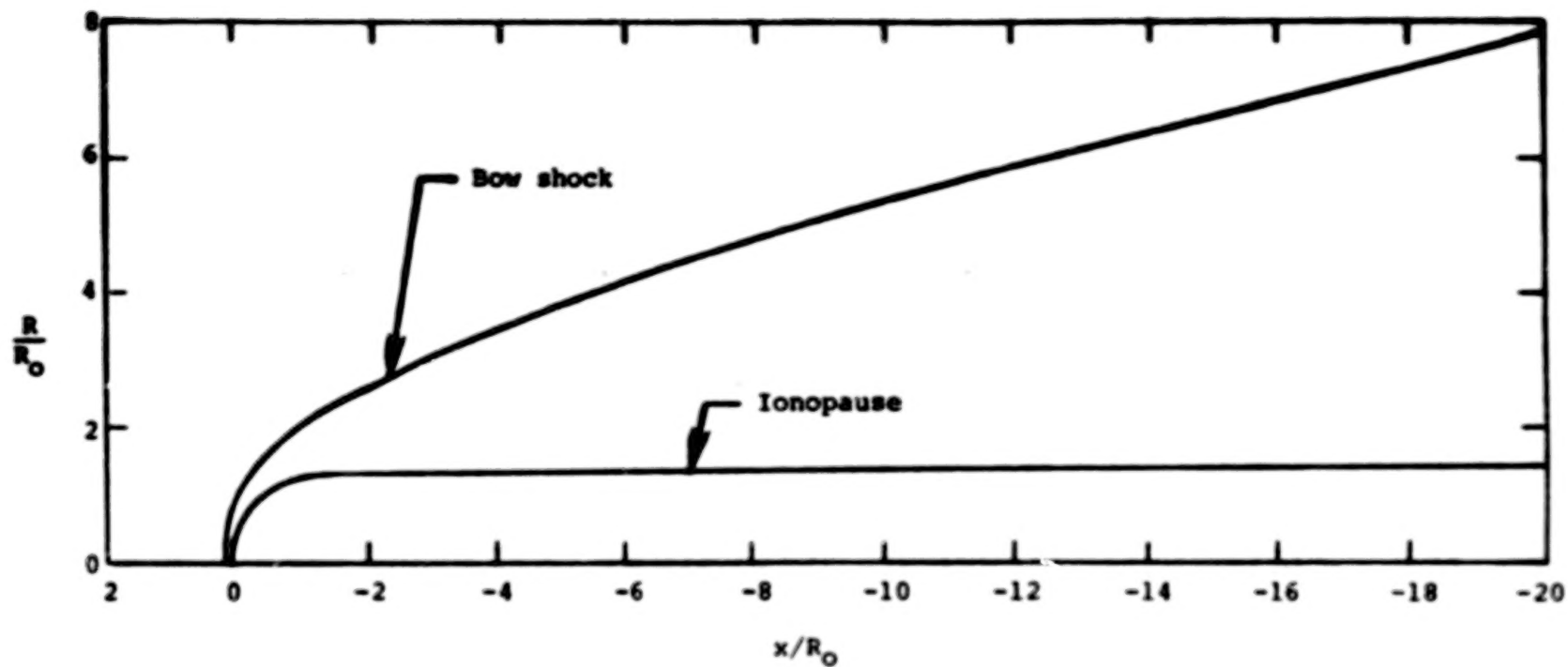
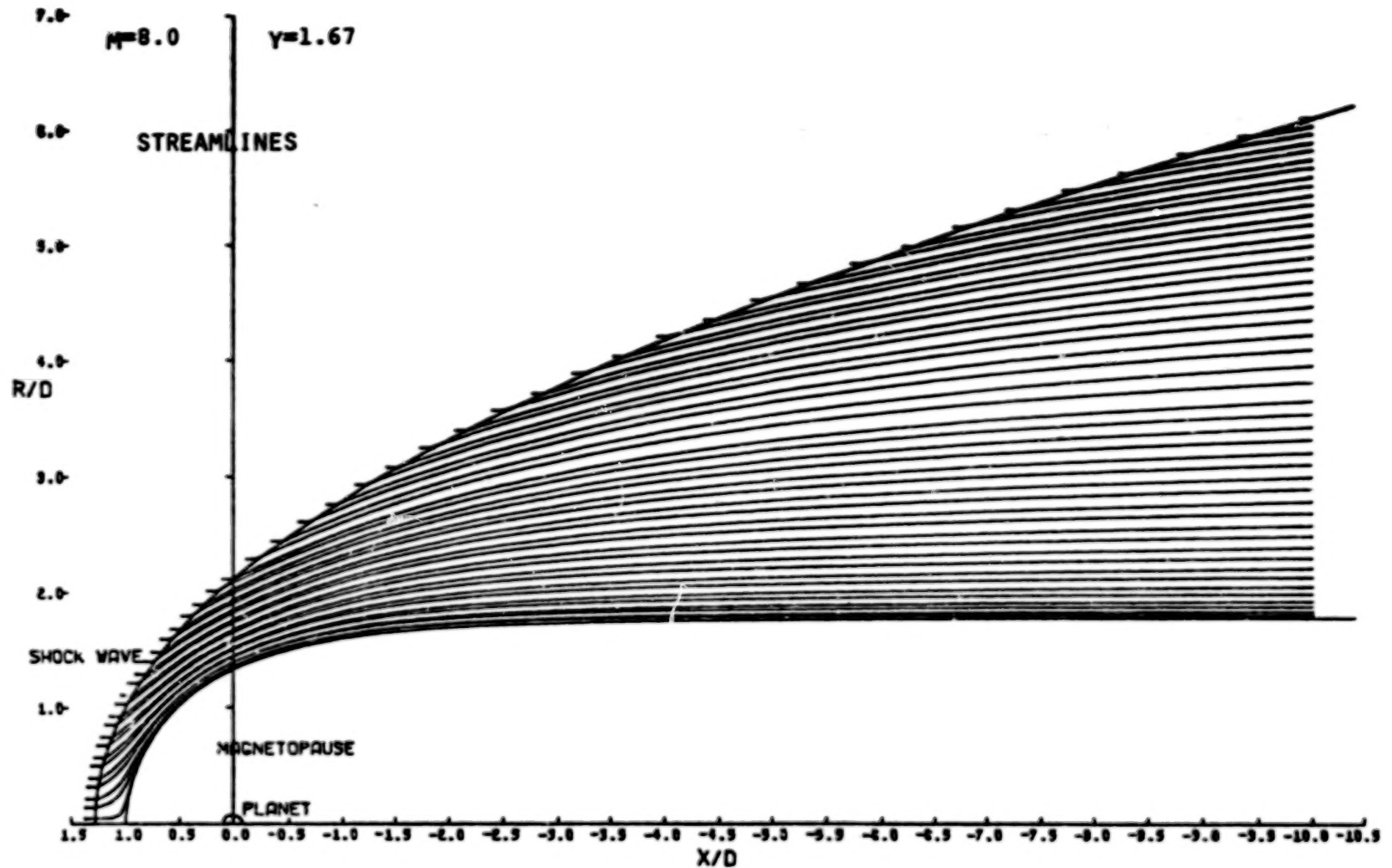
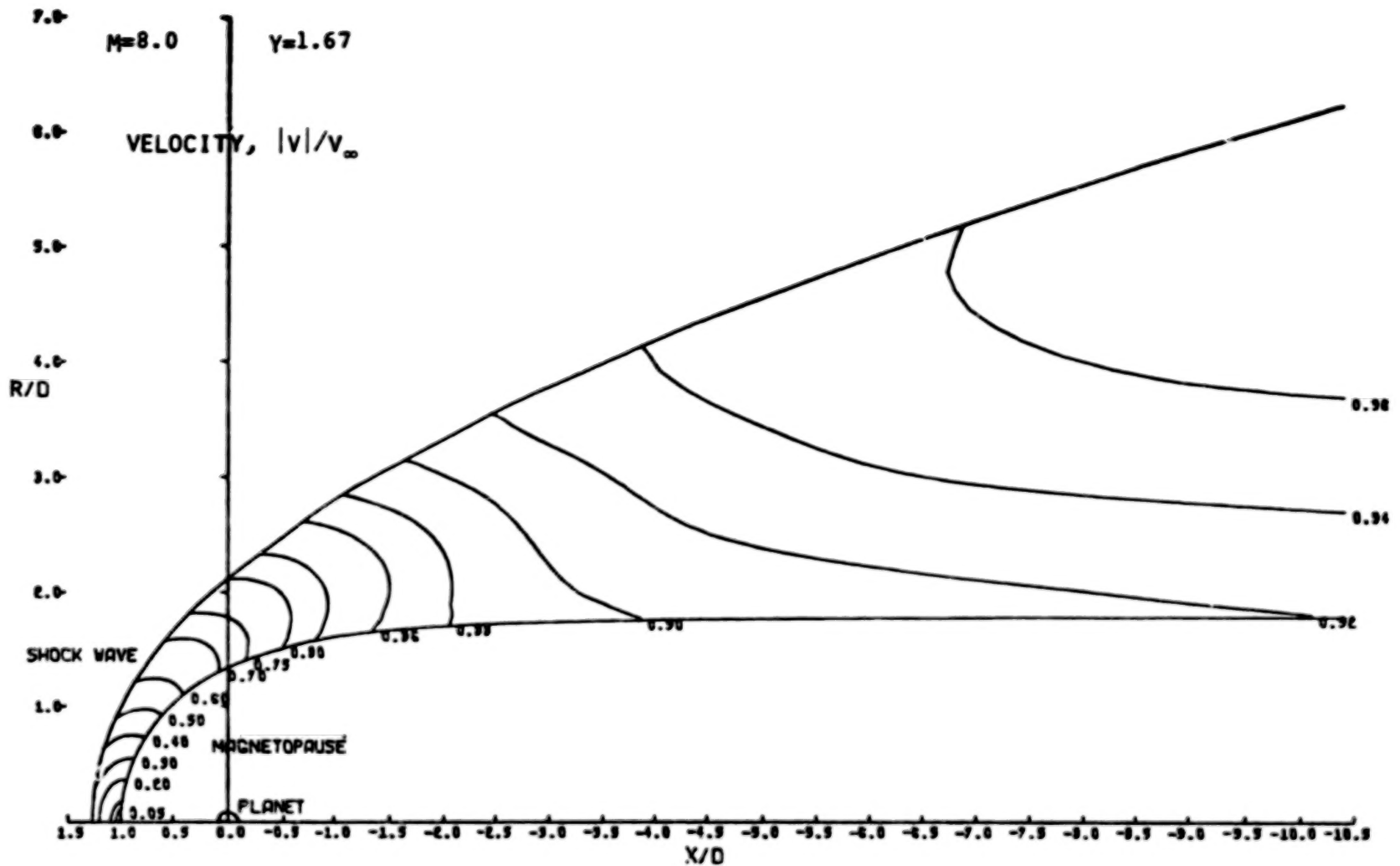


Figure 13. - Shock shape for $M_\infty = 8$, $\gamma = 5/3$ flow past an ionopause shape with $H/R_0 = 0.1$; combined near (blunt body) and far (marching) field solutions.



(a) Streamline Map.

Figure 14. - Streamline, density, and velocity maps for $M_\infty = 8.0$, $\gamma = 5/3$ flow past the rotated equatorial trace of the magnetopause; combined blunt body and marching flow field.



(c) Velocity map.

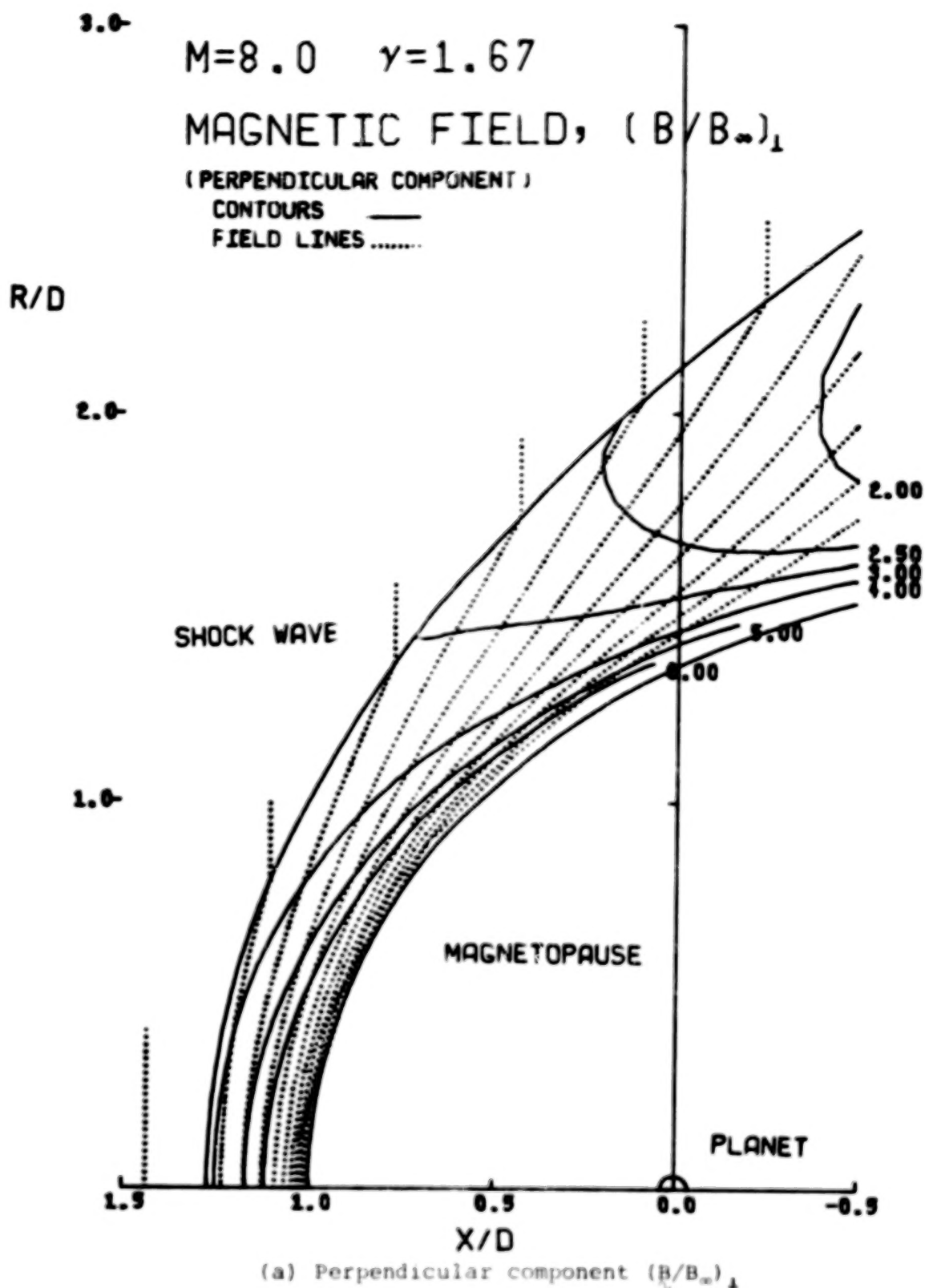
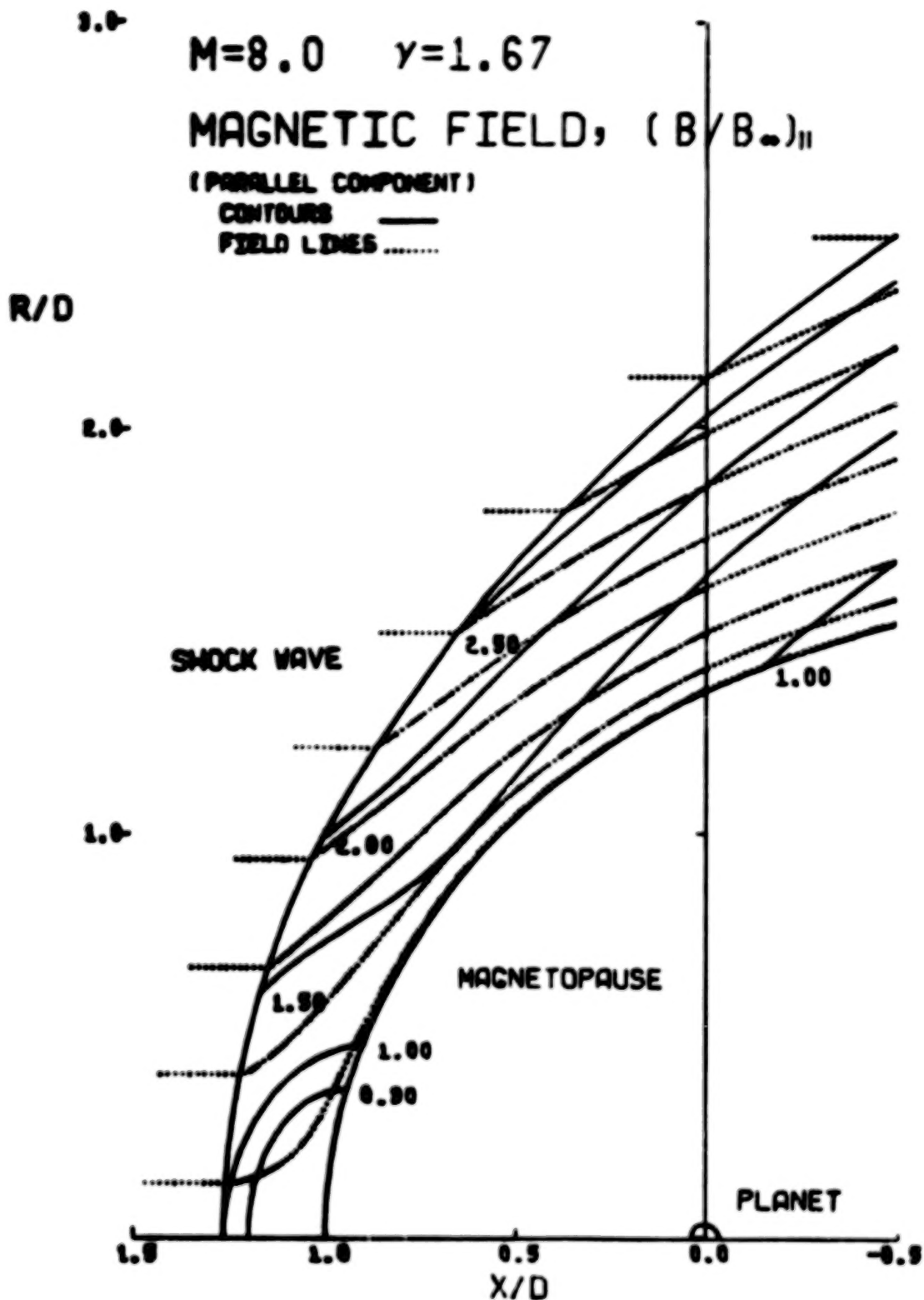


Figure 15. - Contours and field line locations of the in-plane magnetic field components $(B/B_\infty)_1$ and $(B/B_\infty)_2$ for $M_\infty = 8$ and $\gamma = 5/3$ flow past the rotated equatorial trace of the magnetopause.



(b) Parallel component $(B/B_\infty)_\parallel$

Figure 15. - Concluded.

END

April 20, 1981